Geochemical Study of the Back Arc Tsushima Granite Pluton and Its Comparison to the Other Middle Miocene Granites in Southwest Japan

A Dissertation Submitted to

the Graduate School of Life and Environmental Sciences,

the University of Tsukuba

in Partial Fulfillment of the Requirements

for the Degree of Doctor of Philosophy in Science

(Doctoral Program in Integrative Environmental Sciences)

Kicheol   SHIN

Content

Abstract

The Middle Miocene Tsushima granite pluton is composed of leucocratic granites, gray granites and numerous mafic microgranular enclaves (MMEs). The granites have a metaluminous to slightly peraluminous composition and belong to the calc-alkaline series. The Tsushima granites are unique in that they occur in the back arc area of Southwest Japan, contain numerous miarolitic cavities, and show shallow crystallization depth (2–6 km deep) based on hornblende geobarometry. Field, petrological, and geochemical data demonstrate that the MMEs are quenched globules of mafic magma and the gray granites formed by mingling/mixing of the high-temperature mafic and low-temperature granitic magmas. Contamination by sediments was negligible.

The leucocratic granite has higher initial $^{87}Sr/^{86}Sr$ ratios (0.7065 to 0.7085) and lower $\varepsilon_{Nd}(t)$ values (-7.70 to -4.35) than the MMEs (0.7044 to 0.7061 and -0.53 to -5.24), whereas most gray granites have intermediate chemical and Sr–Nd isotopic compositions. The Sr–Nd–Pb isotope data strongly suggest that the mafic magma was derived from two mantle components with depleted mantle material (DMM) and enriched mantle I (EMI) compositions, whereas the felsic magma formed due to partial melting of metabasic rocks in the lower crust by injection mafic magma of EMI-origin. Element data points deviating from the simple mixing line of the two magmas may indicate fractional crystallization of the felsic magma or chemical modification by hydrothermal fluid. The miarolitic cavities and enrichment of alkali elements in the MMEs suggest rapid cooling of the mingled magma accompanied by elemental transport by hydrothermal fluid. The inferred genesis of this magma–fluid system is as follows: (1) the mafic and felsic magmas were generated in the mantle and lower crust, respectively, by a large heat supply and pressure decrease under back arc conditions induced by mantle upwelling and crustal thinning; (2) they

mingled and crystallized rapidly at shallow depths in the upper crust without interaction during the ascent of the magmas through the middle to the upper crust, which (3) led to fluid generation in the shallow crust.

The Outer Zone granites have geochemical features comparable in part to the Tsushima granites; they have calc-alkaline and metaluminous to peraluminous compositions. In detail, the Outer Zone granites have highly fractionated and contaminated geochemical signature, and are abundant in Pb and Rb, and depleted in Ca and Sc than the Tsushima granites. These granites have regional chemical variation resulted from different degrees of contamination; contamination degrees and Sri increasing toward the Pacific Ocean. These features suggest that the Outer Zone granites underwent rather complicated magmatic process during ascent/emplacement of magmas. These granitic magmas are supposedly generated due to partial melting of mafic lower crust by injection of hot mafic magma of mantle origin, as inferred for the Tsushima granites.

Many of the Outer Zone granites plot on a mixing array between high-Mg andesites (sanukitoids) and Shimanto sedimentary rocks in the Sr-Nd diagram. The Sr-Nd plots are however, rather scattered implying that the felsic magmas were originated from rather heterogeneous lower crust. The Ichifusayama granites are especially enriched in radiogenic isotopes. This implies that an older felsic granulite crust, that is silica-rich and enriched in radiogenic Sr-Nd-Pb isotopes, is distributed heterogeneously in the lower crust of the Outer Zone.

The high-Mg andesites, considered to have melted the lower crust of the Outer Zone, have higher Sr and Pb isotopic ratios than the mantle-derived mafic magma in back arc region. The isotopic signature of the high-Mg andesites required involvement of another mantle component for their generation, such as subarc metasomatized mantle contaminated by oceanic sediments, adding to DMM and EMI mantles hypothesized

beneath the Inner Zone. Thus it is considered that the mantle components beneath the Outer Zone crust must be an enriched mantle II (EMII), which represents contaminated DMM by subducted oceanic sediments.

In contrast to the Tsushima granites, mafic magmas of mantle origin, felsic magmas of the lower crust origin and sediments in the upper crust were highly interactive during the ascent and emplacement of the Outer Zone granite magmas. Since the Tsushima granites intruded into the extensional environments, they ascended and cooled rapidly without interacting with the wall-rocks of the middle to upper crusts. In contrast, compressional tectonic environments stimulated degree of the interaction and contamination during magma ascent and emplacement in the forearc region.

Keywords: back arc granite, Outer Zone granites, magma mixing, enclave, Sr-Nd-Pb isotopes, fluid, Middle Miocene, Tsushima Islands.

List of Tables

List of Figures

1. INTRODUCTION

Granite is a major constituent of the upper continental crust of the Earth. The continental crust constitutes only 0.62% of the crust-mantle system of the Earth, but it has a geochemical significance far greater than the number indicated. The continental crust becomes more mafic with depth (Rudnick and Gao, 2003). It has an andesitic bulk composition (Rudnick and Gao, 2003), which cannot be produced directly by accretion of the mantle-derived mafic magmatism. The continental crust is enriched in incompatible elements (Rb, Ba, K, Pb, Th, and U), and involves up to 50 % of the Earth's budget of these elements (Rudnick and Fountain, 1995). Internal processes such as fractional crystallization and/or assimilation were suggested to concentrate these incompatible elements. The upper continental crust is abundant in granites and various rocks with granitic compositions (Wedepohl, 1991). These observations suggest that granites can provide clues to understand how and when the continental crust was developed, and which processes involved in the compositional differentiation to develop a continental crust.

From the late Archaean to late Proterozoic eras, much of the continental crust appears to have been generated in pulses of relatively rapid growth (Figure 1.1) (Condie, 1998). The granites occur in a broad range of plate tectonic setting and thus have diverse sources and underwent various petrogenetic processes (Pitcher, 1997). Nevertheless voluminous occurrence of the granite is restricted in the convergent plate boundaries such as subduction zones and continent colliding zone. The continental crust is thus, formed as a result of accretion of mafic magmas derived from the upper mantle at subduction zones (Marshall and Fairbridge, 1999) but the processes that connect mafic accretion and generation of granitic magma are controversy. The Southwest Japan arc underwent subduction and accretion of oceanic materials and episodic granitic magmatism

1
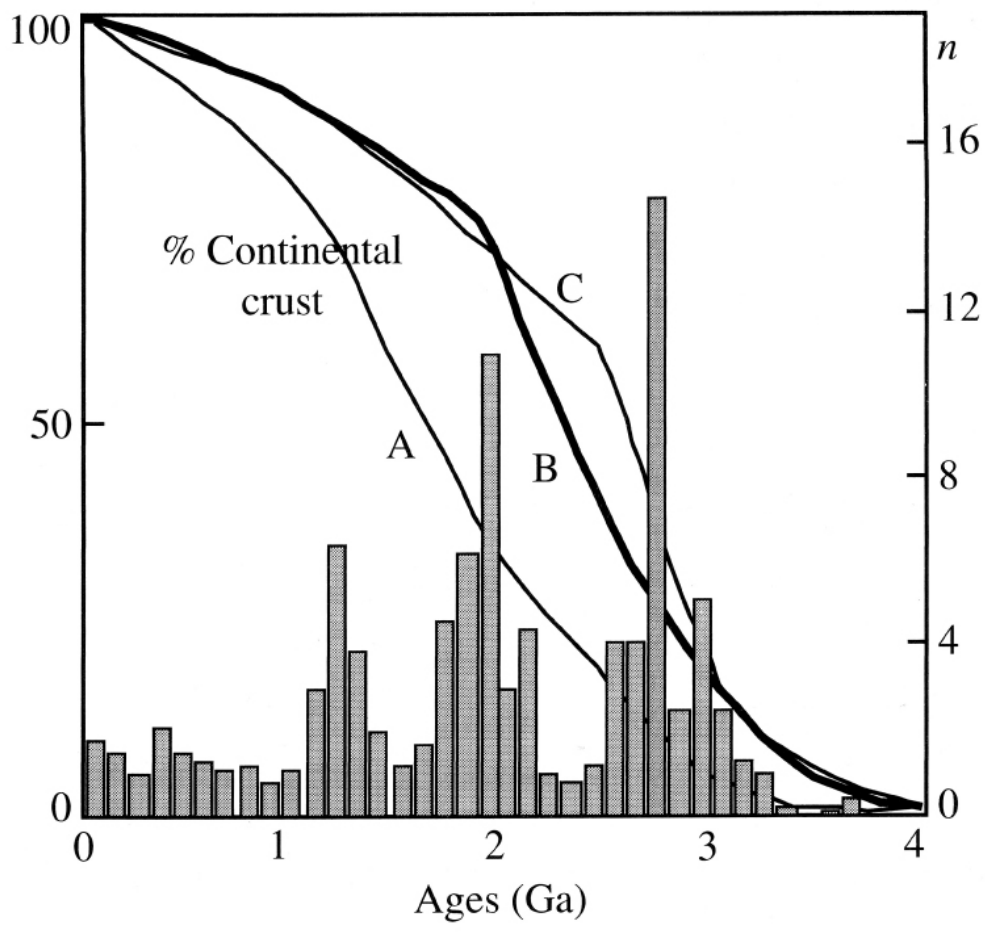
Figure 1.1. Distribution of U/Pb ages from juvenile crust (from Condie, 1998) and continental growth curves. Curves represent different models for the changing volumes of stable continental crust with time (A: minimum curve based on Nd isotopes in shales (authors' compilation); B: from Collerson and Kamber (1999), and similar to Kramers and Tolstikhin (1997); and C: Taylor and McLennan (1985)). Figure is from Kemp and Hawkesworth (2003).

(Takahashi, 1983; Isozaki and Maruyama, 1991; Maruyama, 1997). Framework of Southwest Japan consists of accretionary complexes developed along the margin of the Asia continent since Permian (Taira, 2001). The Southwest Japan is subdivided into two zones bounded by the Median Tectonic Line; the Inner Zone and the Outer Zone (Figure 1.2) (Sugimura and Uyeda, 1973). The Inner Zone consists of Paleozoic and Mesozoic sedimentary and metamorphic rocks, granite batholiths, and acidic volcanic rocks. The granitic magmatism is culminated during the Cretaceous time and continued to the Tertiary period (Sato et al., 1992). The Outer Zone is composed of Jurassic to Paleogene sedimentary rocks and Mesozoic metamorphic rocks (Figure 1.2). The Outer Zone is characterized by small volume of various intrusive rocks. The intrusive rocks are mostly calc-alkaline granites with small amount of gabbroic and alkaline rocks. This magmatic activity characteristically took place within the forearc area close to the trench. This activity is generally considered to have relation with the subduction of the young Philippine Sea plate.

During the Miocene time, the Japanese islands became separated from the Asian continent by the opening of the East Sea (Japan Sea). This opening of the marginal sea and associated mantle upwelling resulted in counterclockwise rotation of the Northeast Japan arc (Otofuji et al., 1985; Tatsumi et al., 1989; 1990; Tamaki, 1995) and clockwise rotation of the Southwest Japan arc (Ishikawa and Tagami, 1991). The Southwest Japan arc obducted onto the young and hot Philippine Sea plate which eventually started to subduct. These tectonic movements generated intensive volcanic activity, mainly of basaltic to andesitic composition, around the East Sea (Cousens and Allan, 1992; Pouclet et al., 1995; S'edin and Sato, 1996) and granitic intrusions in Southwest Japan (Nakada and Takahashi, 1979; Takahashi, 1986) (Figure 1.2). The Middle Miocene alkali basalts around the East Sea, include numerous mantle xenoliths (Arai et al., 2000; Kagami et al., 1993), providing

3
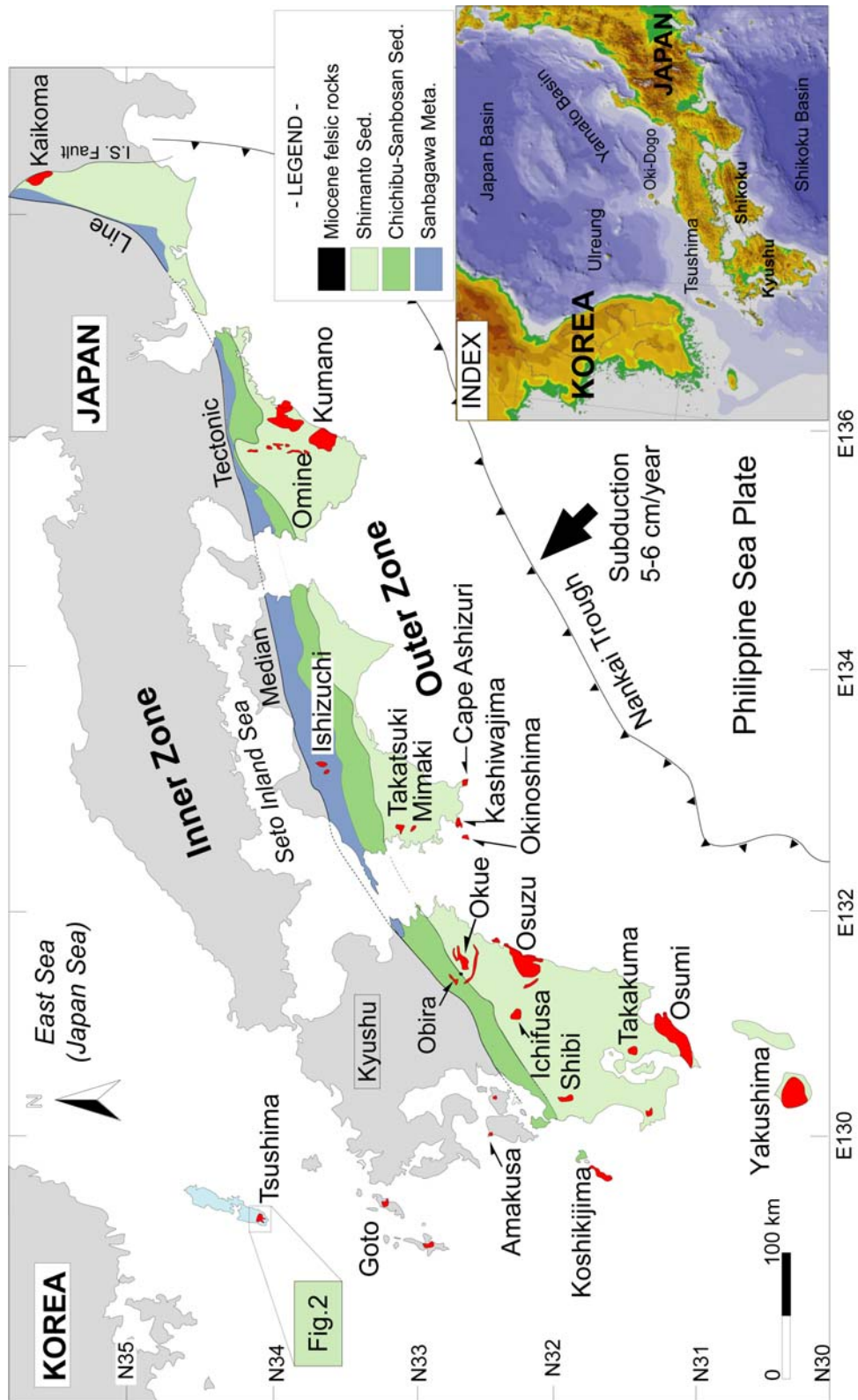
Figure 1.2. Simplified geology and distribution of Middle Miocene granitic rocks in Southwest Japan (after the Geological Survey of Japan, 1992). Inset shows geographical map around Japan.

important information for deep magmatic processes in the upper mantle connected to the back arc opening. Similarly, the Middle Miocene granites provide critical information about shallow magmatic processes during the back arc opening.

Apart from the alkaline Ashizuri pluton distributed southern tip of Shikoku, the Middle Miocene plutons of the Outer Zone of Southwest Japan are all calc-alkaline series granites. The calc-alkaline Outer Zone granites are ilmenite-series granites, with I-type signatures that are characterized by hornblende-bearing mineral assemblages in the northern area, and S-type signatures in the southern area with cordierite as a typical peraluminous mineral. These rocks show geochemical variations such as increasing contents of K_2O, total Fe and normative corundum toward the Pacific Ocean (Nakada and Takahashi, 1979). These chemical variations were caused by contamination with sedimentary rocks of the Shimanto Group in the upper crust (Terakado et al., 1988; Stein et al., 1994; Shinjoe, 1997; Ishihara and Matsuhisa, 1999), and the degree of the contamination decreases from the Outer to the Inner Zone (Nakada and Takahashi, 1979; Nakada and Okamoto, 1984). This regional trend has been attributed to the tectonic difference: a compressional forearc region in the Outer Zone versus an extensional back arc region in the Inner Zone (Ishihara, 1977; Nakada and Takahashi, 1979; Takahashi *et al.*, 1980).

In contrast, the Inner Zone granites of Miocene ages are all classified as magnetite-series, I-type ones. Only few reported petrological characteristics (the Amakusa granite: Hamasaki (1997); the Goto granite and the Tsushima granite: Kitai, 1969; Kawahara et al., 1984) and tectonic model for the intrusion (Ishikawa and Tagami, 1991) of the Inner Zone granites. Few Sr-Nd isotopic data were reported and they are controversy; one suggested a mantle-origin (Shibata and Ishihara, 1979; Ishihara and Imai, 2000) and the other crustal-origin (Ishizaka and Ishikawa, 1990) of the plutons.

5

Among the Miocene granites of Southwest Japan, the Tsushima granite pluton is unique because it is located in the innermost Inner Zone and is thus furthest from the Nankai trough (Figure 1.2) (Otofuji *et al*., 1985; Ishikawa *et al*., 1989). During the opening of East Sea, the Tsushima islands underwent extension and thinning of the arc crust. This suggests the tectonic environment during its formation was relatively extensional (Tamaki, 1995). The location of this pluton, however, corresponds to the hinge of the East Sea opening, which would have been under compressional tectonics during the opening (Ishikawa *et al*., 1989). If extensional stress prevailed over compressional stress, then the Tsushima pluton would be expected to exhibit little contamination from upper crustal materials, and would thus be suitable for the detection and evaluation of deep magma source materials in plutonic processes. Moreover chemical comparison of the granites distributed across the Southwest Japan arc is useful to contrast the character of the back arc calc-alkaline granite.

Recent studies of Quaternary volcanic rocks（Shinjo *et al*., 1999; Hosono *et al*., 2003; Uto *et al*., 2004）have demonstrated that an enriched mantle I (EMI)-like material is distributed underneath the crust of Southwest Japan from the Japan Sea to the Ryukyu Islands, and this material contributes substantially to the volcanic rocks in the area. However, whether a petrological entity from such a deep magmatic source exists and what its genetic relationship to the Middle Miocene granites might be are unclear. It is thus important to understand the origin and development of such regional magmatism with various compositions and modes of emplacement in relation to the tectonic setting.

In this study, I report petrographic description (Chapter 3), abundance of major and trace elements, and Sr-Nd-Pb isotopic data of the Tsushima granite pluton (Chapter 5) to characterize petrochemical features of the "back arc granite" and to elucidate the petrogenesis of a calc-alkaline granitic magma and their source material characteristics

(Chapter 8). A comparison of chemistries between the Tsushima granites and the Outer Zone granites was also attempted to examine the relation between the granite formation and the mantle upwelling (Chapter 9).

2. GEOLOGICAL OUTLINE OF THE TSUSHIMA ISLANDS

The Tsushima Islands, located between the Korean peninsula and the Kyushu islands, consists of two main islands, Kamijima and Shimojima (the North and the South Islands). The islands have an area of about 708km^2 and are composed mainly of Early Eocene to Early Miocene sedimentary rocks of the Taishu Group (Takahashi, 1969; Nakajo and Funakawa, 1996; Sakai and Yuasa, 1998) and Miocene igneous rocks (Figure 2.1).

The Taishu group is composed of massive mudstone and sandstone—mudstone alternation (Takahashi, 1969). The Taishu group sediments are more than 5,400m thick and folded about an axis plunging gently to NE (MITI, 1972). Depositional environments were deltaic to shallow marine (Nakajo and Maejima, 1998; Okada and Fujiyama, 1970) based on marine molluscan fossils (Kanno, 1955; Takahashi and Nishida, 1975) and planktonic microfossils (Ibaraki, 1994; Nakajo and Funakawa, 1996). Paleocurrent directions defined by sedimentary structures such as asymmetrical ripple marks and cross lamination stratification indicate that all of the sediments were derived from north (Sakai, 1993; Nakajo and Maejima, 1998). The Taishu group is subdivided into Upper, Middle, and Lower Formation (MITI, 1972, 1973, 1974). Thin layers of lapilli tuff occur in the boundary zone between the Lower and the Middle Formation. The lapilli tuff layers are subaqueous pyroclastic deposits in Early Miocene to Early Oligocene ages (range from 18.7±1.2 to 30.5±2.5 Ma based on zircon fission-track (FT, hereafter) method (Takahashi and Hayashi, 1985, 1987). The Early Oligocene age is conformable to the Early Eocene radiolarian fossils from the Lower Formation (Nakajo and Funakawa, 1996) and Middle Eocene to Early Oligocene planktonic foraminifers from the basal part of the Upper Formation (Sakai and Nishi, 1990).

Igneous activities in Tsushima Islands culminated in middle Miocene period (Ishikawa and Tagami, 1991; Karakida, 1987; Takahashi and Hayashi, 1987). Igneous rocks, mainly felsic in composition with minor amount of dolerite, intruded into the sedimentary rocks as dikes and sheets after folding events of the Taishu Group. Matsumoto and Takahashi (1987) reported geological relations of these rocks in detail that dacite is older than quartz porphyry and then granite intruded both of them. Dactie and quartz porphyry (to rhyolite) have zircon FT ages of 16.9±1.0 to 18.7±1.0 Ma and 14.2±0.7 to 14.8±0.8 Ma, respectively (Takahashi and Hayashi, 1985, 1987). Quartz porphyry altered into acid clay and porcelain clay by hydrothermal alteration (Suzaki et al., 1970). K-Ar ages of fresh samples range from 14.1 to 19.0 Ma (Karakida, 1987). Dolerite occurs as minor intrusions and considered to intrude at the same period as felsic magmatism (Matsumoto and Takahashi, 1987).

The Tsushima granite pluton is located at the southern end of Shimojima (the South Island) of the Tsushima islands (Figure 2.1). It intruded concordantly into an anticlinal axis developed in the Lower Formation of the Taishu Group (Matsuhashi, 1968) to form thermal metamorphic aureole. The thermal aureole is widespread in the Shimojima, implying the presence of a large cryptodome (Shimada et al., 2000). Biotite-cordierite hornfels extended about 800m to 1500m from the contact (Shimada et al., 2000; Ishihara and Imai, 2000). Exposures of the pluton are limited to topographically low areas such as river valleys and bays, and they are found at the Hikage, Uchiyama, Azamo, Nai-in, and Kuwa localities (Figure 2.1). Although the granites are exposed in separate locations, all of the exposures are considered to be a part of a single continuous pluton on the basis of the distribution of the contact metamorphic aureole (Shimada et al., 2000).

The granites consist of fine- to medium-grained biotite granite, hornblende-biotite granodiorite, and hornblende tonalite. The granites contain mafic microgranular enclave (MME) and sedimentary xenolith (Kaneko and Yaguti, 1980; Ishihara and Imai, 2000).
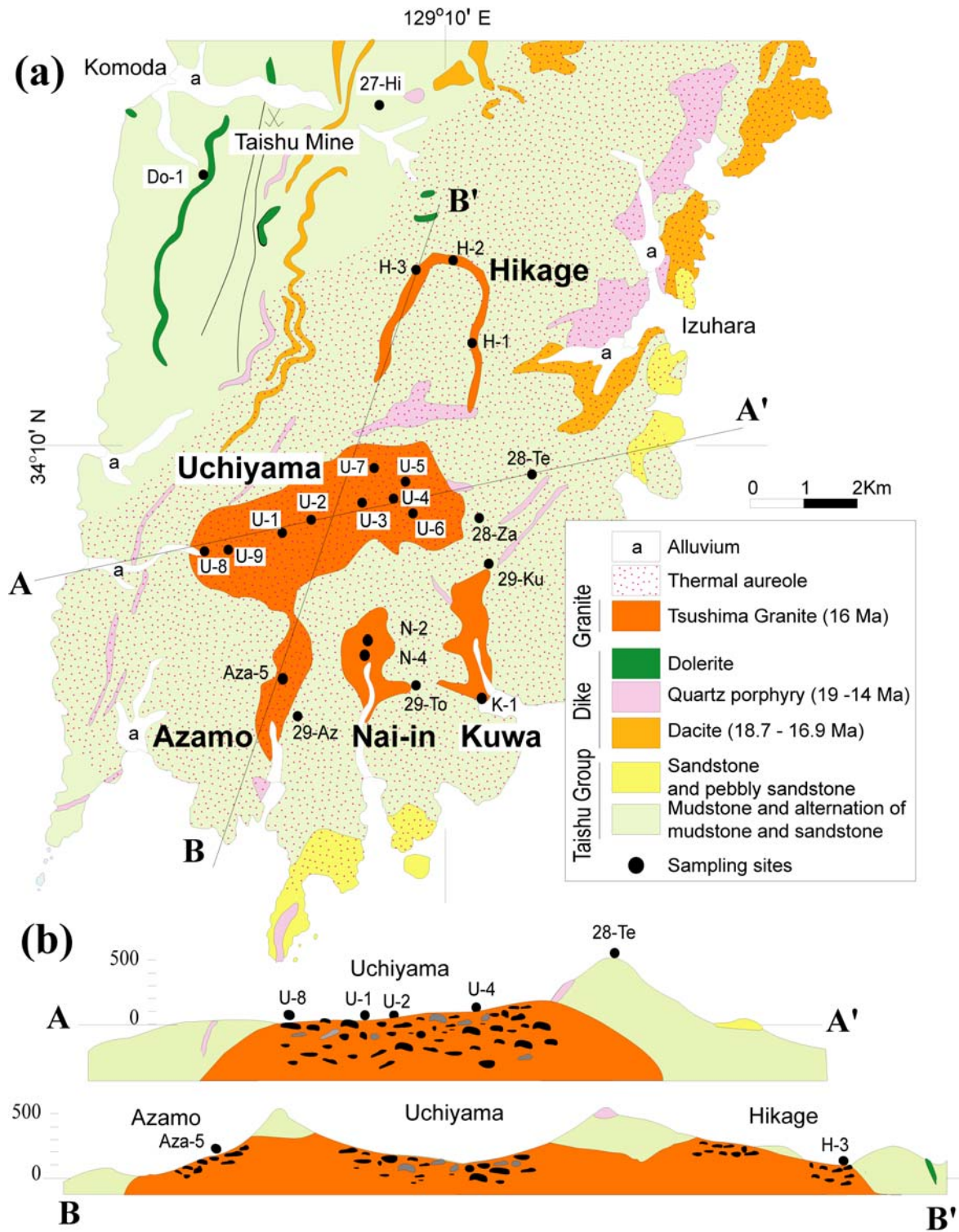
Figure 2.1. (a) Geology and distribution of Middle Miocene granitic rocks in the southern part of Shimojima, southern Tsushima Island archipelago, Japan (modified from Yamada *et al.*, 1990). (b) Simplified geological corss-sections of the study area showing distribution of the Tsushima pluton and the MMEs.

Matsuhashi et al. (1970) considered that the Tsushima granite intruded after or at final stage of the folding event from the geological evidences such as absence in compressional fault in the granite and lack of granitic rocks in the lowermost part of the Lower Formation where folding deformation is the strongest. The Tsushima pluton is a magnetite-series granite, and has an I-type chemistry. Ishihara and Imai (2000) reported that the oxygen isotopic compositions ($\delta^{18}O$ value) of the rocks of the Tsushima pluton to be +9‰ at SiO_2 70%, and $\delta^{34}S$ value to be +1.4 to +9‰, and initial Sr ratio was 0.7037. More enriched isotopic value of the granitic rocks was reported by Ishizaka and Ishikawa (1990). According to them, initial $^{87}Sr/^{86}Sr$ ratios were 0.7056 to 0.7074 and $^{143}Nd/^{144}Nd$ ratio was 0.512334. Ikemi (2001) determined that the $\delta^{18}O$ values of amphiboles range from +7.1 to +8.0‰, biotites from +5.6 to +7.4‰. Hornfels have bulk $\delta^{18}O$ values of +14.2 to +15.1‰. The granite pluton exhibits zoning with respect to magnetic susceptibility, which increases toward the center of the pluton (Shimada et al., 2000).

Reported biotite K–Ar ages for the granitic rocks range from 12 to 19 Ma (Kawano and Ueda, 1966; Karakida, 1987; Ikemi et al., 2001). Ikemi et al., (2001) also determined Hornblende K-Ar age of the granites to be 13.6±0.4 to 17.4±0.4 Ma (Zircon FT ages of 14.9±0.8 Ma (Takahashi and Hayashi, 1985) and 12.8±1.4 to 16.5±1.6 Ma (Ishikawa and Tagami, 1991) were also reported for the granites. These ages correspond to the last stage of the opening of the Japan Sea (15 Ma, Otofuji et al., 1985).

Lead-zinc mesothermal vein-type ore deposits occur along the fracture zone of sedimentary rocks in several areas around the granites. The Taishu ore deposits were impregnated in shear fractures developed along faults striking N-S and NE-SW, and in tension fractures developed along NW faults. These ore deposits were studied in detail with genetic relations to the Tsushima granites (Imai, 1973; Ishihara and Imai, 2000; Matsuhashi, 1968; Ohyama and Shimada, 1988; Shimada, 1977; Shimada et al., 2000). Ore

11

deposits mineralization divided into three stages; Co-As stage, Fe-Zn-Pb stage, and rejuvenation stage (Shimada (1977). The mineralization age was reported to be 15.4 Ma using muscovite K-Ar method (Ikemi et al., 2001).

3. PETROGRAPHY OF THE TSUSHIMA GRANITES

3.1 Granites

The Tsushima granite pluton has three main components: leucocratic granite, gray granite, and mafic microgranular enclaves (MMEs). These three components are hereafter referred to collectively as the TSUG (the Tsushima granites). The MME-free leucocratic part is present at a scale of a few square meters (Figure 3.1b, c) in the TSUG, and we refer to that component as the leucocratic granite. Gray-colored granites, referred to hereafter as the gray granite, are observed only adjacent to MMEs, suggesting mixing of the leucocratic granite magma with the MME magma (Figure 3.1c). The gray granite is easily distinguished from both leucocratic granite and MMEs in the field by its occurrence, mineral assemblage, and texture. Contact zones between granites and sedimentary country rock were observed in Hikage and Kuwa area, where numerous MMEs were distributed.

The leucocratic granite is composed of fine- to medium-grained biotite monzogranite and granodiorite (Figure 3.2 and Table 3.1) and is abundant at the Uchiyama and Hikage localities. Typical specimens have a fine-grained equigranular texture (grain size, 0.5–1.5 mm) (Figure 3.3a); other specimens show a fine- to medium-grained (2–5 mm) equigranular texture. The mineral assemblage is quartz, microperthitic alkali feldspar, plagioclase, and small amounts of biotite, tourmaline, monazite, titanite, and opaques. Hornblende is essentially absent. The opaque minerals are magnetite and ilmenite with small amounts of sulfide minerals such as pyrrhotite. The leucocratic granite often includes miarolitic cavities containing relatively large euhedral crystals of hornblende, tourmaline, titanite, or quartz. These minerals are considered to be the last products of crystallization.

The gray granite usually corresponds to a porphyritic granodiorite (Figure 3.2 and Table3.1) but has variable texture. The mineral assemblage of the gray granite is generally

13
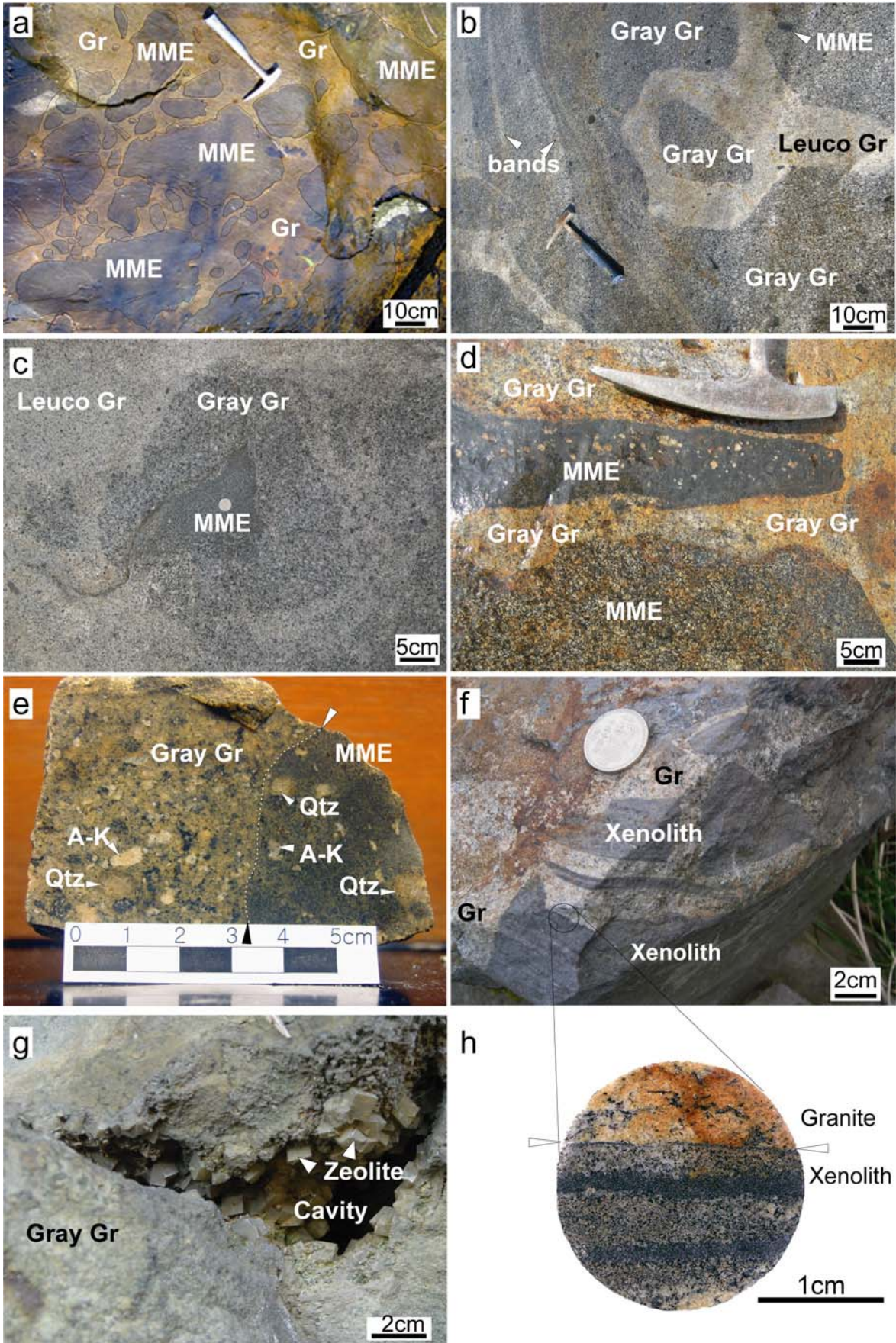
Figure 3.1. Field photographs of the Tsushima granites and sedimentary rocks. (a) Mafic microgranular enclaves (MMEs) in the gray granite (Gray Gr) from Nai-in, Tsushima Islands, Japan (Figure 2.1). (b) Occurrence of leucocratic (Leuco Gr) and gray granites in the Uchiyama locality. Flow banding is observed on the left side of the image. (c) Leucocratic granite, gray granite, and a MME from the Uchiyama locality. (d) Texture variation of MMEs from Hikage locality. Upper MME shows porphyritic texture, having fine matrix with large white phenocrysts (quartz and feldspars). Lower MME shows equigranular texture and has relatively large grains than the upper MME. (e) Diffuse contact between gray granite and MME. Large quartz and alkali feldspar grains were included in the MME. (f) Hornfels xenoliths from Hikage locality. (g) Miarolitic cavity in the gray granite, 20 cm in diameter, from the Nai-in locality. Large euhedral crystals of zeolite (chabazite) (up to 15 mm) are present in the cavity. The miarolitic cavities often contain schorl, hornblende, chlorite, epidote, magnetite, pyrrhotite, chalcopyrite, and/or galena. (h) Contact surface between granite and hornfels xenolith. Xenolith shows clear layers of darker mud and lighter sand.

Table 3.1.　Modal contents of the Tsushima granites[1]

	Mafic Microgranular Enclave (MME)[2]													Leucocratic Granite					
	H-1a	H-2a	H-2b	H-3a	H-3b	N-4a	U-2a	U-2b	U-3a	U-4a	U-5a	U-6a	U-8a	H-2c	H-2e	U-1d	U-1e	U-4c	U-7
Pl[3]	38	52	51	49	48	38	50	57	58	49	49	54	48	47	35	27	30	36	24
Qtz	10	15	18	7	16	4	19	25	13	27	18	22	11	27	32	36	42	42	43
Kfs	0	0	2.1	0.6	1.2	0	0.1	1.3	2.0	5.9	1.8	0.9	0	14	23	32	24	19	30
Bt	22	15	16	14	10	9.6	15	15	6.5	14	6.4	6.0	16	9.3	10	4.6	4.8	1.8	1.5
Hbl	27	18	10	25	20	31	13	1	18	1	17	12	24	0	0	0	0	0	0
sum	97	99	97	96	95	83	97	98	98	97	93	95	99	97	99	100	100	98	99
Cpx	-	-	-	-	-	-	-	-	-	-	tr	tr	-	-	-	-	-	-	-
Opx	tr	tr	-	-	-	-	-	-	-	-	tr	tr	-	-	-	-	-	-	-
Ap	2.1	tr	tr	1.3	1.4	2.3	1.4	1.5	1.5	1.9	2.4	1.9	1.1	tr	tr	tr	-	-	-
Zrn	tr	tr	tr	tr	tr	tr	tr	tr	tr	tr	tr	tr	tr	tr	tr	tr	tr	tr	tr
Mnz	-	-	-	-	-	-	-	-	-	-	-	-	-	-	-	tr	tr	-	-
Ttn	-	tr	-	-	-	-	-	-	-	-	-	-	-	-	-	-	-	-	tr
Act	-	-	-	-	tr	-	tr	-	-	-	tr	-	-	-	-	-	-	-	tr
Ep	-	-	tr	tr	tr	-	-	tr	-	-	-	-	-	tr	tr	tr	-	-	-
Chl	-	-	tr	1.7	1.7	-	-	tr	-	tr	tr	-	-	tr	tr	-	-	1.3	tr
Tur	-	-	-	-	-	tr	-	-	-	-	-	-	-	-	-	-	-	-	tr
Mag	-	-	-	-	-	9.2	tr	-	-	tr	3.3	1.3	-	-	-	tr	-	tr	tr
Ilm	tr	tr	-	tr	tr	5.5	tr	tr	tr	tr	1.1	tr	tr	tr	tr	-	-	tr	-
Sul	-	-	1.6	tr	tr	-	-	-	-	-	-	-	-	tr	tr	-	-	-	-

	Gray Granite																
	H-3c	N-2	N-4b	N-4c	U-1a	U-1c	U-2c	U-3b	U-3c	U-4b	U-5b	U-6b	U-8b	U-8c	U-9	Aza-5	H-1b
Pl	45	49	49	42	33	40	37	56	44	46	54	38	41	31	50	59	43
Qtz	26	23	24	34	33	31	39	24	32	29	22	38	32	38	26	23	37
Kfs	14	5.8	12	15	20	15	15	6.7	11	10	8.6	17	15	25	5.8	3.0	10
Bt	13	20	10	5.9	14	13	8.2	8.4	9.4	14	8.7	6.0	6.8	5.4	14	1.7	8.9
Hbl	1.5	0	3.7	0.8	0	0	0	2.8	2.0	0	2.9	0.7	0	0	3.0	11	0
sum	99	98	99	98	100	99	99	97	98	98	97	100	94	99	99	98	99
Cpx	-	-	-	-	-	-	-	-	tr	-	-	-	-	-	tr	-	-
Opx	-	-	-	-	-	-	tr	-	tr	-	-	-	-	-	tr	-	-
Ap	tr	1.5	tr	tr	tr	tr	tr	1.1	tr	1.0	tr	tr	tr	tr	tr	tr	tr
Zrn	tr	tr	tr	tr	tr	tr	tr	tr	tr	tr	tr	tr	tr	tr	tr	tr	tr
Mnz	-	-	-	-	tr	-	-	-	-	-	-	-	-	-	-	-	tr
Ttn	-	tr	-	-	-	-	-	-	-	-	-	-	-	-	-	tr	-
Act	-	-	-	-	-	-	-	tr	tr	-	tr	-	-	-	-	-	-
Ep	tr	tr	-	-	tr	-	-	-	tr	-	-	-	-	-	tr	-	-
Chl	tr	tr	tr	-	tr	tr	-	-	tr	tr	tr	-	-	-	tr	-	-
Tur	-	-	-	-	-	-	-	-	tr	-	-	-	5.2	tr	-	-	-
Mag	-	tr	tr	1.6	tr	tr	-	tr	tr	tr	1.4	-	-	-	tr	-	-
Ilm	tr	-	tr	tr	-	tr	tr	tr	tr	tr	tr	tr	tr	-	tr	1.0	tr
Sul	tr	-	-	-	-	-	-	-	-	-	-	-	-	-	tr	-	-

[1]Average modes based on 1500 to 2000 points. [2]Sample H, the Hikage locality; Sample N, the Nai-in locality; Sample U, the Uchiyama locality; Sample Az, the Azamo locality. [3]Pl, plagioclase; Qtz, quartz; Kfs, K-feldspar; Bt, biotite; Hbl, hornblende; sum, the sum total of Pl, Qtz, Kfs, Bt, and Hbl; Cpx, clinopyroxene; Opx, orthopyroxene; Ap, apatite; Zrn, zircon; Mnz, monazite; Ttn, titanite; Act, actinolite; Ep, epidote; Chl, chlorite; Tur, toumaline; Mag, magnetite; Ilm, ilmenite; Sul, sulfide.
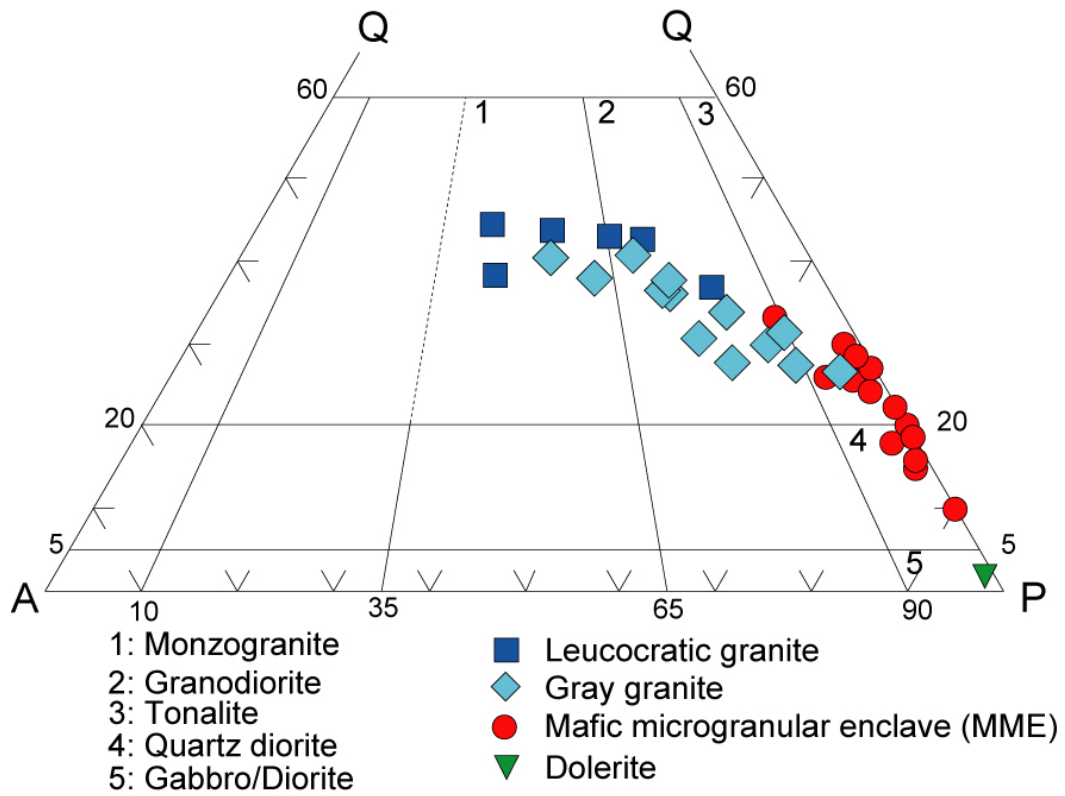
Figure 3.2. Quartz–alkali feldspar–plagioclase (Q–A–P plot) (Le Maitre *et al*., 2002) of the

Tsushima granites.
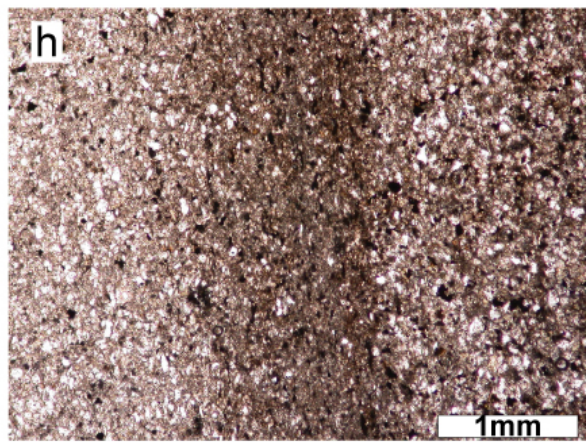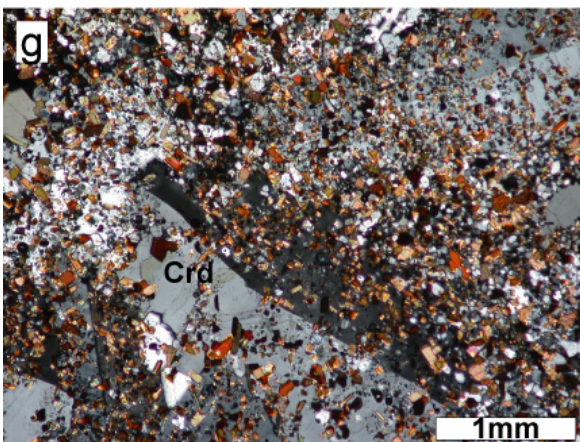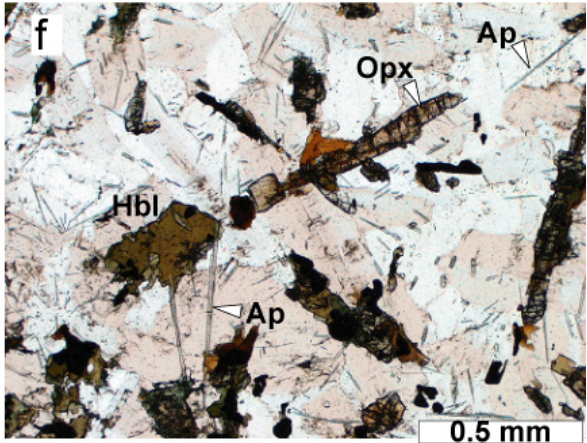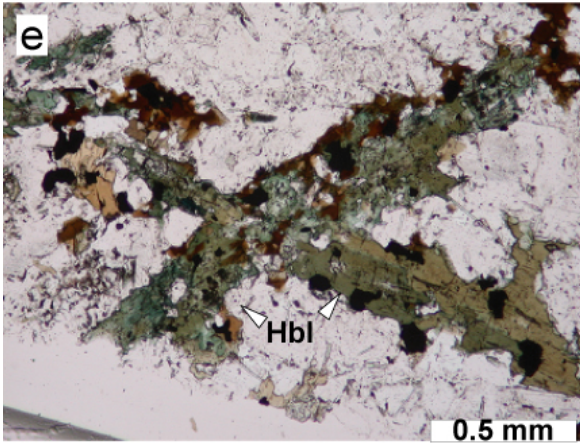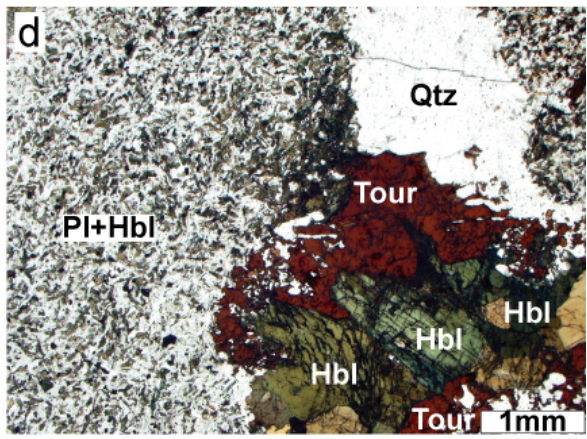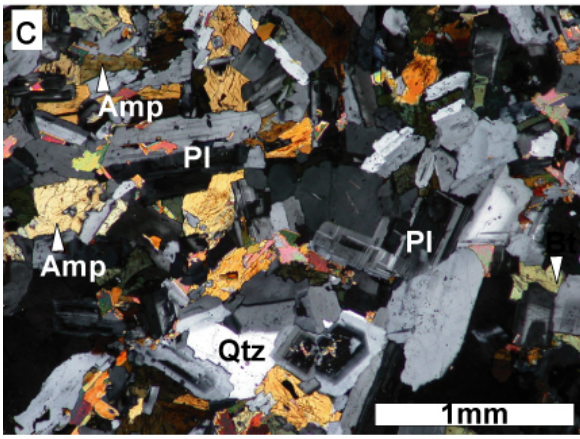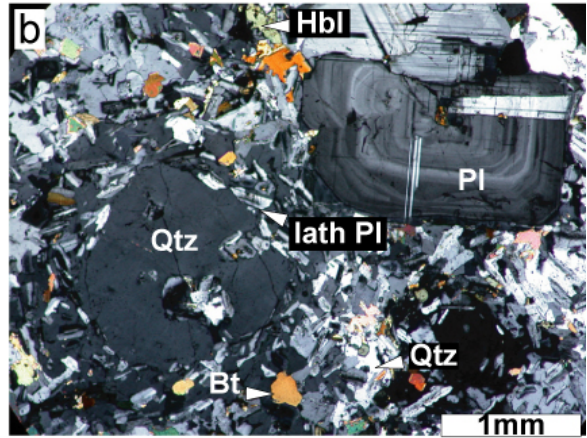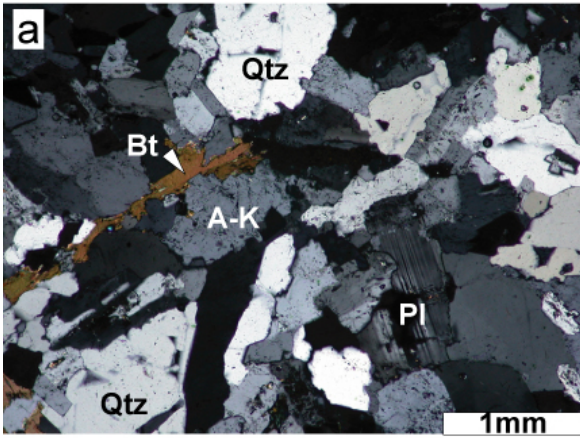
Figure 3.3. Photomicrographs of Tsushima granites under cross polarized light. (a) Fine-grained leucocratic granite from the Uchiyama locality. (b) Porphyritic gray granite with quartz and plagioclase phenocrysts from the Uchiyama locality. (c) Fine-grained equigranular MME from the Uchiyama locality. (d) Aggregate of quartz–hornblende–tourmaline in very fine grained MME from the Nai-in locality. (e) Two elongated hornblendes show crossed growth in MME from Uchiyama locality. (f) Acicular apatite and opx crystals in MME from Uchiyama locality. (g) Hornfels xenolith show large poikiloblastic cordierite with small biotite and quartz inclusions. (h) Sedimentary rock shows alternations of mudstone and sandstone. Abbreviations are the same as in Table 3.1. lath Pl – lath shaped plagioclase.

similar to that of the leucocratic granite, but the accessory minerals differ. Monazite and titanite are rare in the gray granite, whereas apatite, zircon, and magnetite are abundant. Phenocrysts (2–5 mm) comprise mainly quartz with a corrosion rim, zoned plagioclase, and microperthite. Biotite and alkali feldspar phenocrysts are rare. The fine-grained groundmass (0.2–1 mm) is composed of quartz, alkali feldspar, lath-shaped zoned plagioclase, biotite, hornblende, and Fe–Ti oxides (Figure 3.3b). The plagioclase shows complicated textures such as boxy cellular texture, oscillatory zoning with spike zones, or combinations of these textures within a crystal. Alkali feldspar rarely has a rapakivi texture with a plagioclase or corrosion rim. In the Hikage and Uchiyama localities, the texture gradually changes to resemble the texture of the leucocratic granite.

Local-scale mingling of the leucocratic granite with the gray granite or MMEs was often observed (Figure 3.1b, c). The mingled parts are elongated to form curved bands and/or schlieren (Figure 3.1b), suggesting that the viscosity contrast between the two magmas was small. The local-scale mingling is often characterized by the presence of miarolitic cavities in the leucocratic granite part. Such miarolitic cavities, up to 20 cm in diameter, are well preserved at the Nai-in locality (Figure 3.1g). The miarolitic cavities show zoned mineral assemblages of fine-grained quartz–alkali feldspar along the wall, amphibole–chlorite–epidote in the intermediate space, and tourmaline–quartz–zeolite in the center. These assemblages vary from place to place. At the Nai-in locality (N-4), a hornblende–tourmaline–zeolite part is well developed and is accompanied by magnetite, pyrrhotite, chalcopyrite, and galena. A chlorite–zoisite–zeolite assemblage was observed in the cavities at the Hikage locality.

The miarolitic cavities in both gray and leucocratic granites always include borosilicate minerals such as tourmaline. Tourmaline crystals, a few centimeters in size, are abundant in the miarolitic cavities and sometimes occur in the leucocratic granite.

20

Under the microscope, the tourmaline is brown and prismatic. It is schorl and often shows compositional zoning. Most zeolite is stilbite-Ca, and large euhedral crystals of chabazite, up to 15 mm in size, were also observed in miarolitic cavities at the Nai-in locality (Figure 3.1e).

Aplite and pegmatite dikes are very few in the Tsushima pluton. At the Hikage locality, the granite was intruded by 12 thin aplite dikes, from a few centimeters to 40 cm wide, dipping 70°–90° toward N50°–65°E. This orientation parallels the direction of the dominant fractures and joints in the granite body. The aplite dikes include many euhedral chlorite and titanite crystals in the center. Only a few aplite dikes transpose into pegmatite. A quartz vein in the same outcrop is composed of large euhedral quartz crystals, 5 to 10 cm in length, and is accompanied by minor biotite and apatite in the core, and fine-grained quartz and alkali feldspar in the few-centimeter-wide rim. A calcite vein was also observed at the Hikage locality.

3.2 Enclaves

Two types of enclaves, abundant MMEs and a very few metasedimentary xenoliths, are identified in the Tsushima pluton. The MMEs are extensively distributed throughout the pluton and usually form enclave swarms (e.g., Barbarin, 1991; Tobisch et al., 1997). The metasedimentary xenoliths are restricted to the marginal zones of the Hikage and Uchiyama localities, and their abundance is less than 1% of the observed enclaves.

The MMEs are black to dark-gray, rounded or ellipsoidal blobs in the granites, most commonly from 20 cm to 2 m in size (Figure 3.1a). Larger rectangular enclaves (up to 2 m × 5 m) were also observed in the Hikage locality. The common enclaves have a crenulated surface, chilled rim, and sharp or partly diffuse contact with the host leucocratic

granite or gray granite (Figure 3.1e). The grain size is usually 0.1 to 1.0 mm (rarely <0.1 mm; Na-4a sample) and is finer than that of the host granite. Several large grains of the host granite are often incorporated into the MMEs across the contact surfaces (Figure 3.1d, e). These MMEs generally have matrix minerals with finer grain size than those do not have large grains of host origin (Figure 3.1d). In addition, a net-vein structure, and compositional and grain-size variations such as felsic rims are sometimes observed in the MMEs.

The modal mineral composition of the MMEs ranges from quartz diorite to tonalite (Figure 3.2 and Table 3.1), and alkali feldspar is rare. Only one sample was granodioritic (U-4a sample Plagioclase occurs mostly as lath-shaped euhedral grains (0.1–0.7 mm long) with a zonal texture.

Plagioclase phenocrysts (2–5 mm in size) usually have oscillation, patch, or spike zonings, and recrystallized rims (Figure 3.3c). Quartz occurs mainly as small interstitial grains. Large grains of quartz are ovoid and sometimes rimmed by fine-grained biotite and/or hornblende (Figure 3.3d). Biotite exhibits ragged outlines and is sometimes altered to chlorite. The biotite content increases with decreasing SiO_2 content in the MME. Hornblende crystals are acicular, a few millimeters in long, and are sometimes replaced by biotite (Figure 3.3e). Biotite and hornblende rarely occur as phenocrysts. A large, 3-mm-long blade, of hornblende with biotite was observed at the Uchiyama locality. Small relicts of orthopyroxenes and clinopyroxenes are observed in aggregates of hornblende ± biotite. Apatite, zircon, ilmenite, and magnetite occur as accessory minerals. Apatite is abundant and forms acicular crystals up to 3 mm long with aspect ratios varying from 15:1 to 42:1 (Figure 3.3f), whereas apatite in the leucocratic granite forms stubby prismatic crystals with aspect ratios from 4:1 to 15:1. I inferred that crystallization started with opaque minerals and apatite, then continued through plagioclase, hornblende, and biotite,

and ended with quartz. Mineral clusters of quartz ± plagioclase ± biotite with embayed or corroded shapes are often observed in MMEs, which are rimmed by small hornblende and/or plagioclase crystals. Aggregates of fine-grained biotite were observed in MMEs at the Kuwa locality, and coarse-grained quartz–hornblende–tourmaline clusters occur in the MMEs at the Nai-in locality (N-4a) (Figure 3.3d).

Most of the sedimentary xenoliths observed at the Hikage and Uchiyama localities retain their original sedimentary structures of alternating sandstone and mudstone (Figure 3.1f, h). The xenoliths, which are up to 30 cm across, have an angular shape and a sharp contact with the host granites. They usually contain quartz, biotite, alkali feldspar, plagioclase, chlorite, cordierite, and amphibole. The metamorphic grade ranges from the albite–epidote hornfels facies to the pyroxene hornfels facies. Some xenoliths from the Hikage locality contain poikiloblastic cordierite with small biotite and quartz inclusions (Figure 3.3g). None of the metasedimentary xenoliths have traces of melting reaction.

3.3 Dolerites and Sedimentary rocks

Dolerite dikes of 2 to 5 m thick intruded into sedimentary rocks of the Taishu Group in the Komoda area, northeast of the pluton (Figure 2.1). Chilled margins and sedimentary xenoliths were observed within the dikes. The dolerites are composed mainly of olivine, orthopyroxene, clinopyroxene, plagioclase, and minor hornblende, apatite, and biotite. Secondary alteration minerals such as chlorite, calcite, and quartz were also observed. Sedimentary rocks were sampled from the lower Taishu Group. One sample (27-Hi sample) was collected from near Pb–Zn ore deposits. The samples consist of mudstone and alternations of mudstone and sandstone.

4. PETROLOGICAL AND GEOCHEMICAL METHOD

4.1 Sampling and Observation

Procedures of laboratory studies are illustrated in Figure 4.1. The laboratory studies were conducted in two ways; thin-section based microscopic observation, mineral major compositions and fluid inclusion analysis, and chemical analyses on powdered samples, including whole-rock major, trace, and isotopic compositions and. About 70 rock samples of the granites, sediementary rocks, and dolerites were sampled from described outcrops in the Tsushima islands. The samples were taken from the freshest part available at each sampling site. In one outcrop, a pair of granite and MME was collected to examine chemical diversity and textural variation.

Microscopic observation was conducted with polished thin section of 0.03-0.05 mm thick for modal analysis. Counting number for each thin section are about 2,000 points for granites and 1,500 points for MMEs. Mineral major element compositions were determined with electron microprobe analyzer (EPMA). Fluid inclusions were observed with doubly polished thick section (0.2-0.5mm thick). The solid melting temperatures and homogenization temperatures were measured on a Linkam stage THMGS 600.

4.2 Sample preparation and Chemical Analysis

The collected rock samples were dried in an oven at $90^{o}C$ for 1 day and crushed to <1 cm in size in a steel-plated jaw crusher. About 100g of the crushed rocks were then pulverized in a tungsten carbide vessel using HERZOG HSM36 for whole-rock chemical analysis (Nakano and Ito, 1990).

For 34 rock samples of the Tsushima granites, major-element and trace-element compositions and Sr, Nd, and Pb isotopic ratios were analyzed by X-ray fluorescence
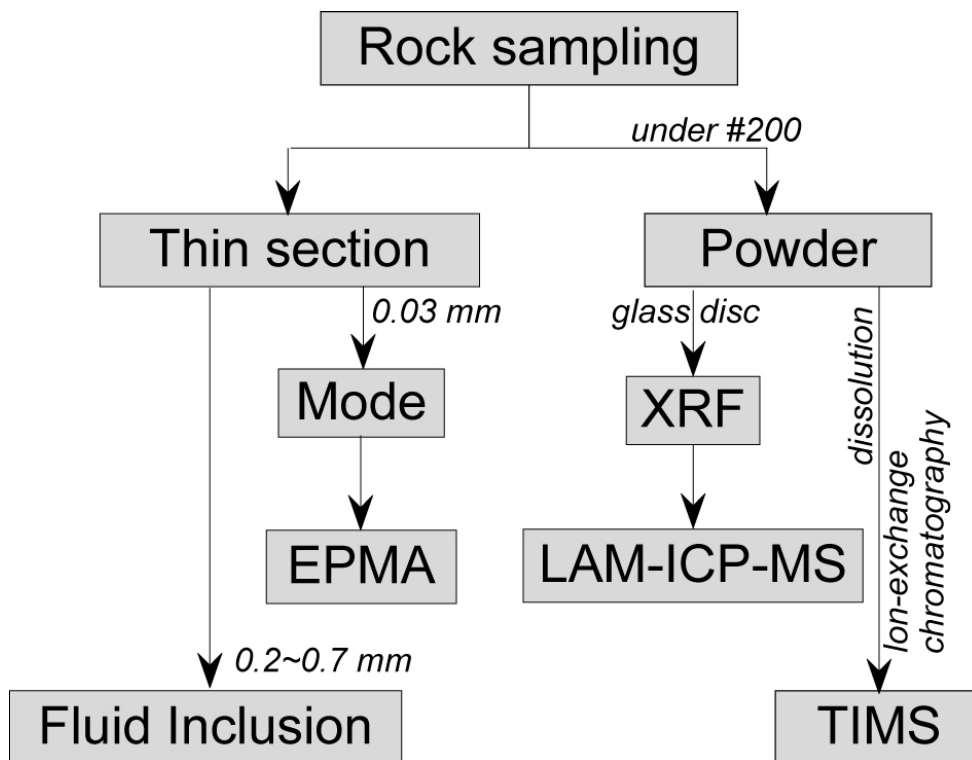
Figure 4.1. The flow chart of research procedures for this study

spectrometry (XRF), laser ablation microprobe-inductively coupled plasma-mass spectrometry (LAM-ICP-MS), and thermal ionization mass spectrometer (TIMS), respectively. The same procedure was applied for the samples of the other Outer Zone granite for the analysis of trace-elements and Sr, Nd, and Pb isotopic ratios by LAM-ICP-MS and TIMS.

XRF analyses were performed on pressed powder pellets using Philips PW1404 X-ray Fluorescence Spectrometer at the Institute of Geoscience, University of Tsukuba. An accuracy of the XRF analyses for element with concentration above 1 wt.% is better than ±3% relative difference (Nakano et al., 1997).

LAM-ICP-MS analyses were carried out on fused lithium-borate glass discs using a Perkin-Elmer Sciex ELAN 6000 ICP-MS and a Q-switched Nd:YAG laser with a wavelength of 266 nm at the Venture Business Laboratory, University of Tsukuba (Kurosawa et al., 2002). The glass discs were prepared with a conventional XRF fusion technique by mixing 2.00 g of the powdered sample with 4.00 g of a lithium tetra-borate. Twenty-nine isotopes (elements) were measured and the quantification was performed by using single-standard internal calibration method. In the isotopes, ^{42}Ca was used as an internal standard because Ca is a good internal standard for the quantification of REE, Zr, Hf, Th and U in minerals and glasses. The concentrations of the internal standards for the rock samples were determined by XRF before the LAM-ICP-MS analyses. For the external standard, the fused-lithium bead of NIST-SRM 610 reference glass material was used. The reference element concentrations of the SRM 610 glass were selected from the preferred values of Pearce et al. (1997). For the present measurement conditions, a precision is 1–5% relative and accuracy for element with concentration above 1 ppm is better than ±10% relative difference.

Isotopic rations of Sr, Nd, and Pb were determined using a Finnigan Mat 262

RPQ multicollector mass spectrometer at the Institute of Geoscience, University of Tsukuba (Na et al., 1995). Approximately 100 mg of each powder sample was completely dissolved in a mixed acid of HF (1.0ml), HNO_3 (0.7ml), and $HClO_4$ (0.2ml). Isolation of Sr, Nd, and Pb were made using a conventional ion-exchange chromatography (Figure 4.2).

The measured $^{87}Sr/^{86}Sr$ and $^{143}Nd/^{144}Nd$ ratios were normalized to $^{86}Sr/^{88}Sr = 0.1194$ and $^{146}Nd/^{144}Nd = 0.7219$, respectively. The $^{86}Sr/^{88}Sr$ value of the NIST SRM 987 reference material throughout the analyses was 0.710247 ± 0.000014 (2σ, n = 8). The $^{143}Nd/^{144}Nd$ ratio of the La Jolla reference material was 0.511856 ± 0.000016 (2σ, n = 14). Precision for the present analyses was better than ±0.000028 (2σ) for $^{87}Sr/^{86}Sr$ and ±0.00002 (2σ) for $^{143}Nd/^{144}Nd$. The Pb isotope ratios were normalized to NIST SRM 981 values ($^{206}Pb/^{204}Pb = 16.9390$, $^{207}Pb/^{204}Pb = 15.4963$, $^{208}Pb/^{204}Pb = 36.7206$). The mean values of NIST SRM 981 throughout this study (n = 26) were $^{206}Pb/^{204}Pb = 16.889 \pm 0.013$ (2σ), $^{207}Pb/^{204}Pb = 15.454 \pm 0.017$ (2σ), and $^{208}Pb/^{204}Pb = 36.603 \pm 0.033$ (2σ).
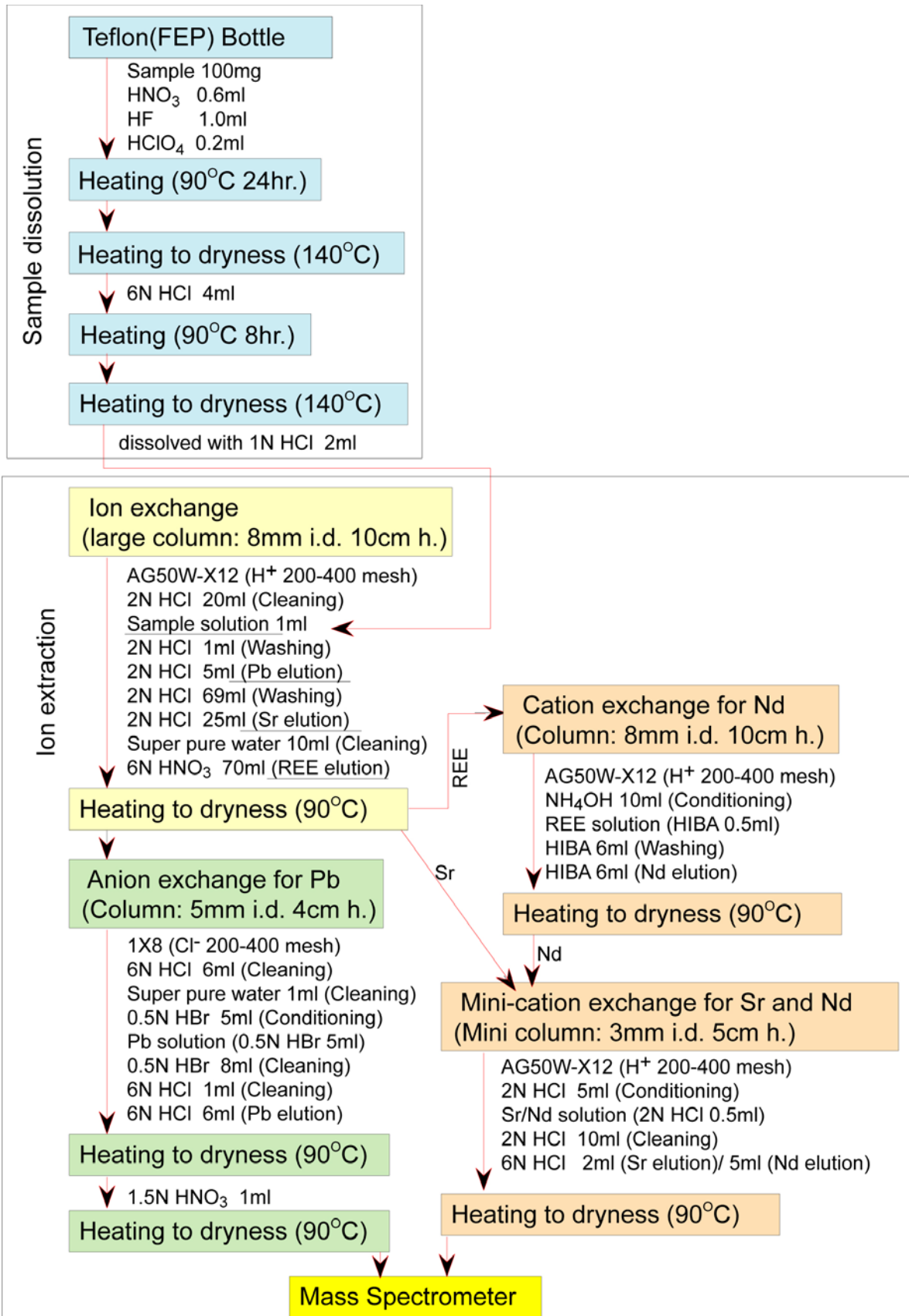
Figure 4.2. Rock dissolution and ion extraction procedure for isotopic analysis.

5. RESULTS

5.1 Mineral chemistry

Plagioclase phenocrysts in the gray granite had $An_{36-52}Ab_{46-63}Or_{1-2}$ (An, anorthite; Ab, albite; Or, orthoclase) compositions (Table 5.1). The CaO content generally increased from core to rim, with the highest content in a spike zone. Small, lath-shaped plagioclases in the MMEs had $An_{23-30}Ab_{70-74}Or_{0-1}$ compositions. Biotite in the gray granites had a Mg/(Fe+Mg) ratio of 0.45 to 0.59 and was relatively poor in Al_2O_3 (12.6 wt. %) (Table 5.1). These data agree with those for granodiorite reported by Ishihara and Imai (2000).

Amphiboles were abundant in the gray granite and the MMEs, occurring mainly as a magnesiohornblende with small amounts of actinolitic hornblende (Table 5.1 and Figure 5.1) (Leake *et al.*, 1997). Mg/(Fe+Mg) ratios of hornblende from the MMEs ranged from 0.5 to 0.6, whereas those from the gray granite were relatively lower, about 0.4 to 0.5. Neither hornblende amphibole was very aluminous (4.5–6.8 wt. % Al_2O_3), suggesting crystallization at low pressure. A few amphiboles plot in the actinolitic hornblende field (Figure 5.1), and their compositions agree with those of actinolitic hornblende reported by Ikemi et al. (2000). The actinolitic hornblende may have formed by alteration and re-equilibration of the primary magnesiohornblende at subsolidus temperatures, because the composition coincides with the breakdown composition of Ca-Al^{VI}-rich amphiboles (Giret *et al.*, 1980). Rarely, cummingtonite was observed in MMEs from the Uchiyama locality (Table 5.1). The chemical composition of most amphiboles in the miarolitic cavities of the leucocratic granite was the same as that of the hornblende in the MMEs.

Orthopyroxenes in the MMEs had Mg/(Fe+Mg) ratios of 0.48 to 0.52 (Table 5.1 and Figure 5.2). The wollastonite component was lower than 4 mol %. Clinopyroxenes were relatively rare in the MMEs, and their composition corresponded to augite (Figure

29

Table 5.1 Representative electron microprobe analyses for rock-forming minerals from the Tsushima granites.

Rock	Plagioclase							Biotite		
	Gray Gr[*1]		MME					Gray Gr		
Sample	U-9ch-1		Aza-1		H-1a	N-4a-3		U-3c-4		
	core	rim	core	rim	middle	middle			core	rim
SiO$_2$[*2]	58.45	57.38	56.07	54.65	60.98	61.26	SiO$_2$	36.69	36.33
TiO$_2$	-	-	-	-	-	-	TiO$_2$	4.15	4.03
Al$_2$O$_3$	25.42	25.31	26	28.34	24.54	23.04	Al$_2$O$_3$	12.55	12.61
Cr$_2$O$_3$	-	-	-	-	-	-	Cr$_2$O$_3$	-	-
FeO	-	0.14	0.21	0.41	0.36	0.28	FeO	21.59	21.62
MnO	-	-	-	-	-	-	MnO	0.26	0.2
MgO	-	-	-	-	-	-	MgO	10.32	10.49
CaO	7.38	7.79	9.02	10.66	6.12	4.77	CaO	-	-
Na$_2$O	7.07	6.05	6.15	5.22	8.08	8.47	Na$_2$O	-	-
K$_2$O	0.27	0.29	0.24	0.22	-	0.13	K$_2$O	9.51	9.39
Total	98.59	96.96	97.68	99.49	100.08	97.95	Total	95.07	94.67
T-site							*Z-site*		
Si[*3]	2.645	2.638	2.577	2.479	2.710	2.771	Si	5.703	5.673
Al	1.355	1.362	1.408	1.515	1.285	1.228	Al	2.297	2.321
(sum)	4.000	4.000	3.986	3.994	3.995	3.999	(sum)	8.000	7.994
M-site							*Y-site*		
Al	0.001	0.009	0.000	0.000	0.000	0.000	Al	0.002	0.000
Cr	0.000	0.000	0.000	0.000	0.000	0.000	Cr	0.000	0.000
Ti	0.000	0.000	0.000	0.000	0.000	0.000	Ti	0.485	0.473
Fe	0.000	0.005	0.008	0.016	0.013	0.011	Fe	2.806	2.823
Mn	0.000	0.000	0.000	0.000	0.000	0.000	Mn	0.034	0.026
Mg	0.000	0.000	0.000	0.000	0.000	0.000	Mg	2.392	2.442
K	0.016	0.017	0.014	0.012	0.000	0.007	(sum)	5.719	5.765
Na	0.620	0.539	0.548	0.459	0.696	0.743	*X-site*		
Ca	0.358	0.384	0.444	0.518	0.291	0.231	K	1.886	1.870
(sum)	0.995	0.955	1.014	1.005	1.001	0.992	Na	0.000	0.000
							Ca	0.000	0.000
							(sum)	1.886	1.870

Note: *1 Gray Gr, gray granite; MME, mafic microgranular enclave. *2 Compositions are quoted in weight %. Total Fe as FeO. *3 Structural formulae, in atoms per formula unit. Calculated on a basis 8 oxygen for plagioclase, 22 oxygen for biotite, 23 oxygen for hornblende and cummingtonite, and 6 oxygen for enstatite and diopside. -; no detection

Table 5.2 (continued)

	Hornblende								Cummingtonite
	Gray Gr[*1]				MME				Gray Gr
	U-3c-3		Aza-5-2		U-6a-10	N-4a-1c	N-4a-4		U-9-2
	core	rim	core	rim	rim	core	core	rim	core
SiO_2[*2]	47.91	46.54	45.64	47.64	47.06	47.59	48.55	47.05	52.74
TiO_2	1.15	1.46	0.74	1.09	1.17	1.2	0.81	1.14	-
Al_2O_3	5.51	5.97	6.75	5.77	5.08	5.84	4.51	5.92	0.26
Cr_2O_3	-	-	-	-	-	-	-	-	-
FeO	18.63	18.5	22.6	18.11	17.44	20.13	16.18	16.41	28.27
MnO	0.74	0.64	0.35	0.26	0.37	0.36	0.29	0.24	1.93
MgO	11.31	10.71	8.07	11.36	11.32	10.24	12.87	12.64	12.97
CaO	10.67	10.57	11.03	11.02	13.76	10.72	10.98	10.88	0.98
Na_2O	1.2	1.53	1.11	0.99	0.87	1.29	1.14	1.41	-
K_2O	0.54	0.69	0.88	0.75	0.61	0.69	0.52	0.83	-
Total	97.66	96.61	97.15	96.98	97.68	98.06	95.85	96.52	97.15
T-site									
Si[*3]	7.188	7.086	7.045	7.178	7.093	7.159	7.325	7.091	8.002
Al	0.812	0.914	0.955	0.822	0.902	0.841	0.675	0.909	0.000
(sum)	8.000	8.000	8.000	8.000	7.995	8.000	8.000	8.000	8.002
B-site									
Mg	0.253	0.194	0.179	0.190	0.000	0.205	0.191	0.211	1.814
Ca	1.715	1.724	1.823	1.780	2.222	1.728	1.775	1.757	0.159
(sum)	1.969	1.918	2.003	1.970	2.222	1.933	1.966	1.968	1.974
C-site									
Mg	2.276	2.237	1.678	2.360	2.543	2.091	2.703	2.629	1.119
Ti	0.130	0.167	0.085	0.123	0.133	0.136	0.092	0.129	0.000
Al	0.163	0.158	0.274	0.202	0.000	0.195	0.126	0.143	0.046
Cr	0.000	0.000	0.000	0.000	0.000	0.000	0.000	0.000	0.000
Fe	2.337	2.355	2.917	2.282	2.198	2.532	2.041	2.068	3.586
Mn	0.094	0.083	0.045	0.033	0.047	0.046	0.037	0.031	0.248
(sum)	5.000	5.000	5.000	5.000	4.921	5.000	5.000	5.000	5.000
A-site									
K	0.103	0.134	0.173	0.144	0.117	0.132	0.100	0.160	0.000
Na	0.349	0.452	0.333	0.290	0.254	0.376	0.333	0.412	0.000
(sum)	0.452	0.586	0.505	0.434	0.371	0.509	0.434	0.572	0.000

Table 5.1 (continued)

Rock	Enstatite							Augite					
	MME[*1]							MME					
Sample	U-5a-2	U-5a-6		U-6a-7		U-6a-8		U-5a-1		U-5a-3	U-5a-4	U-6a-6	
	core	core	rim	core	rim	core	rim	core	rim	core	core	core	rim
SiO_2[*2]	49.76	50.98	51.16	50.76	51.84	51.65	50.13	49.53	50.12	50.49	50.76	52.98	52.69
TiO_2	-	0.26	-	0.21	0.22	-	-	0.79	0.69	0.66	0.54	0.11	-
Al_2O_3	0.61	0.83	0.62	0.48	0.7	0.15	1.06	3.29	2.88	2.56	2.44	0.46	0.48
Cr_2O_3	-	-	-	-	-	-	-	-	-	-	-	-	-
FeO	31.56	30.07	30.85	30.18	28.75	31.98	31.41	13.01	12.61	13.26	12.56	13.15	13.67
MnO	1.28	0.98	1.07	1.07	1.03	1.21	0.96	0.41	0.43	0.43	0.47	0.45	0.59
MgO	13.66	15.09	14.93	16.29	16.01	14.74	15.28	11.62	12.24	11.34	11.74	11.88	11.99
CaO	1.16	1.68	1.47	1.06	2.39	1.09	0.92	19.17	19.17	18.77	20.04	21.64	21.01
Na_2O	-	-	-	-	-	-	-	0.79	0.65	0.54	0.62	0.24	0.24
K_2O	-	-	-	-	-	-	-	-	-	0.24	0.1	-	-
Total	98.03	99.89	100.1	100.05	100.94	100.82	99.76	98.61	98.79	98.29	99.27	100.91	100.65
T-site													
Si[*3]	1.995	1.985	1.994	1.974	1.986	2.006	1.966	1.906	1.919	1.946	1.938	1.994	1.991
Al	0.005	0.015	0.006	0.022	0.014	0.000	0.034	0.094	0.081	0.054	0.062	0.006	0.009
(sum)	2.000	2.000	2.000	1.996	2.000	2.006	2.000	2.000	2.000	2.000	2.000	2.000	2.000
M1-site													
Al	0.023	0.023	0.022	0.000	0.018	0.007	0.015	0.055	0.049	0.063	0.047	0.014	0.012
Cr	0.000	0.000	0.000	0.000	0.000	0.000	0.000	0.000	0.000	0.000	0.000	0.000	0.000
Ti	0.000	0.008	0.000	0.006	0.006	0.000	0.000	0.023	0.020	0.019	0.016	0.003	0.000
Mg	0.816	0.876	0.867	0.945	0.915	0.854	0.893	0.667	0.699	0.652	0.668	0.666	0.675
Fe^{3+}	0.151	0.081	0.102	0.061	0.053	0.124	0.101	0.281	0.252	0.269	0.286	0.318	0.319
(sum)	0.991	0.988	0.992	1.012	0.992	0.984	1.009	1.026	1.020	1.002	1.017	1.002	1.007
M2-site													
Ca	0.050	0.070	0.061	0.044	0.098	0.045	0.039	0.790	0.786	0.775	0.820	0.872	0.851
Fe^{2+}	0.907	0.898	0.903	0.921	0.868	0.915	0.929	0.137	0.151	0.159	0.115	0.096	0.113
Mg	0.000	0.000	0.000	0.000	0.000	0.000	0.000	0.000	0.000	0.000	0.000	0.000	0.000
Mn	0.043	0.032	0.035	0.035	0.033	0.040	0.032	0.013	0.014	0.014	0.015	0.014	0.019
K	0.000	0.000	0.000	0.000	0.000	0.000	0.000	0.000	0.000	0.012	0.005	0.000	0.000
Na	0.000	0.000	0.000	0.000	0.000	0.000	0.000	0.059	0.048	0.040	0.046	0.018	0.017
(sum)	1.000	1.000	1.000	1.000	1.000	1.000	1.000	1.000	1.000	1.000	1.000	1.000	1.000
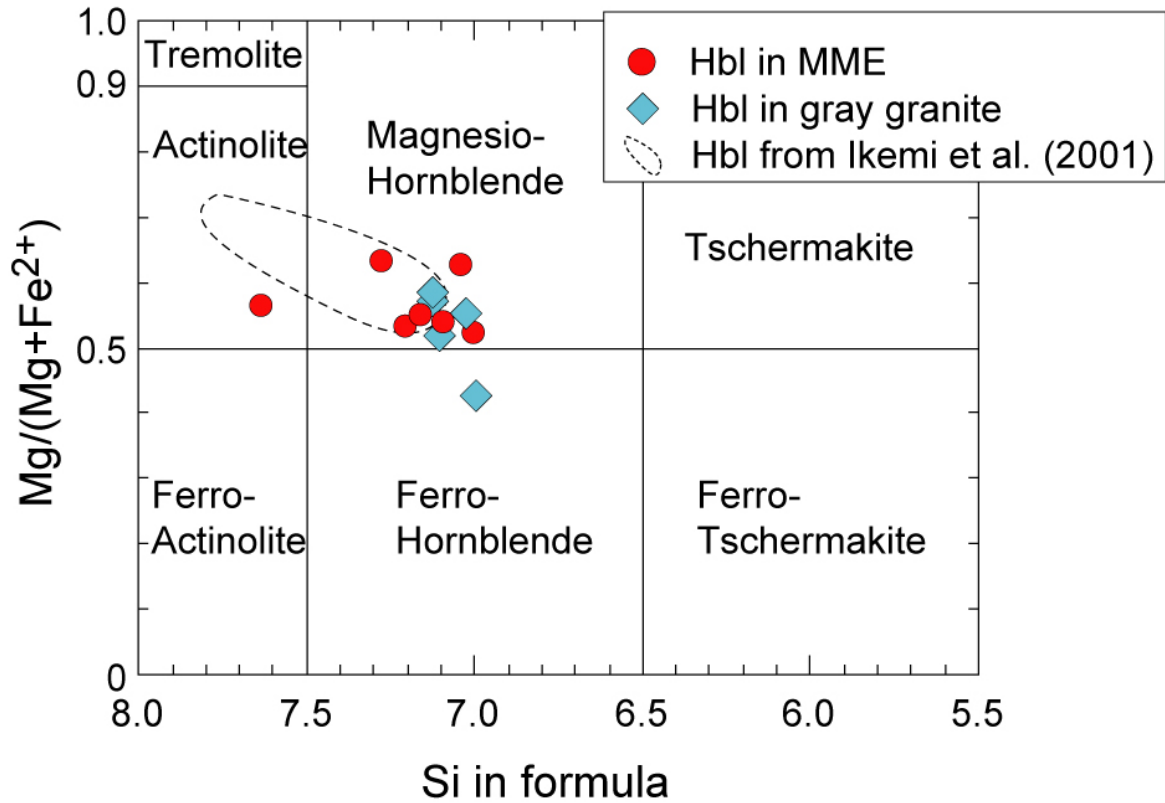
Figure 5.1. Classification of calcic amphiboles in the Tsushima granites according to $Mg/(Mg+Fe^{+2})$ vs. Si^{IV} (Leake et al., 1997)
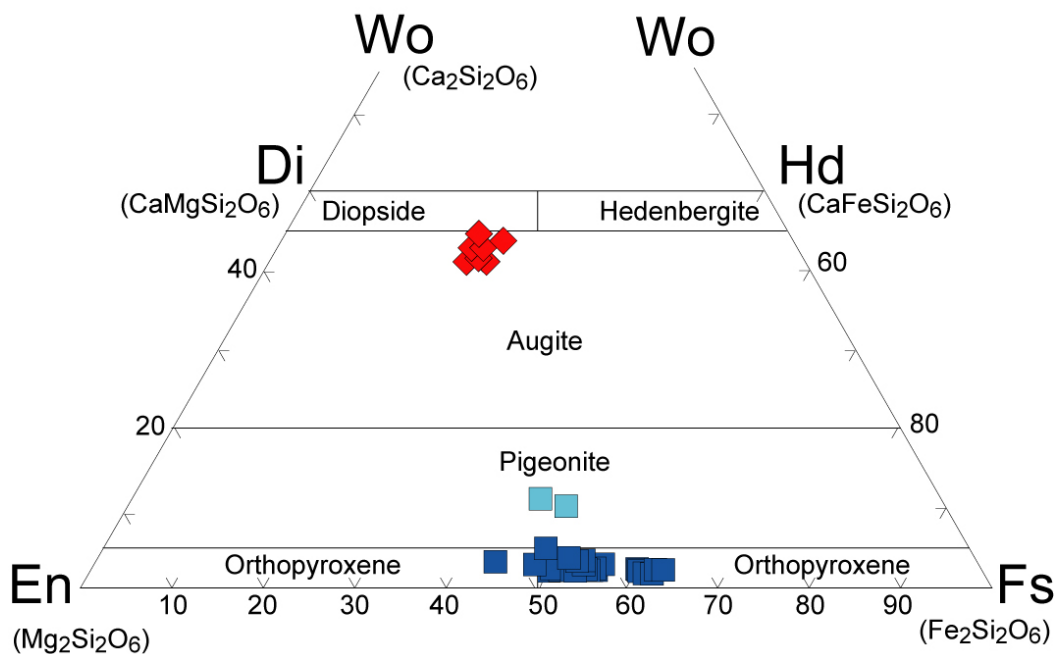
Figure 5.2 Ca-Mg-Fe plot of the analyzed pyroxenes from the MMEs in the Tsushima granites

5.2). I consider these pyroxenes to be early crystallized minerals in a highly undercooling mafic magma because of their relatively evolved Mg/(Fe+Mg) ratios and petrographic occurrence (Figure 3.3).

5.2 Major element compositions of whole rocks

Representative major-element compositions are listed in Table 5.2. The leucocratic granite samples range from 74 to 77 wt.% SiO_2, and the gray granite contain relatively less SiO_2 from 65 to 75 wt.%. Most MMEs have SiO_2 content below 55 wt.% and MgO content above 3 wt.%. Some less mafic MMEs have 61 to 68 wt.% SiO_2 and 1 to 3 wt.% MgO.

Correlations between SiO_2 and major oxides in the TSUG were good ($r^2 > 0.9$). With increasing SiO_2 content, the contents of Al_2O_3, Fe_2O_3, TiO_2, CaO, MgO, MnO and P_2O_5 decreased, whereas the K_2O content increased. The Na_2O content is relatively variable. The dolerite falls outside these trends (Figure 5.3).

In total alkali versus SiO_2 (TAS) and FeO^T/MgO versus SiO_2 diagrams, the Tsushima granites fall into the sub-alkaline and the calc-alkaline fields, respectively (Figure 5.4a, b). The molar ratios of Al_2O_3/(CaO+Na_2O+K_2O) (ASI) range from 0.79 to 1.06 for the MMEs, from 0.88 to 1.12 for the gray granite, and from 0.98 to 1.08 for the leucocratic granite (Table 5.2). Only a few gray granite samples showed high ASI values of 1.2. These values range from metaluminous to slightly peraluminous, except for some of the gray granite. (Figure 5.4c). The low ASI value is consistent with the rarity of metasedimentary xenoliths in the Tsushima pluton.

5.3 Trace-element chemistry of whole rock

Representative trace-element and rare earth element (REE) contents are listed in Table 5.2.

Table 5.2 Chemical compositions of the Tsushima granites, dolerite, and sedimentary rocks.

Sample	Mafic Microgranular Enclave									Gray Granite		
	H-3a	U-8a	N-4a	H-2a	H-2b	H-3b	U-6a	U-2b	U-4a	Aza-5	H-3c	N-2
SiO_2*[1]	54.81	54.97	56.86	61.18	61.89	61.26	62.57	68.13	67.61	67.38	66.91	67.07
TiO_2	1.30	1.08	1.41	1.01	0.99	1.03	1.09	0.65	0.68	0.72	0.83	0.79
Al_2O_3	16.66	16.25	16.17	15.74	15.67	16.01	15.48	14.57	15.26	14.89	15.01	15.65
Fe_2O_3	10.47	10.08	9.18	6.85	6.63	7.59	7.08	4.09	4.41	4.11	4.72	3.67
MnO	0.12	0.17	0.09	0.11	0.11	0.16	0.13	0.09	0.03	0.05	0.06	0.02
MgO	3.56	3.16	3.32	3.02	2.92	2.88	1.96	1.18	1.18	1.43	1.66	1.44
CaO	5.56	5.89	6.01	5.58	5.57	6.12	5.19	2.73	2.96	3.25	3.8	3.31
Na_2O	4.01	4.64	4.90	3.61	3.75	3.38	3.24	3.43	4.89	4.80	2.97	2.93
K_2O	2.29	2.00	1.40	1.91	1.99	1.43	1.75	2.83	2.13	2.93	3.01	2.82
P_2O_5	0.21	0.17	0.24	0.15	0.22	0.18	0.18	0.12	0.15	0.13	0.19	0.14
LOI	0.49	0.49	0.42	0.32	0.32	0.65	0.49	0.65	0.32	0.49	0.65	0.49
Total	99.47	98.88	99.99	99.47	100.05	100.69	99.16	98.44	99.63	100.17	99.81	98.33
Ba*[2]	272	261	169	324	346	267	436	560	340	714	619	638
Rb	245	225	107	129	126	88.5	64	128	133	81.8	147	112
Sr	195	190	183	241	251	281	240	164	155	210	230	215
Cs	18.3	22.7	4.35	7.4	7.03	5.51	3.46	8.21	7.93	2.5	8.07	3.94
Ta	0.41	0.6	0.81	0.8	0.79	0.44	1.09	0.91	1.16	0.78	0.66	1
Nb	6.2	7.85	16.3	8.85	7.34	4.52	14.8	9.28	11.4	7.88	7.87	9.94
Hf	2.35	3.38	3.38	3.35	3.44	2.81	4.11	4.79	4.77	4.73	5.51	5.74
Zr	86	129	130	122	131	103	150	174	185	175	227	220
Y	46.6	44.2	70.2	48.6	38	26.1	75.6	26.4	41.5	32.8	20.4	16
Th	2.96	4.88	4.11	7.32	8.01	5	9.18	7.89	2.07	9.12	3.95	10.3
U	1.22	1.51	1.41	1.71	1.67	1.59	2.25	1.7	3	2.04	1.1	2.66
Sc	29.1	26.7	20.2	20.3	20	22.8	24.9	13.6	15.7	14.8	13.5	15.9
Pb	12.4	5.25	1.19	15.7	15.9	6.23	15.4	7.72	4.4	7.87	7.49	5.85
La	8.77	19.6	45	26.7	24.2	16.9	25	16.5	32.4	15.8	17.4	10.7
Ce	21.6	54.4	93.3	67.6	56.2	35.6	57	32.1	64.7	36.6	34.3	20.7
Pr	3.09	7.25	11.1	8.71	7.13	4.27	7.65	3.71	7.47	5	3.92	2.5
Nd	15.4	32.7	49.6	38.3	30.3	18.7	35.8	16.1	31.1	23.6	17	11.4
Sm	5.36	8.1	12.2	9.14	6.65	4.3	10	3.9	7.02	6.19	3.87	2.6
Eu	1.09	1.31	1.45	1.48	1.39	1.29	1.51	1.14	1.17	1.37	1.4	1.17
Gd	6.12	7.47	11.7	8.15	6.22	4.34	10.2	3.92	6.59	5.51	3.64	2.6
Tb	1.2	1.32	2.01	1.39	1.09	0.75	1.95	0.7	1.12	0.96	0.59	0.42
Dy	8.52	8.34	12.9	8.81	6.74	4.65	12.8	4.47	7.15	5.93	3.68	2.58
Ho	1.8	1.73	2.72	1.86	1.42	0.97	2.79	0.98	1.5	1.26	0.77	0.56
Er	5.11	4.9	7.73	5.16	4.07	2.7	7.76	2.75	4.22	3.45	2.09	1.55
Tm	0.8	0.75	1.17	0.73	0.61	0.41	1.15	0.42	0.62	0.52	0.33	0.25
Yb	6.17	5.39	8.47	5.33	4.35	3	8.07	3.03	4.2	3.6	2.29	1.69
Lu	0.87	0.77	1.17	0.75	0.6	0.43	1.07	0.46	0.63	0.52	0.35	0.28
ASI*[3]	0.87	0.79	0.79	0.87	0.85	0.88	0.93	1.07	0.97	0.88	1	1.13
ZST*[4]	683	700	702	722	726	711	753	791	782	763	803	816

Note: *1 Compositions are quoted in weight %. Total Fe as Fe_2O_3. LOI: loss of ignition above 200˚C.

*2 Concentrations are in weight ppm. *3 ASI: molar $Al_2O_3/(Na_2O+K_2O+CaO)$. *4 ZST: zircon saturation temperature (˚C) based on Miller et al. (2003).

Table 5.2 (continued)

Sample	Gray Granite										Leucocratic Granite	
	N-4b	N-4c	K-1c	U-1a	U-1c	U-4b	U-6b	U-8b	U-8c	U-9	H-2c	U-1d
SiO_2*[1]	65.45	71.1	72.92	70.51	72.00	68.13	74.88	73.54	73.95	66.96	74.86	75.83
TiO_2	0.77	0.52	0.45	0.51	0.5	0.71	0.34	0.27	0.28	0.68	0.29	0.21
Al_2O_3	15.18	13.84	13.89	14.63	14.46	15.02	13.05	13.25	13.6	15.32	13.55	13.34
Fe_2O_3	5.48	3.2	2.54	3.36	2.51	4.39	1.91	1.99	1.94	4.26	2.01	1.08
MnO	0.03	0.02	0.01	0.04	0.04	0.03	0.02	0.03	0.03	0.09	0.02	0.01
MgO	1.41	0.86	0.93	0.92	0.86	1.22	0.48	0.32	0.37	1.3	0.36	0.25
CaO	3.63	2.28	2.56	2.43	2.36	2.7	1.39	1.52	1.6	3.52	1.75	1.22
Na_2O	3.25	2.46	3.18	2.32	3.45	3.93	2.37	2.88	2.59	3.35	3.34	2.78
K_2O	3.38	3.97	1.39	3.27	3.16	2.77	4.54	4.46	4.4	2.71	3.98	5.05
P_2O_5	0.14	0.07	0.09	0.11	0.08	0.11	0.07	0.07	0.04	0.1	0.1	0.05
LOI	0.49	0.32	0.49	0.49	0.51	0.49	0.49	0.65	0.65	0.81	0.65	0.39
Total	99.2	98.64	98.45	98.57	99.93	99.49	99.53	98.96	99.43	99.11	100.88	100.2
Ba*[2]	648	743	334	615	645	441	751	881	770	646	892	939
Rb	139	104	56	178	154	159	104	130	136	152	105	127
Sr	220	107	174	143	138	154	121	128	114	216	140	96.1
Cs	5.68	2.94	0.87	11.7	6.94	9.19	2.17	4.73	4.94	10.8	3.32	3.34
Ta	0.88	0.66	0.87	1.1	1.18	1.03	0.8	0.9	0.88	0.7	0.93	1.03
Nb	8.86	5.76	6.79	11	11.6	12.2	5.63	6.35	7.03	8.55	7.16	7.15
Hf	5.55	5.25	5.41	5.08	5.22	4.95	5.22	4.08	4.34	5.73	4.7	4.28
Zr	216	200	195	186	183	195	172	131	136	226	157	119
Y	22.4	10.3	21.8	32.2	39.4	38.4	22	19.9	22.5	22.9	23	39.4
Th	9.35	9.52	12.3	11.7	12.8	10.7	12.9	14.3	14.8	10.2	14.3	16.9
U	2.43	2.3	2.48	2.72	2.82	2.35	1.96	3.22	3.25	1.38	3.42	2.4
Sc	16.3	11.2	10.5	12.1	12.5	13.3	8.53	7.68	8.16	12.9	8.71	7.98
Pb	5.4	3.76	6.67	10.2	9.41	5.1	8.99	10.9	14.1	7.08	6.95	11.3
La	49.9	8.27	43.3	27.5	43.7	43.9	28.8	26.9	21	36.2	9.88	33.8
Ce	90.2	14.6	86	52.8	81.8	88.2	52.6	50.8	38.9	67.3	16.7	63.5
Pr	9.15	1.74	9.61	5.81	8.77	9.71	5.91	5.39	4.21	7.1	1.82	6.96
Nd	33.5	7.52	38.3	23.6	34.5	38.2	23.2	21.1	16.7	28	7.78	26.9
Sm	5.66	1.73	7.68	5.01	6.75	7.62	4.63	4.17	3.67	5.32	2.08	5.78
Eu	1.45	1.07	1.27	1.13	1.12	1.18	1.06	0.92	0.97	1.61	1.07	0.83
Gd	4.37	1.77	5.78	4.69	5.91	6.68	3.97	3.51	3.47	4.14	2.41	5.25
Tb	0.69	0.27	0.81	0.83	1.03	1.1	0.64	0.57	0.6	0.69	0.49	0.98
Dy	4.08	1.75	4.33	5.47	6.5	6.68	3.94	3.45	3.7	4.16	3.41	6.67
Ho	0.84	0.39	0.83	1.17	1.46	1.42	0.8	0.72	0.81	0.86	0.81	1.44
Er	2.37	1.13	2.25	3.39	4.07	3.88	2.35	2.01	2.34	2.28	2.45	4.41
Tm	0.36	0.18	0.34	0.51	0.62	0.56	0.35	0.31	0.35	0.35	0.38	0.63
Yb	2.67	1.24	2.48	3.79	4.64	4	2.33	2.16	2.46	2.47	2.84	4.53
Lu	0.38	0.22	0.36	0.55	0.66	0.56	0.37	0.31	0.37	0.39	0.41	0.65
ASI*[3]	0.97	1.11	1.22	1.24	1.08	1.05	1.15	1.08	1.14	1.03	1.04	1.09
ZST*[4]	795	811	823	817	801	799	807	775	784	809	786	769

Table 5.2. (continued)

| Sample	Leucocratic Granite			Dolerite	Sample	Sedimentary rocks					
	U-1e	U-4c	U-7	Do-1		27-Hi	28-Te	28-Za	29-Az	29-Ku	29-to
SiO_2*[1]	74.44	76.12	76.48	46.94	SiO_2	62.11	69.72	60.08	67.34	66.03	67.08
TiO_2	0.21	0.2	0.13	0.74	TiO_2	0.98	0.94	1.04	0.99	1.01	1.02
Al_2O_3	13.01	12.85	12.49	15.57	Al_2O_3	15.91	13.67	18.42	15.17	14.78	15.09
Fe_2O_3	1.18	1.37	1.08	8.54	Fe_2O_3	5.46	4.04	4.34	5.52	5.25	5.88
MnO	0.02	0.02	0.01	0.17	MnO	0.09	0.02	0.03	0.02	0.09	0.07
MgO	0.35	0.23	0.11	10.54	MgO	2.53	1.95	2.93	2.1	2.76	2.18
CaO	1.23	0.95	0.77	8.38	CaO	5.51	2.16	2.71	1.47	2.44	1.2
Na_2O	2.7	2.62	3.01	2.47	Na_2O	1.99	1.56	3.15	2.18	3.34	1.39
K_2O	4.98	5.93	5.81	0.22	K_2O	3.06	2.35	3.8	3.42	1.87	3.13
P_2O_5	0.04	0.05	0.06	0.31	P_2O_5	0.17	0.16	0.16	0.15	0.2	0.15
LOI	0.32	0.49	0.32	1.62	LOI	0.32	0.65	0.49	0.65	0.65	0.81
Total	98.46	100.82	100.27	95.5	Total	98.12	97.21	97.13	99	98.42	98.02
Ba*[2]	885	914	850	138	Ba*[2]	509	366	411	550	354	483
Rb	126	111	109	6.82	Rb	141	145	201	158	82.6	156
Sr	96.6	114	72.5	473	Sr	178	162	157	119	154	118
Cs	3.96	1.58	1.54	2.08	Cs	8.56	6.9	10.3	6.44	1.42	5.62
Ta	1.03	0.85	1.13	0.34	Ta	1.51	1.33	1.49	1.49	1.44	1.45
Nb	6.73	3.36	6.92	4.47	Nb	16	14.3	16.1	14.9	15.6	15.8
Hf	3.87	4.2	3.6	2.02	Hf	5.83	7.29	4.85	6.38	6.02	5.99
Zr	113	124	95	88	Zr	218	283	175	243	229	235
Y	39.4	16.6	22	14	Y	28.2	23.1	30.7	27.5	41.8	26
Th	15.8	18	16.7	2.85	Th	14.3	12.4	15	13.1	12.8	12.9
U	2.1	2.49	3.01	1.04	U	3.06	2.69	3.14	2.73	3.17	2.92
Sc	7.86	5.95	6.42	26.9	Cr	98.3	82.1	111.1	89.8	88.5	94.9
Pb	10.8	7.59	9.52	12.4	Ni	43.9	30.7	41.6	40.6	37.9	43.9
La	36.6	39	10.1	14.6	Co	54.1	69	45.6	116	44.1	44.1
Ce	70.4	74.7	18	28.8	Sc	14.7	11.7	17.2	13	14.7	13
Pr	7.65	8.03	2.06	3.37	V	119	99	143	111	109	116
Nd	30.6	30.7	8.28	14.3	Cu	35.7	5.31	11	4.78	5.84	11.4
Sm	6.28	5.42	2.38	3.07	Pb	34.6	4.9	9.6	3	18.5	12
Eu	0.85	0.81	0.56	1.11	Zn	67.3	14.5	19.5	7.5	38.3	29.5
Gd	5.71	3.86	2.62	2.77	La	45.2	26.7	43.4	42	29.8	30.3
Tb	1.02	0.57	0.55	0.43	Ce	84.1	50.2	83.3	79.7	54.3	56.3
Dy	6.53	3.13	3.68	2.58	Pr	9.37	5.72	9.29	8.77	6.15	6.47
Ho	1.43	0.62	0.82	0.54	Nd	36.8	23.1	36.4	34.9	25	25.6
Er	4.14	1.72	2.37	1.49	Sm	6.91	4.56	7.12	6.7	5.65	5.14
Tm	0.63	0.26	0.35	0.22	Eu	1.4	1.1	1.87	1.44	1.26	1.27
Yb	4.48	1.89	2.77	1.53	Gd	5.63	4.29	5.83	5.37	5.88	4.4
Lu	0.64	0.3	0.39	0.23	Tb	0.88	0.67	0.98	0.87	1.12	0.75
					Dy	5.16	4.16	5.72	4.98	7.38	4.63
ASI*[3]	1.08	1.03	0.99	0.8	Ho	1.07	0.85	1.14	1.03	1.55	0.99
ZST*[4]	763	767	741	653	Er	2.83	2.42	3.11	2.72	4.29	2.73
					Tm	0.43	0.34	0.46	0.42	0.61	0.41
					Yb	3.01	2.66	3.18	2.86	4.21	2.89
					Lu	0.42	0.37	0.44	0.42	0.54	0.41
					ASI*[3]	0.96	1.51	1.3	1.52	1.24	1.92

37
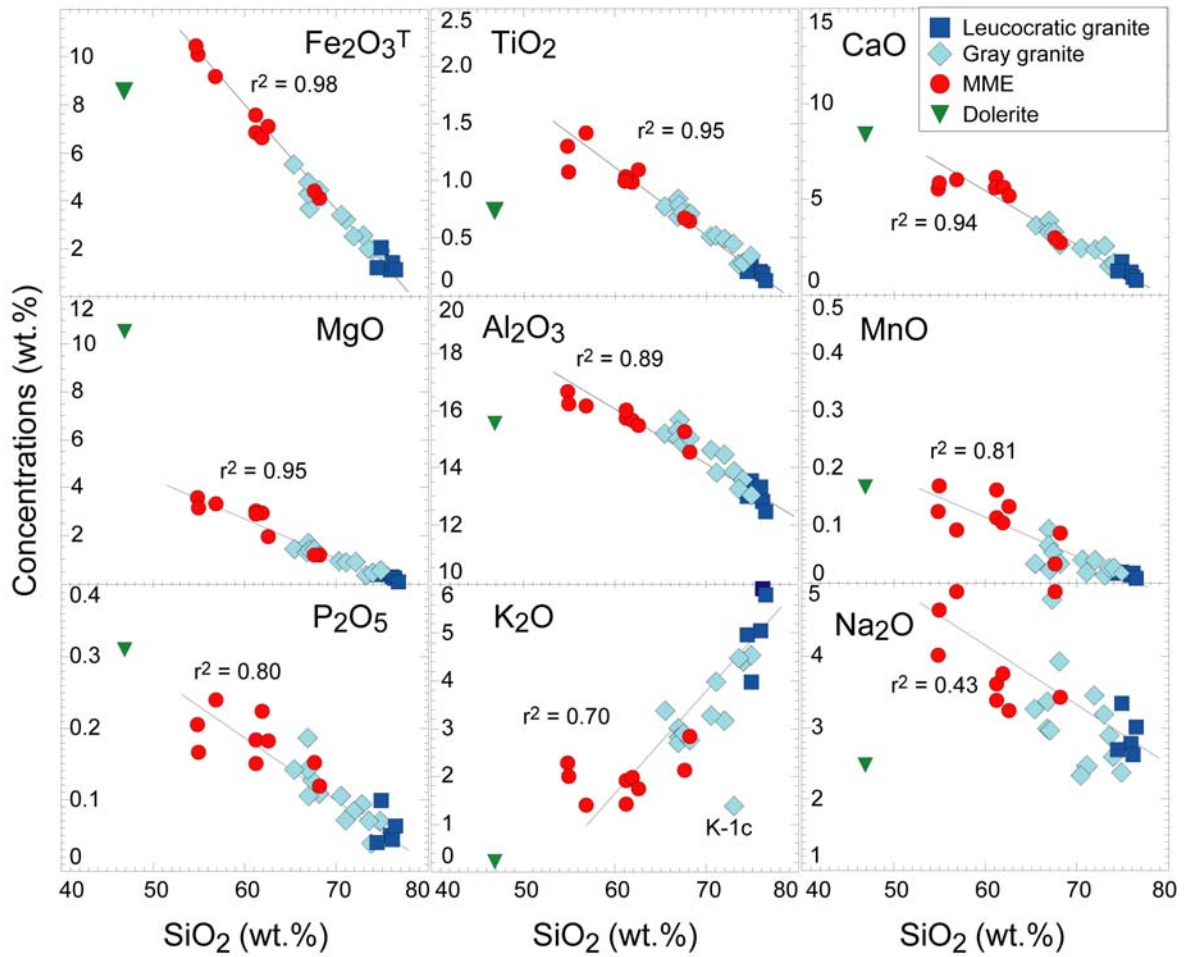
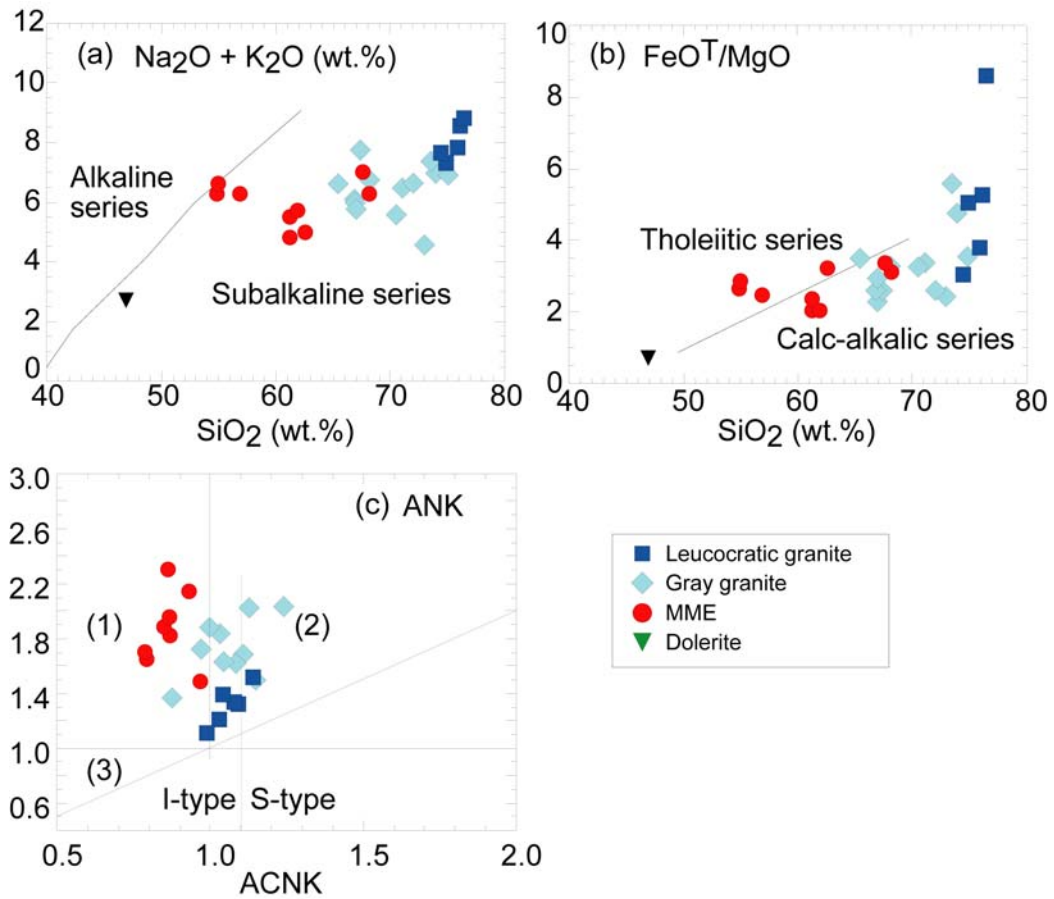Figure 5.3. Harker's variation diagrams for the Tsushima granites.

Figure 5.4. Rock classification diagrams. (a) Total alkali vs. SiO$_2$ diagram. (b) FeO^T/MgO vs. SiO$_2$ diagram. (c) ACNK vs. ANK diagram. (1) metaluminous, (2) peraluminous, (3) peralkaline.

The contents of Y, Zn, and Sc in the TSUG were negatively correlated, whereas those of Ba, Th, U, and Ta, were positively and linearly correlated, with the SiO_2 content (Figure 5.5). Along these correlation lines, the gray granite always lies between the leucocratic granite and the MME. The Sc content correlated with the modal proportion of hornblende (Figure 5.6). In contrast, the contents of Ba and Th correlated strongly with the modal proportion of alkali feldspar (Figure 5.6). Accordingly, the contents of Ba and Th increased linearly with SiO_2 content. The correlation line between Sr and SiO_2 shows a break at 61 wt. % SiO_2 (Figure 5.5). The Sr content correlates well with the modal proportion of plagioclase (Figure 5.6). In the case of Zr and Hf, this break occurs at 67–69 wt. % SiO_2 (Figure 5.5); the Zr content increased with SiO_2 content in the MMEs, whereas it decreased in the gray and leucocratic granites in relation to SiO_2 (Figure 5.5). The Rb and Pb contents of the TSUG showed a weak positive correlation with the modal proportion of biotite and alkali feldspar, respectively (Table 3.1 and Figure 5.6). It is notable that the Rb/Sr ratio exhibited a U-shaped trend against SiO_2 content (Figure 5.5).

Chondrite-normalized REE patterns of the TSUG were variable (Figure 5.7). REE contents of the leucocratic granites were high in U-1d and U-1e but low in H-2c and U-7 (Figure 5.7), implying a fractionation of REE in the leucocratic granitic magma. The MMEs showed a gradual change from a flat but slightly light REE (LREE)-enriched pattern without any Eu anomaly (sample H-3b) to a REE-enriched pattern with a large Eu anomaly (sample N-4a). The dolerite is the most depleted in REE. REE concentrations of the gray granites showed wide variation; one end member was characterized by a REE-depleted pattern with a positive Eu anomaly and the other by a REE-enriched pattern with a negative Eu anomaly. The concentrations of Nd and Yb in the MMEs roughly decreased with that of SiO_2 (Figure 5.5). The chondrite-normalized La/Yb ratios (Figure 5.6) of the MMEs showed relatively low values, ranging from 2.1 to 3.8, whereas those of
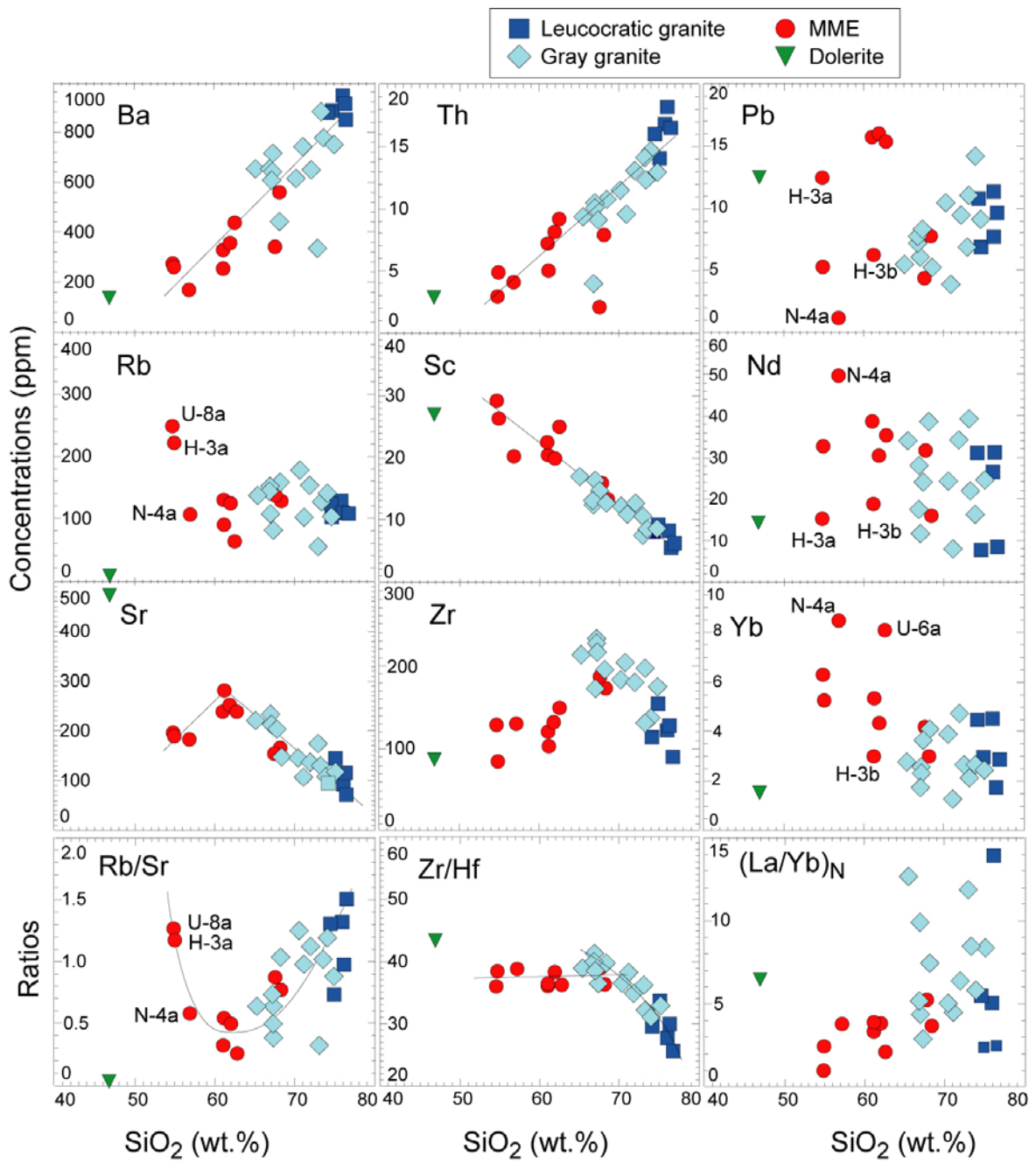
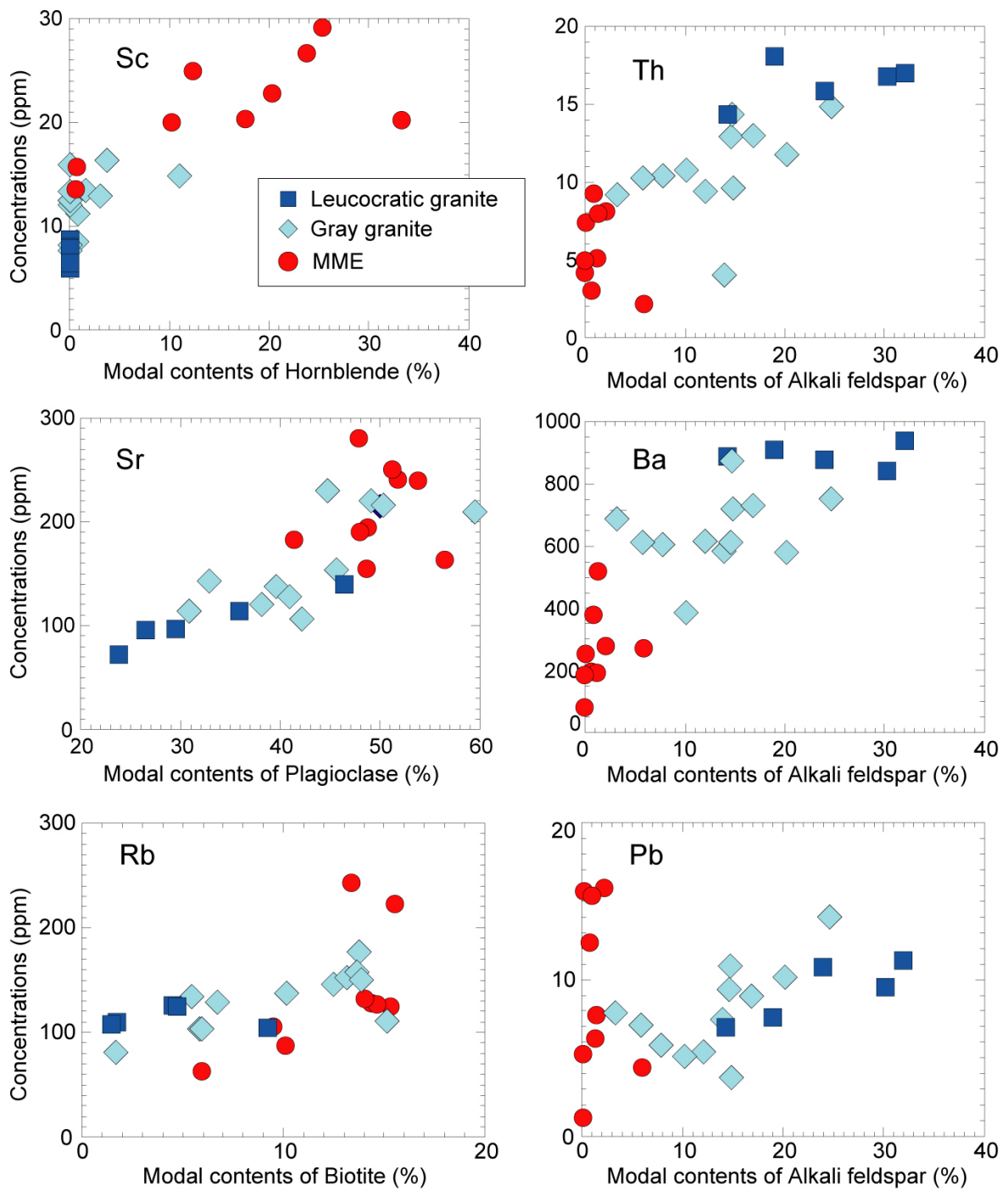Figure 5.5. Trace-element variation diagrams for the Tsushima granites.

Figure 5.6. Modal contents of mineral vs. trace elements variation diagrams
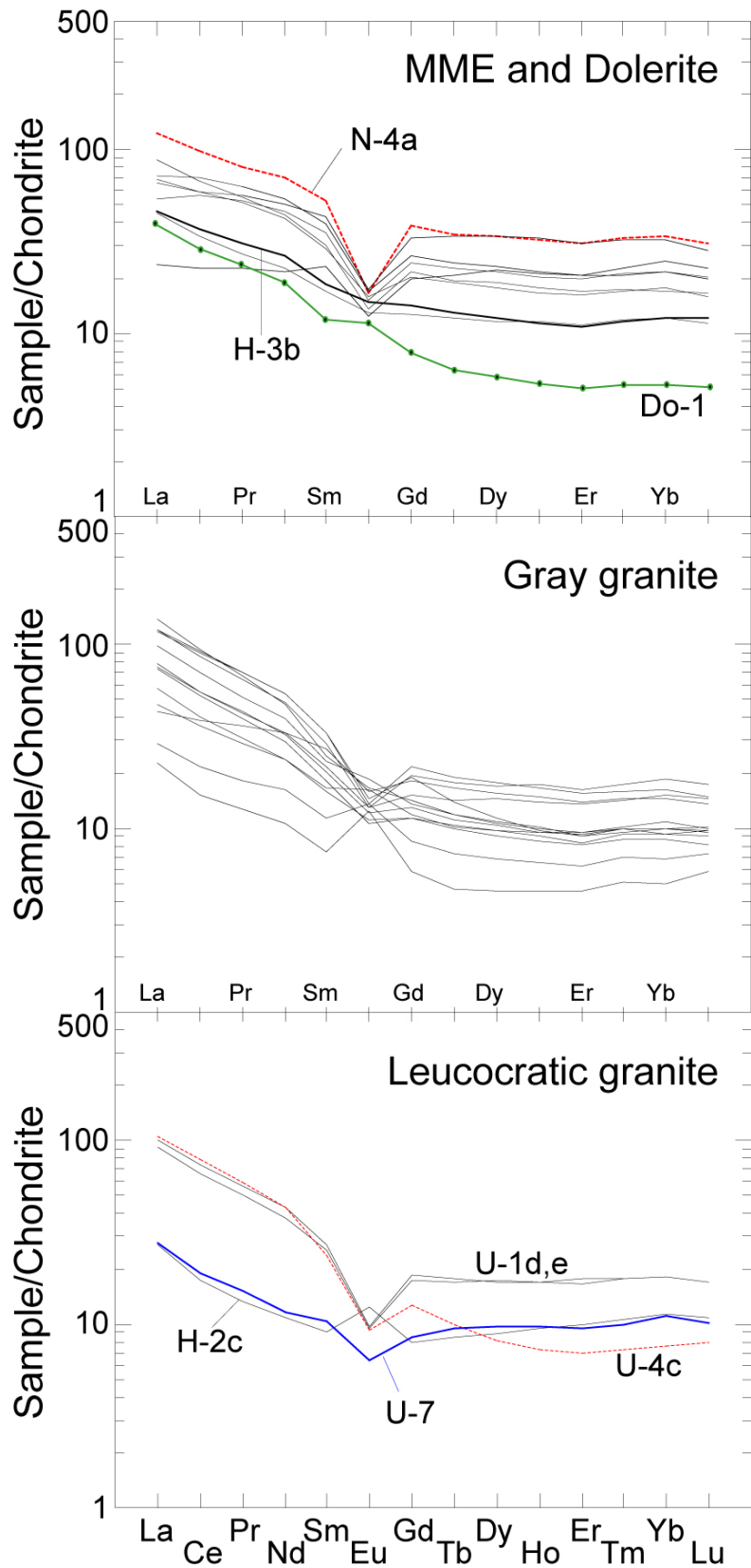
Figure 5.7. Chondrite-normalized rare earth element patterns for the Tsushima granites. Chondrite normalization factors are from Taylor and McLennan (1985).

the gray granite were higher, from 3.0 to 12.7. In contrast, except in one sample (U-4c), the leucocratic granite had a narrow La/Yb ratio in the range of 2.3 to 5.5. LREE contents were variable in all three TSUG components (Figure 5.7).

5.4 Sr–Nd–Pb isotopes

Sr–Nd–Pb isotopic compositions are listed in Table 5.3. We calculated the initial ratios of Sr, Nd, and Pb isotopes for the TSUG by assuming a model age of 16 Ma. The initial $^{87}Sr/^{86}Sr$ ratios and $\varepsilon_{Nd\ (t)}$ values were similar between the leucocratic granites (0.7065–0.7085 and –7.70 to –4.35, respectively) and the gray granites (0.7061–0.7089 and –6.17 to –3.75, respectively), whereas the MMEs had lower initial $^{87}Sr/^{86}Sr$ ratios (0.7044–0.7061) and higher $\varepsilon_{Nd\ (t)}$ values (–0.53 to –5.24). The most depleted isotopic compositions were observed in the less mafic MMEs from the Hikage locality: The initial Sr ratio of sample H-2A was 0.70444, and $\varepsilon_{Nd\ (t)}$ value of sample H-3B is -0.53. These data agree with the values reported by Ishizaka and Ishikawa (1990). The present $^{87}Sr/^{86}Sr$ ratios of an aplite dike and a zeolite- and zoisite-bearing cavity at the Hikage locality were 0.70730 and 0.70848, respectively (Table 5.3). Although the initial ratios were not calculated because of a lack of Rb and Sr concentration data, they were estimated to be comparable to those of the granites.

The TSUG had restricted Pb isotopic ratios, ranging from 18.381 to 18.495 for $^{206}Pb/^{204}Pb$, 15.623 to 15.669 for $^{207}Pb/^{204}Pb$, and 38.676 to 38.923 for $^{208}Pb/^{204}Pb$. The MMEs at the Nai-in locality had the lowest radiogenic lead isotope compositions, whereas those at the Hikage locality had relatively high isotopic values, indicating that the peripheral part of the Tsushima granitic pluton has higher radiogenic Pb components and that the core region has relatively low values. The sedimentary rocks were more enriched in radiogenic Pb than the TSUG, and the marginal zone in the Hikage locality includes many metasedimentary xenoliths. Thus, sediment assimilation may have affected the Pb isotopic composition in

the Hikage locality. Dolerite was the most depleted in radiogenic Pb (Table 5.3).

Table 5.3 Sr, Nd, Pb isotope data for the Tsushima granites, hydrothermal veins, dolerite, and sedimentary rocks.

Sample	Rock*[1]	^{86}Sr/^{87}Sr	^{143}Nd/^{144}Nd	^{87}Sr/^{86}Sr$_i$*[2]	^{143}Nd/^{144}Nd$_i$	εNd$_i$
H-3a	MME	0.706494 (±9)	0.512497 (±4)	0.705664	0.512475	-2.77
U-8a	MME	0.705989 (±10)	0.512412 (±4)	0.705206	0.512397	-4.30
N-4a	MME	0.706354 (±10)	0.512451 (±9)	0.705968	0.512436	-3.53
H-2a	MME	0.704839 (±10)	0.512520 (±5)	0.704485	0.512505	-2.18
H-2b	MME	0.704778 (±10)	0.512546 (±5)	0.704446	0.512532	-1.65
H-3b	MME	0.705220 (±12)	0.512604 (±4)	0.705012	0.512590	-0.53
U-6a	MME	0.706062 (±9)	0.512388 (±6)	0.705885	0.512370	-4.82
U-2b	MME	0.706641 (±11)	0.512364 (±5)	0.706125	0.512349	-5.24
U-4a	MME	0.706455 (±14)		0.705887		
Aza-5	Gray Gr	0.707397 (±11)	0.512436 (±6)	0.707139	0.512419	-3.85
H-3c	Gray Gr	0.707118 (±9)	0.512408 (±6)	0.706695	0.512394	-4.35
N-2	Gray Gr	0.707113 (±10)	0.512411 (±5)	0.706768	0.512396	-4.30
N-4b	Gray Gr	0.706699 (±10)	0.512425 (±2)	0.706281	0.512414	-3.95
N-4c	Gray Gr	0.706703 (±11)	0.512439 (±7)	0.706306	0.512425	-3.75
K-1c	Gray Gr	0.709083 (±10)	0.512380 (±5)	0.708870	0.512367	-4.87
U-1a	Gray Gr	0.707833 (±9)	0.512314 (±6)	0.707010	0.512301	-6.17
U-1c	Gray Gr	0.707680 (±10)	0.512337 (±5)	0.706941	0.512325	-5.69
U-4b	Gray Gr	0.706761 (±9)	0.512347 (±4)	0.706079	0.512334	-5.52
U-6b	Gray Gr	0.707831 (±9)	0.512383 (±5)	0.707263	0.512370	-4.81
U-8b	Gray Gr	0.707265 (±11)	0.512345 (±5)	0.706593	0.512333	-5.54
U-8c	Gray Gr	0.707330 (±10)	0.512337 (±6)	0.706541	0.512323	-5.74
U-9	Gray Gr	0.706744 (±11)	0.512379 (±5)	0.706278	0.512367	-4.88
H-2c	Leuco Gr	0.707001 (±11)	0.512375 (±5)	0.706505	0.512358	-5.05
U-1d	Leuco Gr	0.707815 (±10)	0.512347 (±5)	0.706941	0.512334	-5.52
U-1e	Leuco Gr	0.707421 (±10)	0.512342 (±5)	0.706558	0.512329	-5.62
U-4c	Leuco Gr	0.707429 (±12)	0.512405 (±4)	0.706785	0.512394	-4.35
U-7	Leuco Gr	0.709488 (±12)	0.512241 (±5)	0.708493	0.512222	-7.70
Aplite		0.707302 (±10)	0.512430 (±6)			
Zeolite-zoisite cavity		0.708476 (±10)				
Do-1	Dolerite	0.704229 (±9)	0.512657 (±6)	0.704220	0.512643	0.51
27-Hi	Sediment	0.716929 (±11)	0.512002 (±6)	0.716405	0.511991	-12.22
28-Te	Sediment	0.716443 (±9)	0.511987 (±18)	0.715851	0.511974	-12.54
28-Za	Sediment	0.717169 (±11)	0.512041 (±6)	0.716321	0.512029	-11.47
29-Az	Sediment	0.718540 (±9)	0.512017 (±5)	0.717661	0.512005	-11.95
29-Ku	Sediment	0.714709 (±12)	0.511993 (±6)	0.714354	0.511979	-12.45
29-to	Sediment	0.716884 (±11)	0.511993 (±5)	0.716009	0.511981	-12.42

Note: *1 MME, mafic microgranular enclave; Gray Gr, gray granite; Leuco Gr, leucocratic granite. *2 ^{87}Sr/^{86}Sr$_i$ ^{143}Nd/^{144}Nd$_i$ ^{206}Pb/^{204}Pb$_i$, ^{207}Pb/^{204}Pb$_i$, ^{208}Pb/^{204}Pb$_i$: age corrected for 16 Ma. Nd$_i$: deviation in parts per 10^4 from bulk earth values at 16 Ma (^{143}Nd/^{144}Nd =0.512617).

Table 5.3 (continued)

Sample	Rock*[1]	$^{206}Pb/^{204}Pb$	$^{207}Pb/^{204}Pb$	$^{208}Pb/^{204}Pb$	$^{206}Pb/^{204}Pb_i$	$^{207}Pb/^{204}Pb_i$	$^{208}Pb/^{204}Pb_i$
H-3a	MME	18.5059 (±16)	15.6545 (±14)	38.8637 (±37)	18.490	15.654	38.851
U-8a	MME	18.4899 (±18)	15.6351 (±16)	38.7910 (±42)	18.444	15.633	38.742
N-4a	MME	18.5709 (±25)	15.6545 (±25)	38.9148 (±77)	18.381	15.646	38.733
H-2a	MME	18.5019 (±19)	15.6347 (±19)	38.8119 (±57)	18.485	15.634	38.787
H-2b	MME	18.5025 (±14)	15.6699 (±19)	38.9492 (±54)	18.486	15.669	38.923
H-3b	MME	18.5108 (±17)	15.6335 (±20)	38.8080 (±37)	18.470	15.632	38.766
U-6a	MME	18.5178 (±32)	15.6447 (±33)	38.8578 (±95)	18.495	15.644	38.827
U-2b	MME	18.4558 (±126)	15.6267 (±113)	38.7687 (±295)	18.421	15.625	38.715
U-4a	MME	18.5049 (±16)	15.6395 (±14)	38.8285 (±37)	18.494	15.639	38.826
Aza-5	Gray Gr	18.5359 (±14)	15.6421 (±11)	38.8830 (±29)	18.494	15.640	38.822
H-3c	Gray Gr	18.4716 (±16)	15.6336 (±15)	38.8266 (±37)	18.448	15.633	38.799
N-2	Gray Gr	18.4558 (±126)	15.6267 (±113)	38.7687 (±295)	18.383	15.623	38.676
N-4b	Gray Gr	18.4877 (±49)	15.6268 (±1000)	38.8455 (±1058)	18.416	15.624	38.754
N-4c	Gray Gr	18.5222 (±19)	15.6489 (±16)	38.8769 (±43)	18.421	15.644	38.744
K-1c	Gray Gr	18.5549 (±21)	15.6486 (±19)	38.9363 (±50)	18.495	15.646	38.839
U-1a	Gray Gr	18.4866 (±14)	15.6449 (±13)	38.8153 (±36)	18.444	15.643	38.755
U-1c	Gray Gr	18.4800 (±13)	15.6344 (±12)	38.8059 (±31)	18.432	15.632	38.734
U-4b	Gray Gr	18.5222 (±53)	15.6338 (±45)	38.9116 (±114)	18.449	15.630	38.801
U-6b	Gray Gr	18.5245 (±16)	15.6404 (±14)	38.8795 (±38)	18.490	15.639	38.804
U-8b	Gray Gr	18.5075 (±15)	15.6434 (±14)	38.8689 (±36)	18.460	15.641	38.800
U-8c	Gray Gr	18.4905 (±16)	15.6387 (±18)	38.8285 (±36)	18.454	15.637	38.773
U-9	Gray Gr	18.4846 (±20)	15.6438 (±18)	38.8300 (±50)	18.454	15.642	38.754
H-2c	Leuco Gr	18.5402 (±21)	15.6559 (±21)	38.9154 (±64)	18.461	15.652	38.807
U-1d	Leuco Gr	18.4758(±17)	15.6674 (±26)	38.9423 (±37)	18.442	15.666	38.863
U-1e	Leuco Gr	18.4966 (±18)	15.6609 (±16)	38.8880 (±37)	18.466	15.660	38.811
U-4c	Leuco Gr	18.5440 (±21)	15.6477 (±18)	38.9379 (±49)	18.492	15.645	38.813
U-7	Leuco Gr	18.4909 (±20)	15.6334 (±18)	38.7889 (±44)	18.440	15.631	38.697
Aplite		18.4625 (±20)	15.6253 (±17)	38.7545 (±42)			
Zeolite-zoisite cavity							
Do-1	Dolerite	17.8847 (±44)	15.5374 (±17)	38.0182 (±19)	17.872	15.537	38.006
27-Hi	Sediment	18.6365 (±10)	15.6658 (±8)	39.0294 (±21)	18.622	15.665	39.008
28-Te	Sediment	18.6251 (±45)	15.6932 (±44)	39.2048 (±113)	18.537	15.689	39.071
28-Za	Sediment	18.5603 (±16)	15.6626 (±15)	39.0036 (±94)	18.508	15.660	38.921
29-Az	Sediment	18.5713 (±16)	15.6629 (±14)	38.9794 (±38)	18.425	15.656	38.749
29-Ku	Sediment	18.6619 (±16)	15.6830 (±14)	39.3319 (±35)	18.634	15.682	39.295
29-to	Sediment	18.7761 (±16)	15.6856 (±13)	39.6315 (±35)	18.737	15.684	39.574

6. PRESSURE AND TEMPERATURE CONSTRAINTS

The two-pyroxene geothermometer of Kretz (1982) yielded an equilibrium temperature of 730 to 860 °C for two MME samples (U-5a and U-6a) from the Uchiyama locality. These temperatures indicate conditions at an early stage of crystallization of mafic magma.

Solidus temperatures of the leucocratic granites (normative An content is 3%–8%) estimated from the Qtz–Ab–Or–An–H_2O compositions were 720 to 730 °C, assuming 100 MPa of pressure and water-saturated conditions (Johannes & Holtz, 1996) (Figure 5.8). The solidus temperature for the gray granites ranged from 740 to 780 °C.

Using the Fe/(Fe+Mg) ratios and Al contents of hornblendes in the gray granite and the MME, the hornblende geobarometer of Anderson and Smith (1995) in most cases yielded model pressures from 50 to 150 MPa, using a calibration temperature of 770 °C obtained above from the average solidus temperature of the gray granites. Amphibole–plagioclase geothermometer (Blundy and Holland, 1990) also indicates that the MME crystallized from 50 to 150 MPa at temperatures of 980–800 ˚C. I estimated the emplacement level of the Tsushima granites to be from 2 to 6 km. This shallow intrusion is consistent with the presence of abundant miarolitic cavities in the leucocratic and gray granites.

Magmatic temperatures of granitic rocks have also been estimated using zircon solubilities in granitic melts (Miller et al., 2003; Piccoli and Candela, 2002). Zircon is a common accessory mineral in all rocks of the Tsushima granites, and the estimates are suitable for the present samples. The zircon saturation thermometry is calculated based on the distribution coefficient of Zr between zircon and the granitic melt and the cation ratio (Na+K+2Ca)/(Al*Si) of the granitic melt. The equation is

$$T_{Zr} (^{o}C) = 12900/[\ln(496000/Zr_{melt})+2.95+0.85M) -273$$

where Zr_{melt} is Zr concentration (ppm) in the melt and M is cation ratios. Representative cation ratios of the Tsushima granites range from 1.9 to 1.3, and the temperature estimates range from 823 to 763 ˚C for the gray granite and 786 to 741 ˚C for the leucocratic granite. The MMEs show increasing temperature with SiO_2 content from 683 to 791˚C. This result might be related either to the inflection in the $Zr–SiO_2$ correlation plot (Figure 5.5), in which Zr is relatively undersaturated in the MMEs (constant Zr/Hf ratios) and reaches saturation point in the gray granite, or to the transportation of granitic zircon from the host granites during their mixing. If the former is true, it may represent a near-solidus temperature of enclave magma. In case of the later the zircon saturation temperature may not provide true magmatic temperature, but may imply that mixing was occurred in a restricted range of temperature in the granitic magma or the granitic magma was relatively unfractionated Zr/Hf ratios. The crystallization temperatures of zircon in the leucocratic granites (Normative An content is 3-8%) is higher than the solidus temperatures of about 720-730 ˚C from the system $Qtz–Ab–Or-An-H_2O$ compositions at 100 MPa under water-saturated conditions (Johannes and Holtz, 1996).
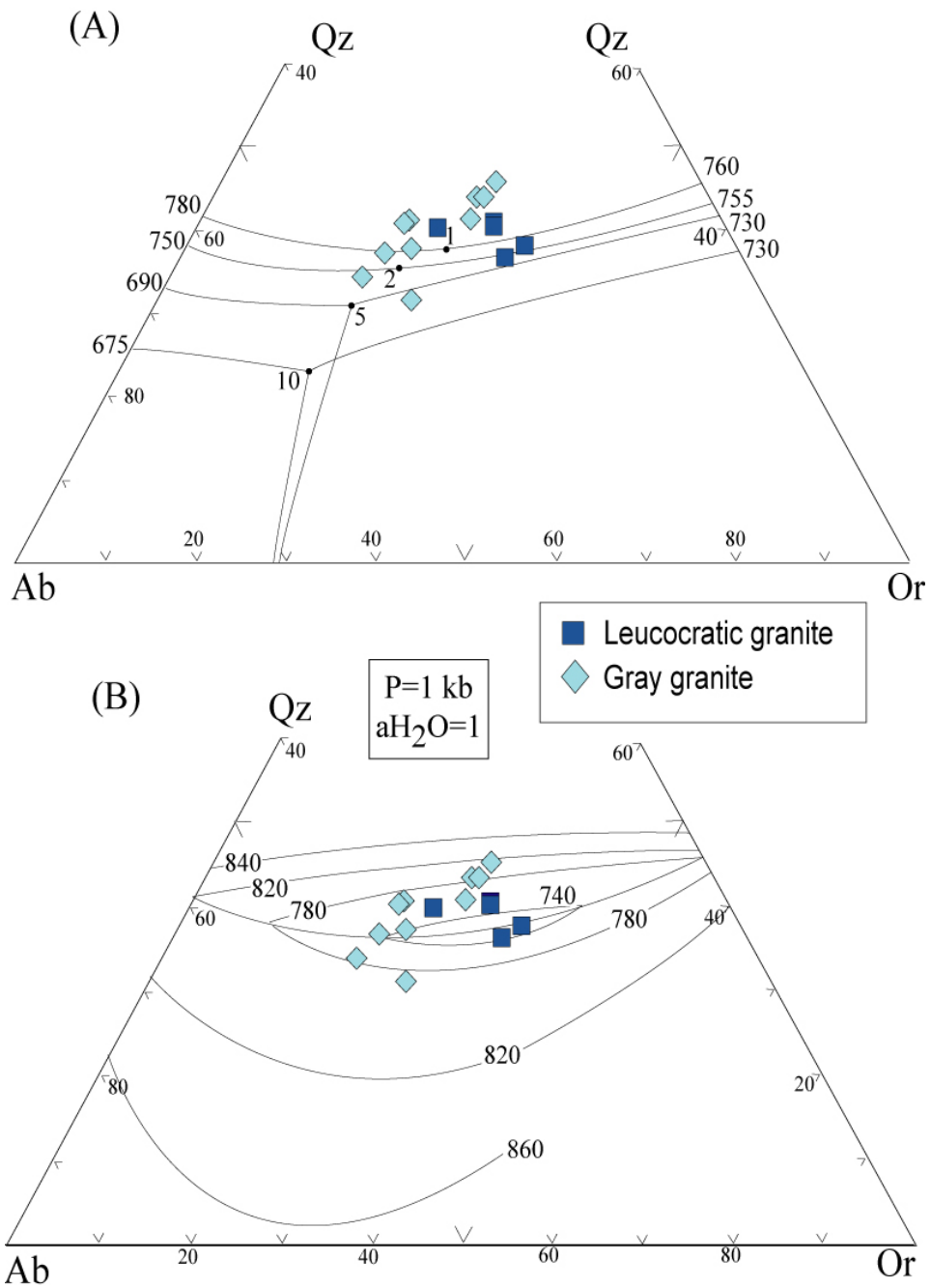
Figure 6.1. Normative Q-Ab-Or triangle diagram for the gray and leucocratic granites (Johannes and Holtz, 1996).

7. FLUID INCLUSIONS

Quartz grains from the TSUG often contain fluid inclusions. Salinity and homogenization temperatures were analyzed using a Linkam stage THMGS 600. The quartz crystals were separated from MME, host granite, miarolitic cavity, and pegmatites. However, inclusion in quartz crystals from the granite and MMEs were too small. Salinity and homogenization temperatures were therefore determined only from the miarolitic cavities and pegmatites. Three types of inclusions were observed (Figure 7.1); 1) liquid water and vapor, 2) liquid water, vapor and solids, and 3) silicate melt inclusions. The solid phases in the fluid inclusions are mostly halite and minor sylvite, unknown transparent and opaque minerals (Figure 7.1b, c). Silicate melt inclusions were observed only in one crystal from the Hikage locality.

On the heating microscope stage, most of the vapor phase disappeared at 210 to 450 ^{O}C and rarely remained up to 600 ^{O}C. The halite crystals melted at 130 to 530°C. Only one halite did not melt up to 600 ^{O}C. The salinity was calculated with equation reported by Sterner et al., (1988). The salinity ranges from 28 to 64 wt. % and high salinity inclusions over 45 wt.% were observed in the quartz from the miarolitic cavity (Figure 7.2). Similar hypersaline fluid inclusions have also been reported in quartz from the granite (34–56 wt. % NaCl equivalent; Imai *et al*., 1971).
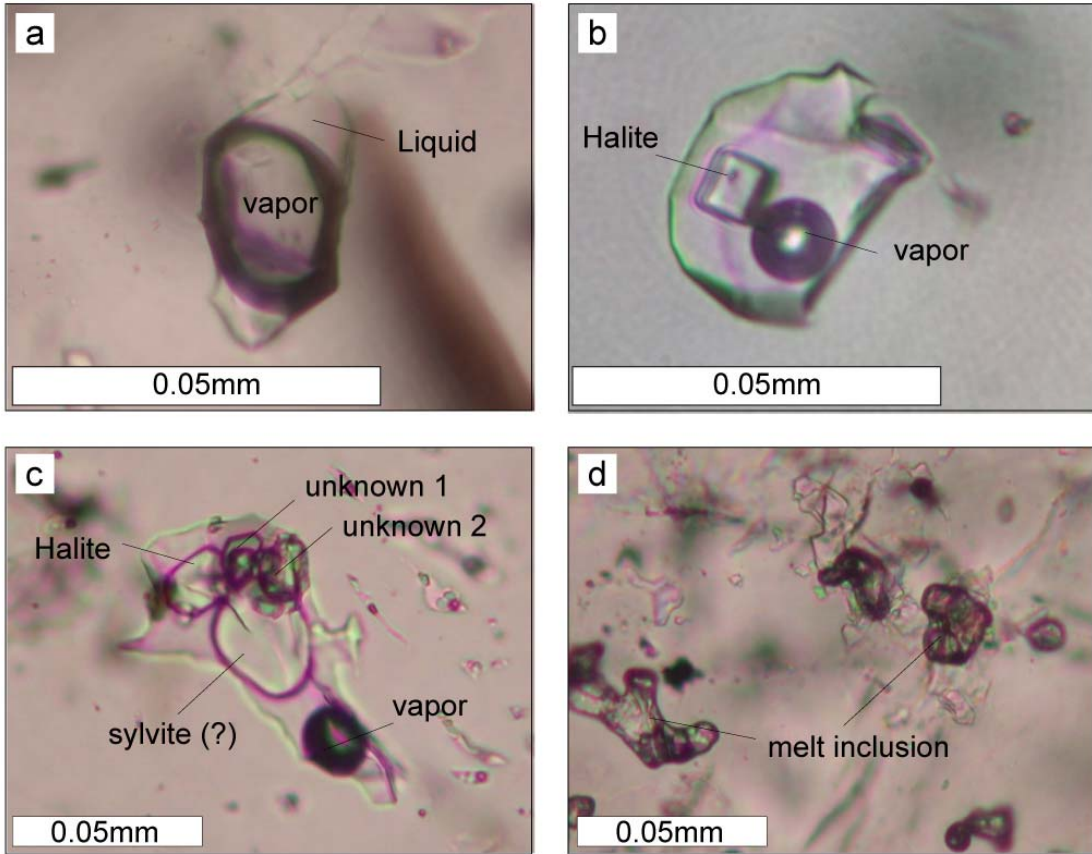
Figure 7.1. Photomicrographs of fluid inclusions in under plane polarization. (a) Liquid + vapor type inclusion. (b) Liquid + vapor + one solid (halite) type inclusion. (c) Liquid + vapor + multi solid (halite ± sylvite ± unknown solids) type inclusion. (d) melt inclusion

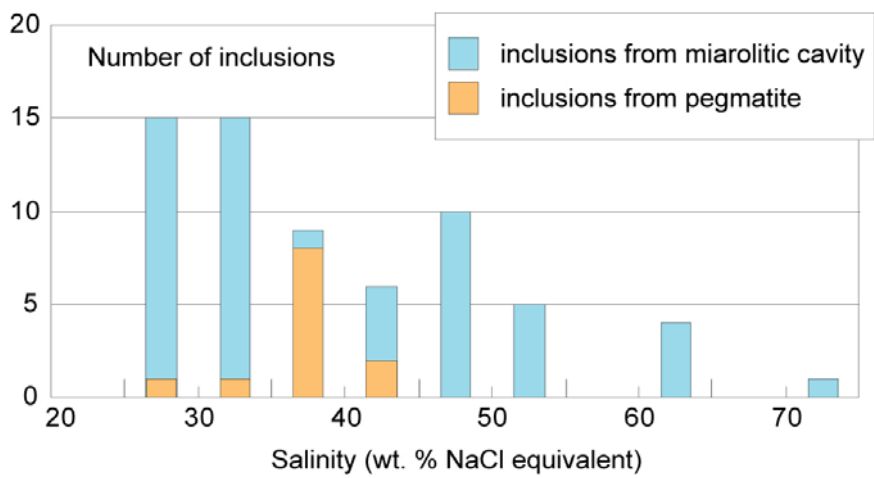Figure 7.2. Frequency vs. salinity histogram from fluid inclusion microthermometric data.

8. ORIGIN AND EVOLUTION OF THE TSUSHIMA GRANITE

8.1 Magma mingling and mixing in the TSUG

The mode of occurrence of MMEs in the Tsushima pluton, with rounded shape, crenulate surface, chilled margin, and sharp but partly diffuse contact, suggests that the MMEs were formed by injection of mafic magma with a high temperature and low viscosity into a felsic magma/crystal mush with a low temperature and high viscosity (Barbarin & Didier, 1991, 1992; Wiebe & Collins, 1998). Thus, I consider the MMEs to be globules of mafic magma variably hybridized with the host felsic magma (Hibbard, 1981; Vernon, 1984; Huppert & Sparks, 1988; Barbarin & Didier, 1991). The acicular shape of apatite, hornblende and orthopyroxene in the MMEs (Figure 3.3), a common texture reflecting magma mixing (Hibbard, 1981), indicates rapid growth in an overcooled mafic magma (Wyllie *et al*., 1962).

Furthermore, the corroded texture of quartz and the overgrowth rim of plagioclase phenocryst in the MME are clear evidence for the incorporation of these two minerals, which originally crystallized in felsic magma, into a hotter mafic magma (Hibbard, 1981; Vernon, 1991). The ovoid quartz crystals fringed by fine-grained mafic minerals also suggest that the quartz crystals were derived from felsic magma that was partly dissolved in the MME-forming mafic magma, and that the tiny mafic minerals then crystallized on the surface of the quartz crystals (Hibbard, 1981). Thus, the chemical variation of the MME from basaltic to dacitic composition can be attributed to differences in the amounts of felsic minerals mixed into the molten mafic magma.

The chemical difference also respond to the crystallization of hornblende in the

MMEs. The crystallization of hornblende also explains the REE patterns and the isotopic signatures of the MMEs: the MMEs resemble to the leucocratic granites in their REE patterns, and the most felsic MME (sample H-3b) shows the most depleted REE pattern (Figure 5.7). This is because the apparently mafic MMEs include abundant hornblende formed by reaction of clinopyroxene with fluid released from the leucogranitic melt. These apparently mafic samples also show higher initial $^{87}Sr/^{86}Sr$ ratios and lower initial $^{143}Nd/^{144}Nd$ ratios (Table 5.3). The initial Sr ratios increase and the initial Nd ratios decrease with increasing modal contents of hornblende (and with decreasing SiO_2 content) in the mafic MMEs (Figure 8.1).

The gray granite has intermediate chemical and Sr–Nd isotopic compositions, between those of the leucocratic granite and the MME. The quartz and plagioclase phenocrysts of the gray granite are indistinguishable from those of the leucocratic granite under microscope. In contrast, the groundmass of the gray granite is more mafic and enriched in hornblende. These features indicate that (1) a large amount of coarse-grained plagioclase and quartz in the gray granite must have already been formed in the felsic magma/crystal mush, and (2) the fine-grained, hornblende-enriched part of the gray granite might have formed by the fractional crystallization of the felsic magma at high temperature, which may have been compositionally altered by mixing with mafic magma or heated by injection of mafic magma, because hornblende in granitic magma commonly crystallizes at high temperatures. Thus, the gray granite can be explained in terms of the injection of mafic magma and the interaction between the mafic magma and partly crystallized felsic magma. The absence of K-feldspar phenocrysts in the MME indicates that the mingling of the two magmas must have occurred before the K-feldspar crystallization in the felsic magma. This result is consistent with the finding that in felsic magma with high SiO_2 content, quartz can crystallize at an earlier stage than alkali feldspars (Whitney, 1975).
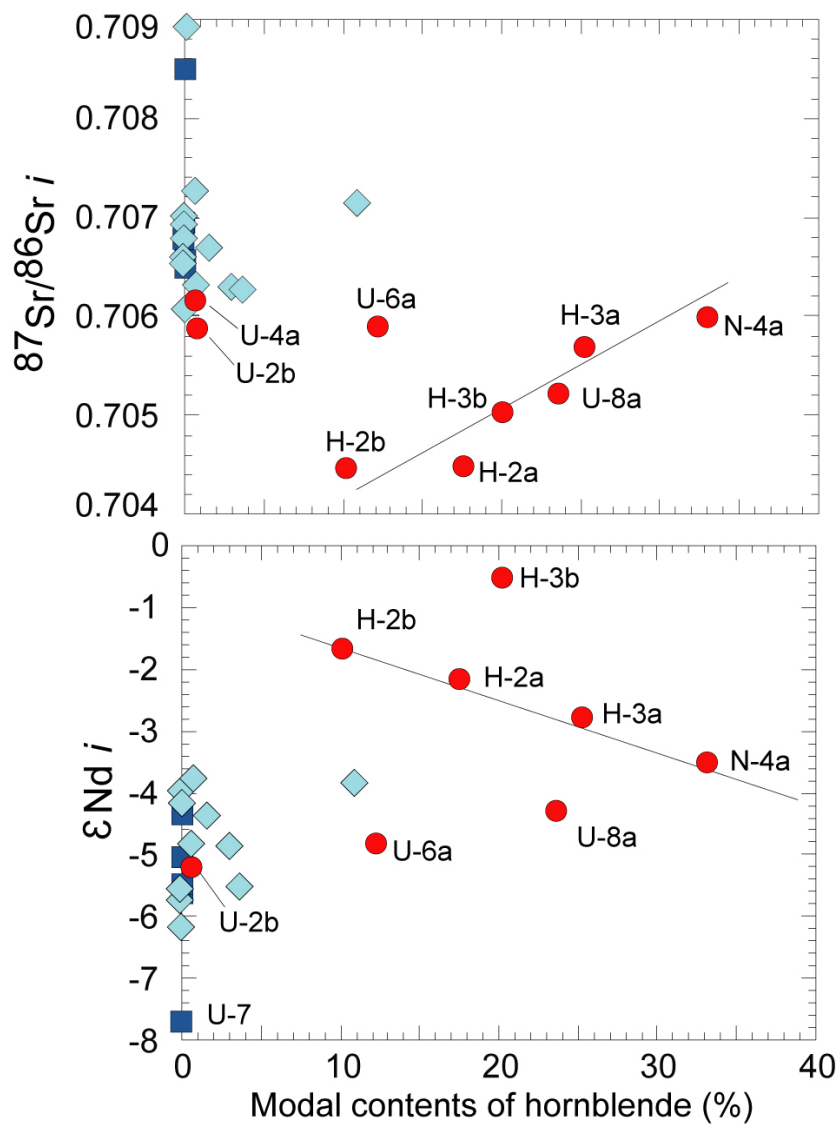
Figure 8.1. Modal contents of hornblende vs. initial Sr isotopic ratios and εNd I values diagrams.

The trends for Sr and Zr (Hf) (Figure 5.5) can be explained by the accumulation of plagioclase and the crystallization of zircon during the mixing respectively. The decrease of Zr (Hf) and Zr/Hf ratios in the both granites might reflect crystallization and accumulation of zircon as a result of temperature decrease of the granitic magma. In peraluminous granitic melts the solubility of zircon on a molar basis is five times greater than hafnon, though Hf and Zr have similar chemical properties (Linnen and Keppler, 2002). Zr content increasing with SiO_2 contents of MMEs is controlled either by crystal fractionation in mafic magma or by the effect of granitic zircon transportation during magma mixing. The constant Zr/Hf ratio in the MMEs with various composition supports crystal fractionation of zirconium. Because Zr/Hf ratio of the MMEs is similar to that of gray granite and considerably different from that of the leucocratic granite, if any, only restricted mixing of zircon from gray granite is expected. This suggests that the both gray granites and leucocratic granites are a series of rocks fractionated from an original granitic magma and the MMEs are minglied only with gray granite.

8.2 Magma source

The linear relationships of most major elements (Figure 5.3) and some trace elements (Ba, Th, and Sc in Figure 5.5) in relation to SiO_2 contents of the TSUG also agree with mingling and mixing between mafic and felsic magmas. Information regarding the source materials of the two magmas can be obtained by comparing initial Sr–Nd–Pb isotopic ratios of the TSUG with those of volcanic and plutonic rocks in Southwest Japan. It is notable that the TSUG and the Miocene and Quaternary volcanic rocks of Southwest Japan constitute an array on the $^{87}Sr/^{86}Sr$ and ε_{Nd} diagram (light yellow area in Figure 8.2), demonstrating that these igneous rocks are derived from similar source materials.

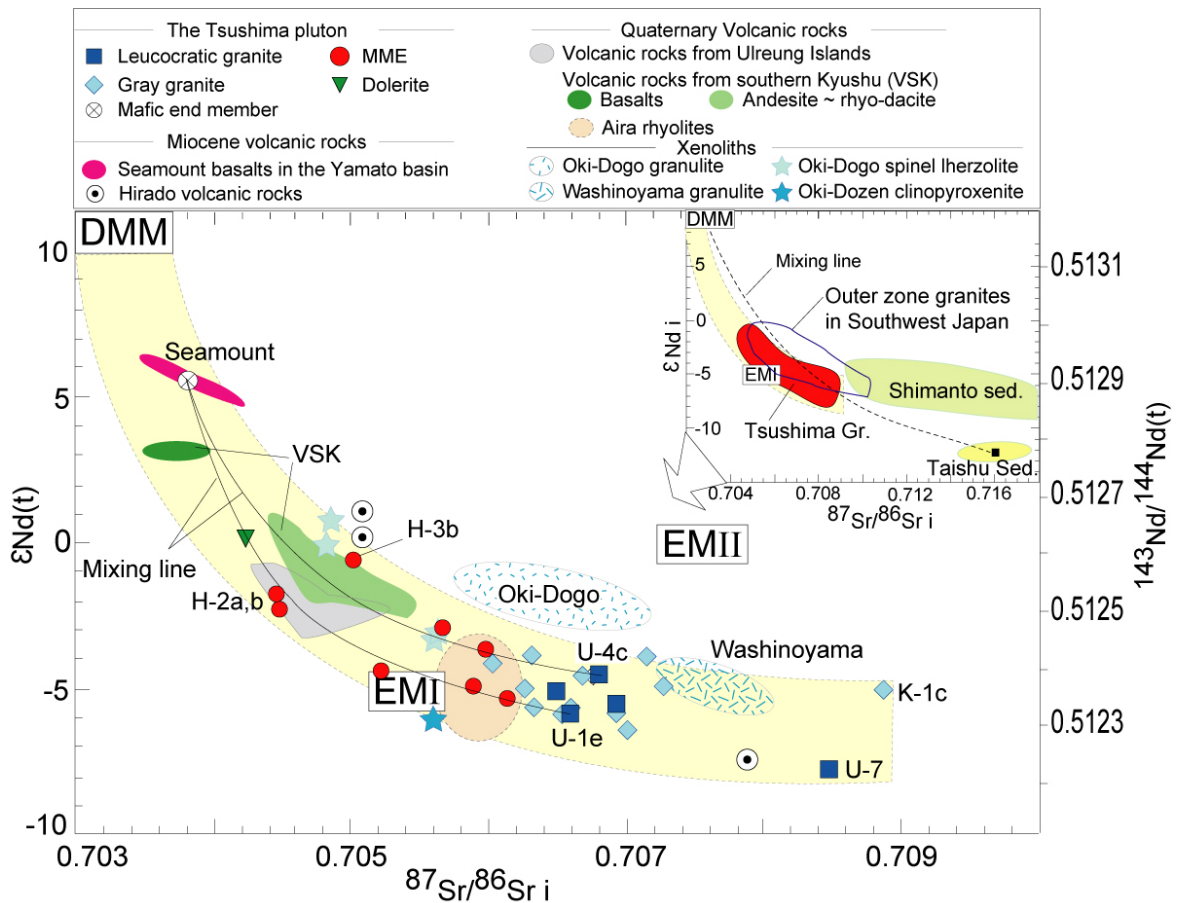Depleted mid-ocean ridge basalt (MORB) mantle (DMM: Hart, 1988) and EMI

Figure 8.2. Relationship between initial Sr and Nd isotope ratios for the Tsushima granites and volcanic rocks from Southwest Japan. The two solid lines represent mixing between basaltic magma from the Yamato basin seamount and felsic magmas of samples U-4c and U-1e. Data sources: seamount basalts of the Yamato Basin and alkali volcanic rocks of the Ulreung islands, Tatsumoto and Nakamura (1991); Hirado volcanic rocks of northern Kyushu, Uto *et al*. (2004); volcanic rocks of the Hishikari area in southern Kyushu, Hosono *et al*. (2003); rhyolites from the Aira volcano in southern Kyushu, Arakawa *et al*. (1998); and xenoliths from Oki-Dogo and Washinoyama, Kagami *et al*. (1993, 1995), and from Oki-Dozen, Ikeda *et al*. (2001), Southwest Japan. The dashed line in the inset shows a simple mixing line between depleted MORB mantle material (DMM) and the Taishu sedimentary rocks. The open blue encircled area represents Sr-Nd isotopes of the Middle Miocene granites from Southwest Japan (Terakado *et al*., 1988; Dai *et al*., 1993; Shinjoe, 1997; Anma *et al*., 1998). Data for Shimanto Sedimentary rocks are from Terakado *et al*.

57

(1988) and Hosono *et al*. (2003). Values for DMM and enriched mantle materials (EMI and EMII) are from Hart (1988).

(Hart, 1988) plot on the extension of the trend established by the volcanic rocks and the MMEs on the Sr–Nd isotope diagram (Figure 8.2). Mantle xenoliths of clinopyroxenite from Oki-Dozen (Ikeda *et al*., 2001) and some spinel lherzolite from Oki-Dogo (Kagami *et al*., 1993) have Sr–Nd isotope values close to those of EMI (Figure 8.2). The Sr–Nd isotopic ratios of mantle xenoliths from 15 Ma are similar to their present values. Therefore, we can assume that DMM and EMI are two major source materials of the mafic magma. Basalts from the Yamato basin seamount and southern Kyushu and dolerite from Tsushima have higher ε_{Nd} values and lower $^{87}Sr/^{86}Sr$ than other rocks on the array, suggesting that these mafic rocks are enriched in the DMM component.

Mantle with an EMI-like composition, similar to that of the mantle xenoliths, probably occurs beneath the continental crust of Southwest Japan. The leucocratic and gray granites had higher initial $^{87}Sr/^{86}Sr$ ratios and lower ε_{Nd} values than the MMEs (Figure 6.2). Most leucocratic and gray granites plot between the EMI and granulite values from Oki-Dogo islands and Mt. Washinoyama (Figure 1.2) (Kagami *et al*., 1993, 1995), which may represent lower crustal material in Southwest Japan. Because the MMEs seldom affected the isotopic composition of the leucocratic granites and because partial melting of metabasic materials can produce a felsic melt leaving a granulitic restite (Beard & Lofgren, 1991), the main source material for the felsic magma can be ascribed to that of the granulites. Partial melting of the metabasic rocks in the lower crust must have been induced by injection of basaltic magma with EMI composition derived from the upper mantle. This contention is consistent with the results that basalts in Southwest Japan, andesite and dacite from the Hishikali area (Hosono *et al*., 2003) and rhyolite from the Aira volcano (Arakawa *et al*., 1998), southern Kyushu, have Sr and Nd isotope ratios close to those of the EMI component (Figure 8.2). Thus, it is likely that the mafic magma responsible for the formation of the MMEs originated from mantle with DMM and EMI

compositions, whereas the felsic magma and granulitic restites were formed in the lower crust by the partial melting of metabasic rocks resulting from the injection of basaltic melts with EMI composition. Two leucocratic granites (samples U-7 and K1-c) had extremely high initial $^{87}Sr/^{86}Sr$ ratios, indicating contamination by sedimentary rocks of the Taishu Group.

The Pb isotopic data are partly consistent with the above results. The TSUG have intermediate Pb isotopic ratios between those of volcanic rocks from Kyushu Island and those of sedimentary rocks of the Taishu Group (Figure 8.3). It is notable that these rocks constitute an array on the diagram of Pb isotopic ratios, and that the seamount basalt from the Yamato basin plots as an extension of the array. Furthermore, the Pb isotopic ratios of the seamount basalt lie close to the intersection between this array and the mixing line connecting the DMM and EMI components. The Pb isotopic ratios of dolerite from Tsushima Island are also close to those of the Yamato seamount basalt. These results are compatible with the Sr–Nd isotopic ratios, supporting the view that the mafic magma for the TSUG originated from two mantle sources, DMM and EMI.

Pb isotopes are a sensitive indicator of sediment contamination, therefore the plot (Figure 8.2) reveals even slight crustal assimilation in the Tsushima granitic magma during the intrusion. However, unlike the Sr–Nd isotope ratios, the Pb isotopic ratios of the TSUG are similar irrespective of rock type and differ markedly from those of the EMI component. Instead, the values of the TSUG are close to those of the Taishu sedimentary rocks (Figure 8.3). There are two possible explanations for this result. The first is that metabasic rocks in the lower crust, which formed the felsic component of the TSUG, have similar Pb isotopic ratios to those of the TSUG. Two data points of sedimentary rocks (hornfels) overlap the granite field, probably reflecting the effect of magmatic fluids released from the granite body to the surrounding sedimentary rocks, taking into account the highly mobile nature of
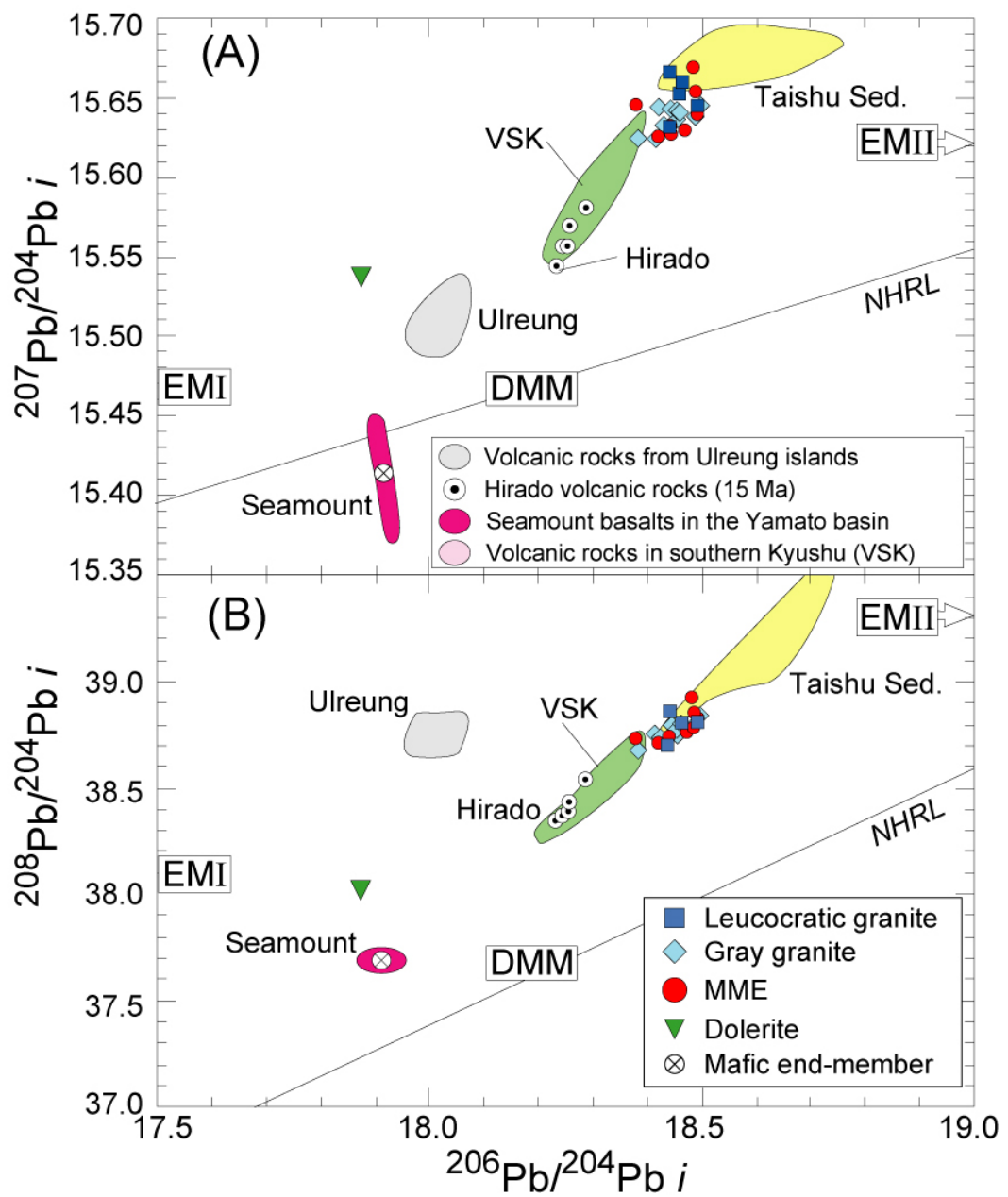
60

Figure 8.3. Initial Pb isotopic composition of the Tsushima granites. Data sources are the same as those indicated in the caption of Figure 8.2. NHRL represents Northern Hemisphere reference line with Th/U = 4.0 (Hart, 1984).

Pb in fluid. However there is no Pb isotope data available for the granulite and hence no direct evidence to support the former possibility. Thus, a systematic Pb isotope study of granulites and other possible materials of the lower crust are necessary. The second possibility is that the TSUG-forming magma was contaminated with Pb from the Taishu sedimentary rocks through assimilation or fluid circulation. The possibility of assimilation involvement has been ruled out from field observation and geochemical and Sr-Nd isotopic signatures. The latter possibility of fluid involvement has generally been ruled out because the solidifying granitic magma can expel magmatic fluid into the surrounding rocks. Nevertheless, Shimada et al (2000) reported that the magnetic zoning of the Tsushima pluton was resulted from reduction of ferric iron by external volatile buffer system. Experiments showed that base metals (such as Cu, Zn, Mn, and Pb etc) strongly partitioned into the aqueous phase during the aqueous phase released from granitic melts (Holland, 1972; Urabe, 1984; Audétat et al., 2000). The partition ratio is highly correlated with chlorine concentration in aqueous phase. The high concentration of Cl in the Tsushima granites (Terashima and Ishihara, 1980) supports the elevated concentration of Pb in the fluid phase and their circulation through in the solidifying the Tsushima pluton. The presence of numerous miarolitic cavities in the TSUG supports the possible incorporation of Pb in the Taishu Group into the TSUG-forming magma by fluid circulation. Since Pb concentrations in the upper mantle are generally very low compared with those of crustal rocks, even a small amount of contamination by crustal materials can substantially affect the Pb isotopic ratios of mantle-derived mafic magma. Basalts from Hirado Island and the Hishikari area, which are likely little affected by upper crustal materials on the basis of Sr–Nd isotopes, are enriched in radiogenic Pb compared with the DMM and EMI (Figure 8.3).

62

8.3 Formation process of the TSUG

Figure 8.4 shows the relationship between the molar [Mg/(Mg+Fe)] value $\times$ 100 of the whole rock (Mg#) and the initial $^{87}Sr/^{86}Sr$ ratio of the TSUG. The MMEs plot along a line on the diagram (line A), forming an array. This result is consistent with the previously mentioned view that the MMEs were derived from two components, one being a mafic magma with low initial $^{87}Sr/^{86}Sr$ ratio and high Mg# value and the other a felsic magma with high initial $^{87}Sr/^{86}Sr$ ratio and low Mg# value. The former end member is considered to correspond to seamount basalt from the Yamato basin because the basalt plots on an extension of line A (Figure 8.4). On the other hand, most of the leucocratic and gray granites, excluding samples K-1c and U-7, have similar $^{87}Sr/^{86}Sr$ ratios but variable 1/Sr and Mg# values (Figure 8.4), thus forming another array (line B) on the diagram. The latter trend indicates that the two granites resulted from fractional crystallization of a felsic magma with a relatively uniform $^{87}Sr/^{86}Sr$ ratio. The 100/Mg# value discriminating the gray granite from the leucocratic one is about 3.0. We assume that this value corresponds to the other end member, a felsic magma with a high $^{87}Sr/^{86}Sr$ ratio, because it is located at the intersection of the two arrays in Figure 8.4. The exceptional granites, samples K-1c and U-7, plot apart from the other granites. Thus, the higher $^{87}Sr/^{86}Sr$ ratio of the two granites might be attributable to contamination by Taishu Group sedimentary rocks.

Although the gray granite has abundant plagioclase and quartz phenocrysts, its composition is more mafic than that of the leucocratic granite because the groundmass of the gray granite is rich in hornblende. The similar $^{87}Sr/^{86}Sr$ ratios of the gray and leucocratic granites are consistent with the inference that the hornblende may have precipitated from the gray granite magma at a high-temperature stage and was not derived from the mafic magma. The quartz and plagioclase phenocryst minerals and the groundmass hornblende in the gray granite may have accumulated by melt flow. The
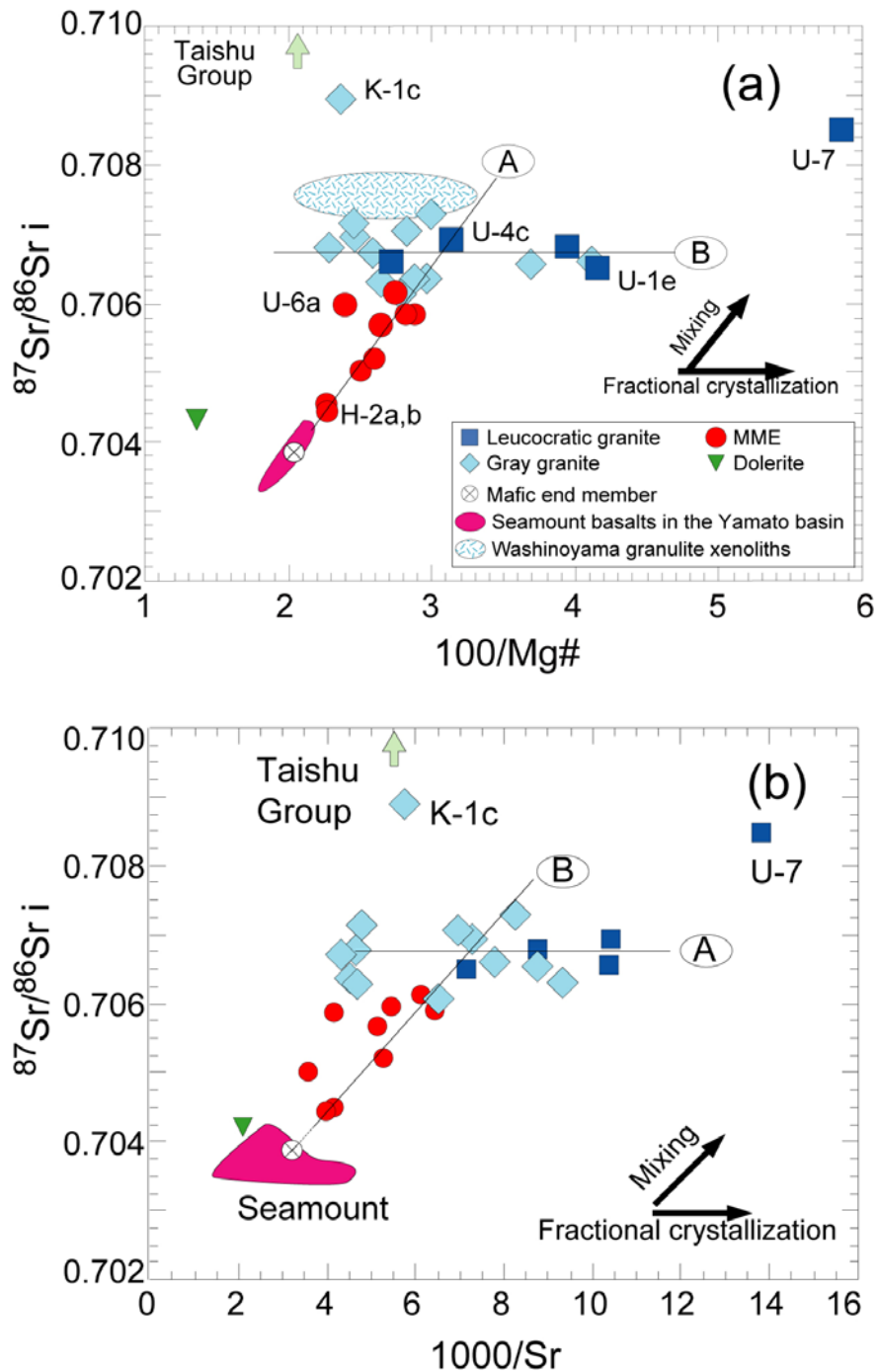
Figure 8.4. (a) Initial Sr isotopic ratio vs. 100/Mg# diagram. Lines A and B represent the mixing trend and the fractional crystallization trend, respectively. Mg#, 100 × molar [Mg/(Mg+Fe)] value of whole rock. Data for the seamount basalts of the Yamato basin are from Tatsumoto and Nakamura (1991), and data for the Washinoyama granulite xenoliths are from Kagami *et al.* (1995). (b) Initial Sr isotopic ratio vs. 1000/Sr diagram.

occurrence of the gray granite, restricted to between leucocratic granite and MMEs, and the presence of flow foliations in the gray granite may also suggest that mechanical mingling near the emplacement level were responsible for the formation of this granite (Figure 8.5). The higher SiO_2 contents and lower Mg# values of the leucocratic granite compared with the gray granite also suggest that the leucocratic granite formed at later stages, after the solidification of the gray granite around the MMEs.

The granulites, which have a more mafic composition and higher initial $^{87}Sr/^{86}Sr$ ratios than the TSUG granites, do not plot on the MME mixing line (Figure 8.4). In our previous discussion of the Sr–Nd isotopic system, we suggested that the felsic magma of the TSUG formed by partial melting of metabasic rocks as a result of heating by intrusions of mafic magmas with EMI composition and that the granulite was left behind as a restite. If the felsic magma was derived from metabasic rocks and the EMI component, we can estimate the contribution of each component by simple comparison of $^{87}Sr/^{86}Sr$ ratios among the TSUG granite (0.7068), granulite (0.7076), and EMI components (0.7055). We calculated the proportion of EMI-derived Sr in the felsic magma to be 0.38. As the concentration of Sr in basalt is in general two or three times that in granite (Faure & Mensing, 2005), the estimated EMI contribution is around 20% at maximum, suggesting that the felsic magma derived largely from the partial melting of the metabasic rocks.

High K_2O/Na_2O and Rb/Sr ratios in the leucocratic granites imply that the source rocks were enriched in K and Rb and that they probably contained biotite. The chemical features of the leucocratic granites can be explained by assuming partial melting of metabasic rocks with high K contents. Relatively hydrous basaltic rocks with medium to high K contents have been reported to generate a metaluminous to weakly peraluminous granitic melt with 4–5 wt. % K_2O by a low degree of partial melting (Sisson *et al.*, 2005). In addition, a partial melting of metabasic rocks without garnet can explain the REE
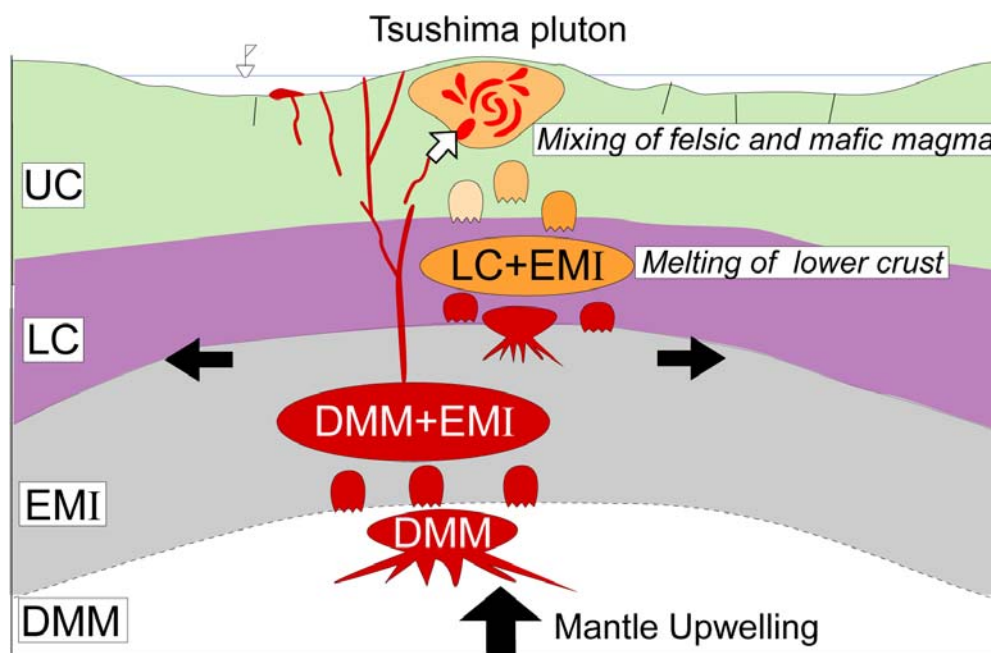
Figure 8.5. Schematic illustration of the generation of felsic and mafic magmas in the back arc region. Abbreviations: UC, upper crust; LC, lower crust; EM, enriched mantle; DMM, depleted MORB mantle.

patterns of the leucocratic granites: relatively flat heavy REE (HREE) patterns with a pronounced negative Eu anomaly. These results support the view that partial melting of metabasic rocks in the lower crust was responsible for the generation of the felsic magma for the TSUG and residual granulites. This partial melting would have been induced by injection of basaltic magma derived from the underlying mantle with EMI composition.

8.4 Fluid generation and chemical modification

The presence of numerous miarolitic cavities in the gray and leucocratic granites strongly indicate enrichment of volatiles and fluid generation during magma mixing. Fluid generation and elemental transport by fluid may have affected the trace-element contents in the TSUG. Their Rb content was positively correlated with the modal content of biotite (Figure 5.6), whereas it showed no correlation with alkali feldspar or plagioclase. The high contents of Rb and K in the MMEs are attributable to the replacement of amphibole by biotite, implying mineral–fluid interaction (e.g., Johnston & Wyllie, 1988). The large amount of biotite in the MMEs also explains the U-shaped trend of the Rb/Sr ratios vs. SiO_2 (Figure 5.5). The MMEs with the highest Rb (samples U-8a and H-3a) also had high K_2O, and Cs contents. These alkali elements are commonly enriched in granites and are easily mobilized via fluid flow.

We estimated the hydrothermal fluid to be enriched in B and Cl as well as in alkali elements from the mineral assemblages of the miarolitic cavities and the hypersaline fluid inclusions. In addition, the similarity of the present $^{87}Sr/^{86}Sr$ ratios between the aplite dike and zeolite–zoisite cavity in the Tsushima pluton (0.70730 and 0.70848 in Table 5.3) and the leucocratic granite indicates that the fluid was Sr-isotopically magmatic in origin. A shallower intrusion might generate hypersaline fluid by the boiling of magmatic fluids due to decompression. The fluids expelled from the granite magmas might generate a

67

convecting hydrothermal system in the surrounding rocks, whose mobile elements might thus have been incorporated into the magmas.

Taking the presence of fluid during the latest magmatic stage and the greater mobility of Pb in fluids into account, Pb isotopic ratios in the TSUG may be affected by hydrothermal fluid. The Pb isotope ratios of the TSUG are similar to those of the sedimentary rocks of the Taishu Group (Figure 8.3). This finding seems to suggest that radiogenic Pb in the TSUG magmas was incorporated from the Taishu sediments by fluid transport rather than from felsic magma of lower-crust origin, as Hosono *et al.* (2003) proposed. Rapid crystallization of the MMEs during magma mingling and mixing, which was enhanced by rapid cooling of the TSUG magma system as a result of the shallow intrusion, may have nicely preserved records of fluid release and rock–fluid interaction. The shallow intrusion and rapid cooling of the TSUG-forming magma would have been enhanced by the crustal thinning associated with the opening of the Japan Sea (Tamaki *et al.*, 1992).

9. COMPARISON BETWEEN THE TSUSHIMA GRANITE AND THE OUTER ZONE GRANITES

9.1 Geology and General feature of the Outer Zone granites

The Outer Zone is composed of three east-west trending tectonic provinces; Sambagawa metamorphic belt, Chichibu-Sanbosan belt, and Shimanto belt (Sugimura and Uyeda, 1973; Figure 1.2). The rocks of the Sambagawa metamorphic belt are composed of Triassic mafic volcanic rocks with some sandstone and shales. The Chichibu-Sanbosan belt is composed of Jurassic sandstones and shales with minor cherts and mafic volcanic rocks. Shimanto belt consists of Cretaceous-Paleogene sedimentary rocks of sandstones and shales with minor conglomerates, limestones, cherts and submarine mafic volcanic.

The Outer Zone granites of Middle Miocene ages, contemporaneous to the Tsushima pluton, are distributed widely in the forearc region of Southwest Japan (Figure 1.2). Most of the Outer Zone granites are emplaced into the Shimanto Group; the Yakushima granite in the western end of the Outer Zone, through the Osumi granite, the Takakumayama granite, the Shibisan granite, the Ichifusayama granite, the Osuzuyama granite, the Okueyama granite, the Okinoshima granite, the Kashiwajima granite, the Mimaki granite, the Takatsuki (Uwajima) granite, the Omine granite, the Kumano granite, and the Kaikoma granite in the eastern end of the Outer Zone. The Ishizuchiyama granite in Shikoku islands intruded into the Sanbagawa belt. The Obira granite in Kyushu and northern part of the Ohmine granite in the Kinki district intruded into the Chichibu-Sanbosan belt.

All the Outer Zone granites are classified as calc-alkaline and ilmenite-series granites, except the Ashizuri alkaline rocks. The calk-alkaline granites are subdivided into two types; the I-type granites with hornblende-bearing mineral assemblages distributed in

the northern area, and the S-type granites in the southern area with cordierite as a typical peraluminous mineral. These rocks have contents of K_2O, total Fe and normative corundum increasing toward the Pacific Ocean (Nakada and Takahashi, 1979). This regional variation was attributed to the degree of contamination of the sedimentary rocks of the Shimanto Group in the upper crust (Nakada and Takahashi, 1979; Nakada and Okamoto, 1984).

The Outer Zone granites were deduced to develop by mixing of basaltic to high magnesian andesitic magma of mantle origin with the sedimentary rocks of Shimanto belt based on Sr-Nd isotopic studies (Terakado et al., 1988; Stein et al., 1994; Shinjoe, 1997). Ishihara and Matsuhisa (1999) suggested similar processes based on oxygen isotopic ratios. They also estimated about 30-64 wt% contributions of the sedimentary rocks to form the granite melts. Dai et al. (1993) suggest that the granitic magma that formed the Kashiwajima-Okinoshima pluton were generated by partial melting of meta-sedimentary rocks at a depth of about 20 km, and then mixed with Shimanto sedimentary rocks. Anma et al. (1998) suggested that the magmas that formed the Yakushima pluton were developed along the top surface of the subducting plate by dehydration-enhanced melting of oceanic plate and sediments sank with the subducting slab, and then rose obliquely toward inner-wall of trench axis as a diapir.

9.2 Samples and Analytical Process

To compare the Tsushima granite with the Outer Zone granites, the author analyzed representative 31 powered rocks samples collected from 12 granites (the Takakumayama, Shibisan, Ichifusayama, Osuzuyama, Okueyama, Obira, Okinoshima, Kashiwajima, Mimaki, Takatsuki, Ishizuchiyama, and Kumano granites; see Table 9.1) by Dr. Ishihara. The mineral assemblages, major elements, and oxygen isotope compositions of the

Table 9.1 Chemical compositions of the Outer Zone granites.

Sample	Takakumayama		Shibisan			Ichifusayama		
	57T-305	57Z-111	SB1601	SB1602	SB1705	75KY-115	75KY-116	75KY-118
SiO_2*1	73.76	68.00	67.06	66.17	66.61	67.28	78.67	65.03
TiO_2	0.04	0.28	0.61	0.66	0.74	0.67	0.41	0.66
Al_2O_3	14.65	16.59	15.59	15.88	15.38	15.00	9.50	15.85
FeO^T	0.99	2.54	3.67	4.10	3.74	4.39	2.30	4.67
MnO	0.09	0.06	0.07	0.07	0.06	0.10	0.05	0.09
MgO	0.31	0.88	1.13	1.33	1.17	2.22	0.87	2.30
CaO	0.85	2.67	2.90	2.44	3.16	3.23	1.18	3.50
Na_2O	3.85	3.19	3.38	3.34	3.44	2.52	1.84	3.07
K_2O	4.25	4.07	4.42	4.46	4.08	2.95	3.80	2.94
P_2O_5	0.03	0.08	0.18	0.20	0.17	0.12	0.06	0.15
Total	98.82	98.36	99.01	98.65	98.55	98.48	98.68	98.26
ASI*2	1.17	1.14	1.00	1.08	0.97	1.14	1.02	1.09
Ba*3	38.0	487	827	931	763	529	891	535
Rb	573	198	194	201	181	128	104	128
Sr	15.4	155	217	214	235	198	179	219
Cs	59.5	17.7	9.74	11.5	8.92	7.65	3.35	5.51
Ta	9.60	1.78	3.32	3.40	3.06	1.28	0.82	1.42
Nb	18.9	12.9	33.9	35.0	31.3	14.2	7.62	15.8
Hf	4.49	4.67	5.54	5.49	5.83	4.58	5.89	5.29
Zr	61.5	147	212	210	220	179	229	212
Y	102	38.2	25.0	23.8	23.6	20.9	12.6	23.3
Th	19.0	24.8	27.8	17.7	16.9	9.23	7.28	10.6
U	15.4	4.93	5.79	1.96	3.93	2.06	1.78	2.21
Sc	7.99	9.92	9.40	8.18	8.63	14.0	5.41	13.6
Pb	115	30.9	17.9	29.2	15.2	21.8	13.6	19.9
La	18.2	44.7	66.6	53.0	46.6	30.5	24.9	32.2
Ce	45.2	90.5	111	91.5	79.4	59.8	45.9	61.8
Pr	5.70	9.80	10.9	9.49	8.01	6.46	5.11	6.65
Nd	23.7	39.2	39.0	35.1	30.2	24.6	19.4	25.4
Sm	10.2	8.22	6.59	6.28	5.46	4.70	3.51	5.00
Eu	0.08	0.92	1.20	1.37	1.23	1.12	0.78	1.22
Gd	11.3	6.90	4.94	4.90	4.41	3.92	2.76	4.01
Tb	2.50	1.17	0.80	0.74	0.72	0.64	0.41	0.70
Dy	17.1	6.77	4.53	4.31	4.19	3.91	2.28	4.35
Ho	3.72	1.40	0.91	0.87	0.87	0.80	0.47	0.90
Er	11.2	3.76	2.48	2.31	2.50	2.07	1.34	2.34
Tm	1.89	0.57	0.38	0.36	0.36	0.32	0.20	0.35
Yb	15.1	4.02	2.74	2.63	2.56	2.19	1.31	2.49
Lu	2.13	0.54	0.41	0.38	0.40	0.31	0.22	0.37

Note: *1 Compositions are quoted in weight %. Total Fe as FeO^T. *2 ASI: molar $Al_2O_3/(Na_2O+K_2O+CaO)$. *3 Concentrations are in weight ppm.

Table 9.1 (continued)

Sample	Osuzuyama			Okueyama				Obira		
	75KY-109	75KY-110	75KY-112	75OK-100	75OK-89	75OK-95	75OK-98	75OB-59	75OB-60	75OB-65
SiO_2	67.95	75.23	70.53	75.89	65.82	72.44	76.26	75.45	58.22	66.97
TiO_2	0.71	0.08	0.36	0.17	0.69	0.27	0.06	0.15	1.03	0.77
Al_2O_3	15.11	13.22	14.25	12.81	15.77	14.40	12.92	12.81	15.98	15.34
FeO^T	4.53	1.58	2.79	1.21	4.39	2.04	0.75	1.32	6.17	3.78
MnO	0.08	0.04	0.06	0.02	0.09	0.03	0.01	0.02	0.12	0.08
MgO	1.47	0.04	0.76	0.26	1.66	0.51	0.04	0.18	5.22	1.04
CaO	2.33	0.30	1.48	0.84	3.84	1.60	0.34	0.96	6.50	3.12
Na_2O	3.15	2.86	2.87	2.86	3.40	3.12	3.11	3.35	3.32	3.95
K_2O	3.30	5.24	4.20	5.38	3.50	4.95	5.95	4.82	2.16	3.52
P_2O_5	0.17	0.20	0.17	0.02	0.14	0.06	0.01	0.02	0.27	0.15
Total	98.80	98.79	97.47	99.46	99.30	99.42	99.45	99.08	98.99	98.72
ASI	1.16	1.21	1.19	1.06	0.96	1.07	1.06	1.03	0.81	0.96
Ba	621	79.0	682	189	628	383	23.0	268	445	669
Rb	158	207	155	288	153	202	386	225	87.0	149
Sr	153	24.3	101	43.8	222	95.7	5.62	51.4	298	229
Cs	12.4	9.53	3.69	15.7	9.60	10.9	8.44	13.9	6.86	9.46
Ta	1.23	1.39	1.20	2.57	1.50	1.94	4.26	1.74	0.88	1.20
Nb	14.8	8.53	11.5	15.0	18.5	14.1	19.4	12.7	10.0	13.9
Hf	7.53	1.89	5.36	3.90	5.88	4.72	3.63	4.73	3.79	7.71
Zr	306	48.0	197	102	232	149	62.3	123	150	318
Y	30.4	17.4	31.3	40.2	23.7	29.0	74.0	30.4	19.7	26.9
Th	14.0	4.30	11.9	20.1	7.08	13.7	22.1	17.4	6.01	11.5
U	2.53	4.20	3.05	7.14	1.78	4.43	14.2	4.45	1.71	2.83
Sc	11.7	2.62	8.01	5.91	12.5	6.88	4.50	5.29	19.4	12.8
Pb	27.4	21.2	27.3	26.4	16.0	15.4	36.2	29.5	18.2	17.5
La	44.2	5.52	29.9	33.7	32.2	26.1	19.8	37.8	23.1	39.9
Ce	90.5	12.7	60.9	66.2	60.3	49.2	44.7	76.2	47.4	78.9
Pr	9.71	1.53	6.79	7.03	6.56	5.03	5.11	8.08	5.19	8.44
Nd	39.1	5.17	26.7	26.1	26.3	19.5	20.7	30.6	21.7	33.0
Sm	7.69	1.83	6.13	5.67	5.33	4.38	6.64	6.40	4.65	6.49
Eu	1.12	0.20	0.81	0.29	1.05	0.55	0.04	0.29	1.23	1.30
Gd	6.21	2.29	5.44	5.19	4.50	4.09	7.81	5.83	3.94	5.21
Tb	0.98	0.46	0.94	1.05	0.72	0.78	1.70	0.90	0.63	0.86
Dy	5.66	3.30	5.65	6.94	4.38	5.02	12.1	5.40	3.69	4.92
Ho	1.17	0.64	1.18	1.46	0.90	1.03	2.61	1.14	0.76	1.02
Er	3.04	1.84	3.20	4.08	2.45	2.93	7.50	3.14	2.06	2.75
Tm	0.45	0.34	0.45	0.62	0.35	0.44	1.16	0.45	0.30	0.40
Yb	3.18	2.16	3.19	4.50	2.47	3.00	8.20	3.21	2.03	2.98
Lu	0.45	0.38	0.44	0.65	0.36	0.40	1.14	0.45	0.29	0.42

72

Table 9.1 (continued)

Sample	Okinoshima			Kashiwajima			Mimaki	Takatsukiyama	
	58A-302	58A-303	58A-309	58A-328	58A-331	58A-336	70S-97	75TS-38	75TS-44W
SiO_2	68.00	65.74	75.23	72.70	69.43	69.88	73.51	66.61	65.92
TiO_2	0.76	0.99	0.13	0.25	0.52	0.55	0.27	0.79	0.75
Al_2O_3	14.95	15.42	13.48	14.30	14.98	14.66	13.73	15.35	15.49
FeO^T	3.95	4.60	1.26	2.15	2.61	2.48	1.29	3.99	4.03
MnO	0.09	0.10	0.03	0.04	0.09	0.04	0.03	0.14	0.11
MgO	1.20	1.73	0.07	0.25	0.82	1.19	0.59	1.85	1.95
CaO	2.55	3.37	0.92	1.36	2.31	2.18	1.47	3.20	3.55
Na_2O	3.20	3.24	3.42	3.43	3.00	3.04	2.80	2.92	2.88
K_2O	3.24	2.78	4.70	4.25	4.49	4.30	4.99	3.90	3.70
P_2O_5	0.14	0.20	0.04	0.07	0.13	0.11	0.06	0.14	0.14
Total	98.08	98.17	99.28	98.80	98.38	98.43	98.74	98.89	98.52
ASI	1.12	1.07	1.09	1.12	1.07	1.08	1.08	1.03	1.02
Ba	580	490	438	581	508	558	253	597	595
Rb	126	133	192	177	189	143	181	158	141
Sr	155	186	61.3	90.4	155	180	93.7	210	221
Cs	6.52	7.14	9.50	11.7	16.8	9.45	12.5	13.5	8.97
Ta	1.08	1.19	0.89	0.92	1.58	2.21	1.92	1.66	1.57
Nb	11.5	12.9	8.20	9.26	14.6	15.2	9.45	16.2	16.3
Hf	5.86	4.92	3.80	4.73	5.26	5.71	4.30	5.74	5.65
Zr	217	197	115	165	185	195	115	220	214
Y	28.9	24.8	35.4	36.8	21.9	26.0	33.5	25.1	24.4
Th	12.2	7.80	11.4	12.2	17.1	16.7	23.7	13.2	12.7
U	1.82	2.55	2.84	3.64	4.03	4.81	6.11	3.24	3.12
Sc	12.9	12.7	7.13	9.33	8.17	8.93	4.95	11.9	12.2
Pb	20.6	21.8	30.4	34.2	83.9	13.0	39.4	96.7	14.9
La	33.9	29.6	22.2	31.7	36.9	41.0	38.2	38.9	38.3
Ce	69.9	61.2	48.6	66.8	71.5	79.4	78.3	74.8	73.7
Pr	7.48	6.72	5.34	7.14	7.36	8.27	8.22	7.87	7.72
Nd	30.3	27.7	21.0	29.5	27.2	30.1	29.3	29.8	29.9
Sm	5.92	5.75	5.39	6.44	4.88	5.58	5.85	5.57	5.61
Eu	1.13	1.23	0.47	0.73	0.83	0.94	0.47	1.11	1.14
Gd	5.42	4.75	5.09	6.02	4.17	4.72	4.72	4.86	4.52
Tb	0.89	0.78	0.97	1.03	0.67	0.75	0.87	0.77	0.76
Dy	5.28	4.58	6.28	6.60	3.89	4.54	5.40	4.55	4.40
Ho	1.10	0.94	1.35	1.39	0.83	0.94	1.17	0.96	0.92
Er	2.95	2.47	3.57	3.81	2.24	2.74	3.56	2.52	2.39
Tm	0.47	0.38	0.51	0.57	0.33	0.42	0.58	0.38	0.35
Yb	3.35	2.73	3.74	3.76	2.49	2.74	4.14	2.69	2.53
Lu	0.46	0.36	0.50	0.55	0.34	0.43	0.58	0.40	0.38

73

Table 9.1 (continued)

Sample	Ishizuchiyama		Kumano	
	70S-303	70S-304	kumano-4	kumano-5
SiO_2	64.58	73.06	70.13	74.17
TiO_2	0.74	0.18	0.61	0.23
Al_2O_3	16.42	14.53	14.54	13.55
FeO^T	4.24	1.76	3.01	1.90
MnO	0.11	0.04	0.05	0.03
MgO	2.04	0.29	1.09	0.64
CaO	3.52	1.08	1.85	0.60
Na_2O	3.34	3.66	3.48	2.65
K_2O	3.60	4.61	3.52	4.83
P_2O_5	0.15	0.04	0.16	0.15
Total	98.74	99.25	98.78	98.97
ASI	1.04	1.12	1.13	1.27
Ba	564	392	749	379
Rb	136	195	122	168
Sr	214	63.8	179	49.5
Cs	8.32	13.6	4.67	5.02
Ta	1.33	1.46	1.10	0.99
Nb	14.0	12.8	11.4	7.14
Hf	4.58	3.45	6.51	2.93
Zr	175	90.8	246	91.0
Y	19.9	14.7	28.8	28.5
Th	10.5	11.7	15.4	7.55
U	2.49	3.35	2.57	3.76
Sc	10.7	5.46	9.44	4.75
Pb	20.3	39.0	17.1	18.3
La	31.6	24.9	39.3	14.0
Ce	63.9	53.7	81.4	30.1
Pr	6.54	5.73	8.66	3.31
Nd	26.0	22.2	35.0	13.3
Sm	4.84	5.23	7.05	3.50
Eu	1.09	0.43	1.05	0.41
Gd	4.11	4.27	6.03	3.54
Tb	0.62	0.65	0.95	0.72
Dy	3.64	3.28	5.50	4.74
Ho	0.75	0.50	1.13	1.03
Er	2.04	1.07	3.04	2.90
Tm	0.28	0.14	0.46	0.43
Yb	2.05	0.87	2.90	2.97
Lu	0.29	0.12	0.43	0.41

provided samples were reported by Ishihara and Matsuhisa (1999).

The author analyzed trace-elements and Sr-Nd-Pb isotopic compositions using LAN-ICP-MS and TIMS, respectively. The sample preparation and analytical procedure is the same as those for the TSUG. The measured $^{87}Sr/^{86}Sr$ and $^{143}Nd/^{144}Nd$ ratios were normalized to $^{86}Sr/^{88}Sr$ = 0.1194 and $^{146}Nd/^{144}Nd$ = 0.7219, respectively. The $^{86}Sr/^{88}Sr$ values of NIST-SRM987 throughout the analyses were 0.710256 ± 0.000012 (2σ, n = 10). The $^{143}Nd/^{144}Nd$ ratios of the Johnson Mass standard materials were 0.511301 ± 0.00001 (2σ, n = 6), respectively. Precision for the present analyses was better than ±0.000025 (2σ) for $^{87}Sr/^{86}Sr$ and ±0.00002 (2σ) for $^{143}Nd/^{144}Nd$. The Pb isotope ratios were normalized to NIST-SRM981 values ($^{206}Pb/^{204}Pb$ = 16.9390, $^{207}Pb/^{204}Pb$ = 15.4963, $^{208}Pb/^{204}Pb$ = 36.7206). The mean values of NIST-SRM981 throughout this study (n = 14) were $^{206}Pb/^{204}Pb$= 16.9110 ± 0.0015 (2σ), $^{207}Pb/^{204}Pb$= 15.4601 ± 0.0017 (2σ), and $^{208}Pb/^{204}Pb$= 36.5878 ± 0.0041 (2σ).

9.3 Whole rock geochemistry of the Outer Zone granites

Major and trace-element compositions of the Outer Zone granites are listed in Table 9.1. The SiO_2 contents range from 58 to 78 wt.%. The newly analyzed samples of the Outer Zone granites show good correlation with reference data of the Outer Zone granites (e.g., Aramaki *et al*., 1972; Nakada, 1983; Okamoto *et al*., 1987; Tsusue *et al*., 1987; Dai *et al*., 1993; Stein et al., 1994; Shinjoe, 1997; Anma *et al*., 1998; Shinjoe et al., 2007) (Figure 9.1). Thus the author uses these newly analyzed data to represent geochemical features of the Outer Zone granites.

The major element concentrations of the Outer Zone granites are comparable to those of the TSUG. Only CaO contents are slightly lower than that of the TSUG at the same SiO_2 content (Figure 9.2). Trace and rare-earth element (REE) contents in the TSUG
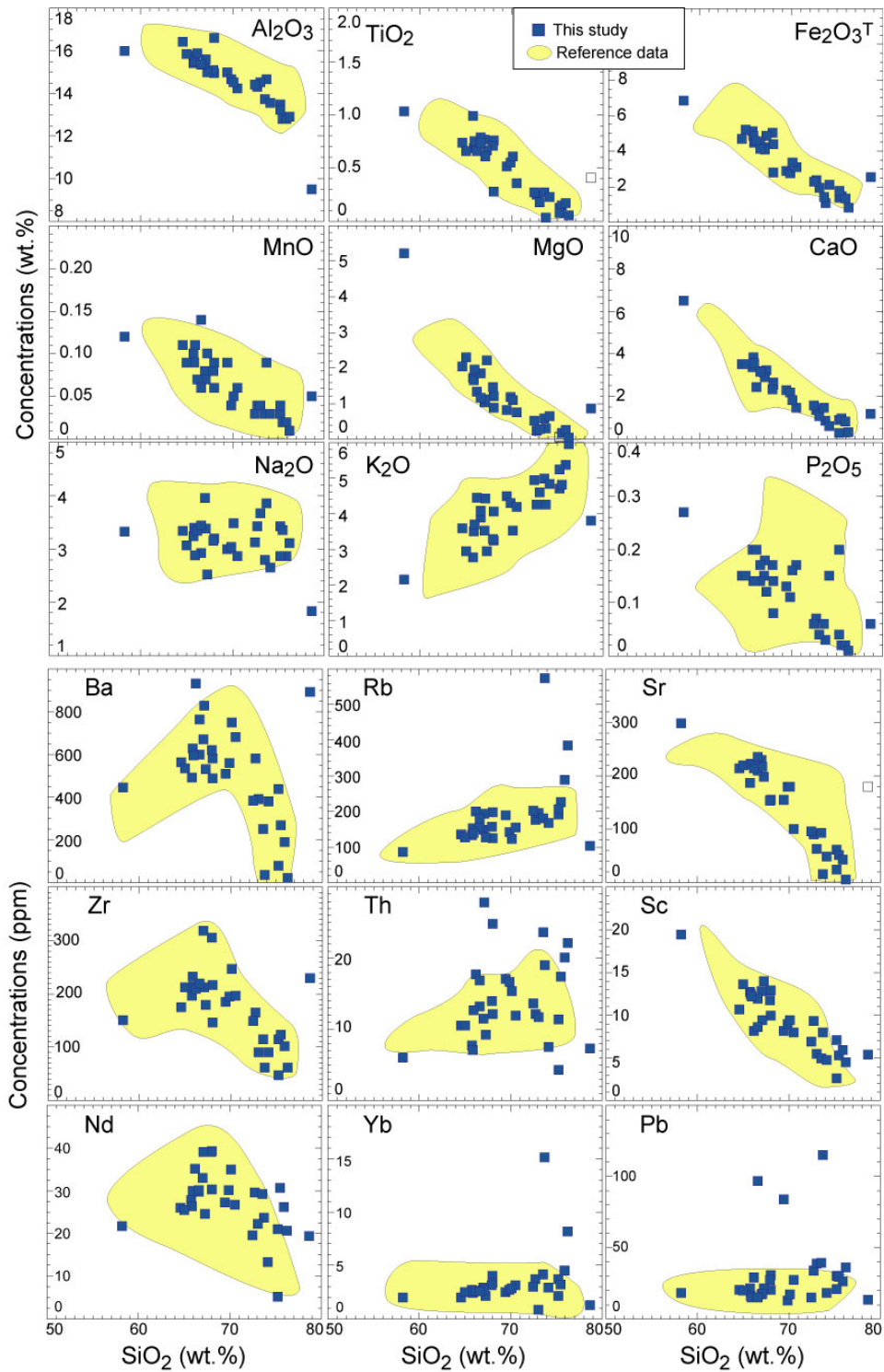
Figure 9.1 Chemical composition of newly analyzed data and reference data of the Outer Zone granites. Data sources: Aramaki *et al*., 1972; Nakada, 1983; Okamoto *et al*., 1987; Tsusue *et al*., 1987; Dai *et al*., 1993; Stein *et al*., 1994; Shinjoe, 1997; Anma *et al*., 1998; Shinjoe *et al*., 2007

are in part comparable to those of the Outer Zone granites (Figure 9.2). The TSUG have lower Rb and Pb content than those of the Outer Zone granites (Figure 9.2). Nb, Cs, and Ta contents are slightly lower in the TSUG, whereas Sc content is slightly higher (Figure 9.2) than other Outer Zone granites. Ba content of the TSUG positively correlated with increasing SiO_2 contents, whereas the Outer Zone granites show negative correlation with SiO2 contents (Figure 9.2). The patterns of Ba contents suggest either different crystallization behavior of alkali feldspar during fractional crystallization or different degree of sedimentary assimilations. In high silica range (> 70 wt. % SiO_2), Sr content is higher in TSUG than those of the Outer Zone granites (Figure 9.2).
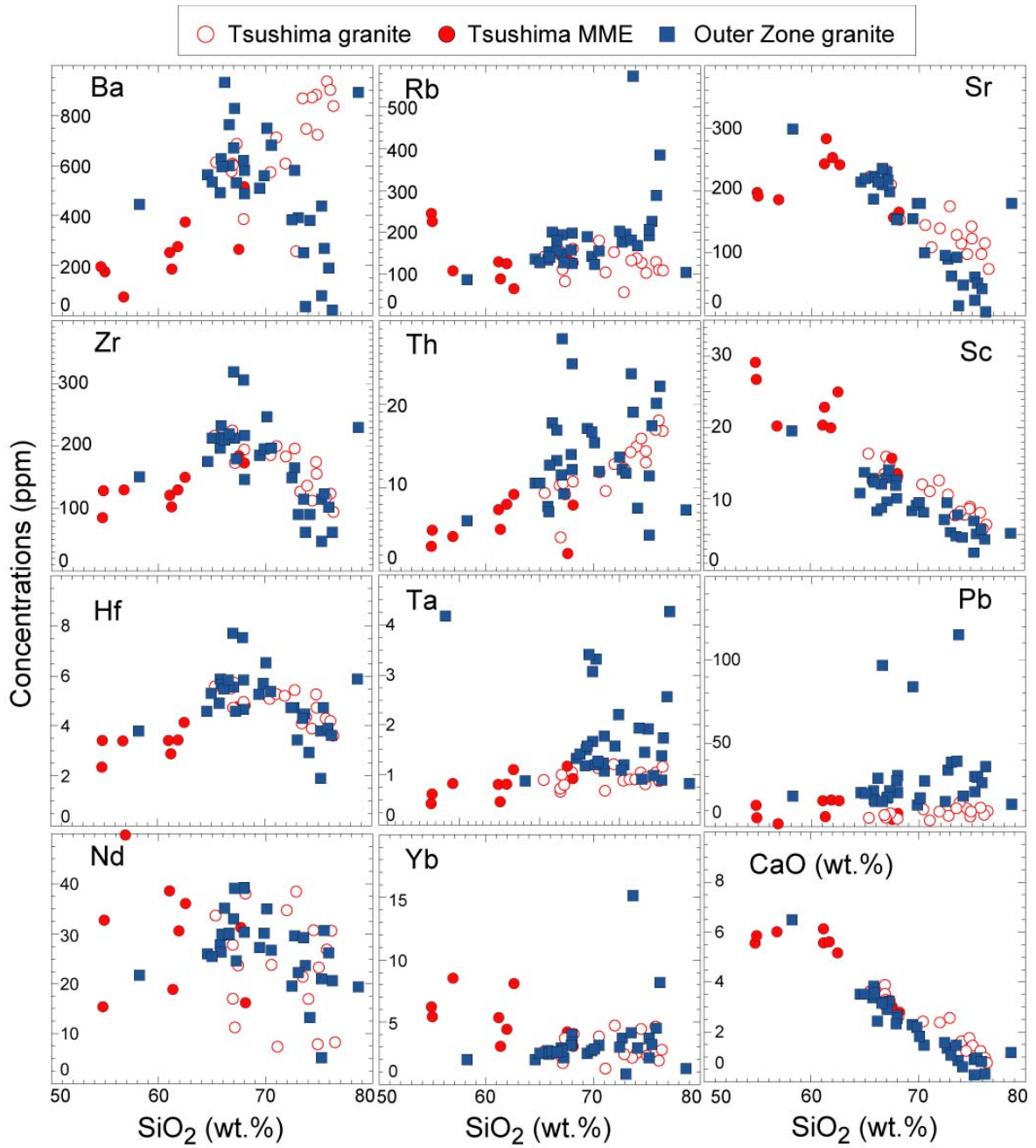
Figure 9.2 Elements variation diagrams of the TSUG and the Outer Zone granites.

9.4 Sr-Nd-Pb isotope compositions of the Middle Miocene granites

Sr-Nd isotope compositions of the Outer Zone granites are listed in Table 9.2. Initial Sr-Nd isotopic ratios of the newly analyzed rock samples plot in slightly wider field compared to the reference data of the Outer Zone granites (Terakado *et al*., 1988; Dai *et al*., 1993; Stein et al., 1994; Shinjoe, 1997; Anma *et al*., 1998) (Figure 9.3). The granites from Shibisan pluton have the highest $\varepsilon_{Nd}(t)$ values among the Outer Zone granites. Most of the Outer Zone granites plot on an array that extended from the field of high-Mg andesite of mantle origin (Shimoda, 1998; Tatsumi et al., 2003) to the field of Shimanto sedimentary rocks. Several samples have lower $\varepsilon_{Nd}(t)$ values and plot in a lower field of the array in the Sr-Nd diagram (Figure 9.3). One sample of the Ichifusayama has extremely high initial $^{87}Sr/^{86}Sr$ ratio (0.71590) and low $\varepsilon_{Nd}(t)$ value (-14.6).

Unlike the Outer Zone granites, the TSUG granites have relatively restricted and lower isotopic ranges than those of the Outer Zone granites (Figure 9.3), and most are plotted on a mixing array between the mafic magma of mantle origin (Seamount and VSK in Figure 8.2) and the lower crust component (IZLC in Figure 8.2). The MMEs in the Tsushima pluton have lower $^{87}Sr/^{86}Sr$ ratios, and slightly higher $\varepsilon_{Nd}(t)$ values than those of the Middle Miocene plutons of Southwest Japan (Figure 9.3).

The Outer Zone granites have scattered Pb isotopic ratios (Figure 9.4), ranging from 18.035 to 18.449 for $^{206}Pb/^{204}Pb$, 15.573 to 15.642 for $^{207}Pb/^{204}Pb$, and 38.549 to 38.857 for $^{208}Pb/^{204}Pb$. These values are relatively less radiogenic than those of the TSUG and the Shimanto sedimentary rocks. Several samples of the Osuzuyama and Ichifusayama granites have low $^{206}Pb/^{204}Pb$ ratios to plot on the left side from the other granites in the $^{207}Pb/^{204}Pb$-$^{206}Pb/^{204}Pb$ diagram (Figure 9.4).

Table 9.2. Sr, Nd, Pb isotopic data for the Middle Miocene granitic rocks.

	SAMPLE	$^{87}Sr/^{86}Sr$	$^{143}Nd/^{144}Nd$	$^{87}Sr/^{86}Sr\ i$[*1]	$^{143}Nd/^{144}Nd\ i$	$\varepsilon_{Nd\ i}$[*2]
Takakumayama	57T-305	0.728047 (± 10)	0.512264 (± 6)	0.706601	0.512240	-7.4
	57Z-111	0.709233 (± 11)	0.512268 (± 6)	0.708498	0.512256	-7.1
Shibisan	SB1601	0.705986 (± 10)	0.512548 (± 5)	0.705472	0.512539	-1.6
	SB1602	0.707509 (± 13)	0.512460 (± 5)	0.706969	0.512450	-3.3
	SB1705	0.706181 (± 10)	0.512528 (± 5)	0.705738	0.512518	-2.0
Ichifusayama	75KY-115	0.710867 (± 10)	0.512220 (± 5)	0.710495	0.512209	-8.0
	75KY-116	0.716239 (± 09)	0.511880 (± 4)	0.715905	0.511870	-14.6
	75KY-118	0.709047 (± 10)	0.512333 (± 6)	0.708711	0.512322	-5.8
Osuzuyama	75KY-109	0.710317 (± 09)	0.512343 (± 5)	0.709723	0.512332	-5.6
	75KY-110	0.715761 (± 09)	0.512351(± 21)	0.710857	0.512331	-5.6
	75KY-112	0.710314 (± 10)	0.512361 (± 5)	0.709431	0.512348	-5.3
Okueyama	75OK-100	0.710398 (± 11)	0.512454 (± 5)	0.706615	0.512442	-3.5
	75OK-89	0.706121 (± 10)	0.512489 (± 6)	0.705725	0.512478	-2.8
	75OK-95	0.707730 (± 08)	0.512498 (± 6)	0.706516	0.512486	-2.6
	75OK-98	0.745507 (± 10)	0.512467 (± 5)	0.705852	0.512449	-3.3
Obira	75OB-59	0.709871 (± 09)	0.512397 (± 4)	0.707352	0.512385	-4.6
	75OB-60	0.706020 (± 08)	0.512470 (± 5)	0.705852	0.512458	-3.2
	75OB-65	0.707352 (± 11)	0.512396 (± 5)	0.706978	0.512385	-4.6
Okinoshima	58A-302	0.709145 (± 11)	0.512361 (± 5)	0.708677	0.512350	-5.3
	58A-303	0.709472 (± 11)	0.512284 (± 5)	0.709061	0.512273	-6.8
	58A-309	0.709451 (± 19)	0.512388 (± 5)	0.707649	0.512374	-4.8
Kashiwajima	58A-328	0.708652 (± 10)	0.512373 (± 6)	0.707526	0.512361	-5.1
	58A-331	0.707392 (± 10)	0.512403(± 10)	0.706691	0.512393	-4.4
Mimaki	70S-97	0.707800 (± 10)	0.512389 (± 9)	0.706689	0.512378	-4.7
Takatsukiyama	58A-336	0.707640 (± 13)	0.512416 (± 5)	0.707183	0.512406	-4.2
	75TS-38	0.707423 (± 12)	0.512394 (± 5)	0.706990	0.512384	-4.6
	75TS-44W	0.707421(± 12)	0.512403 (± 5)	0.707054	0.512393	-4.4
Ishizuchiyama	70S-303	0.706746 (± 15)	0.512453 (± 5)	0.706380	0.512443	-3.5
	70S-304	0.708299 (± 09)	0.512403 (± 5)	0.706541	0.512390	-4.5
Kumano	kumano-4	0.708225 (± 09)	0.512475 (± 6)	0.707833	0.512464	-3.0
	kumano-5	0.708622 (± 09)	0.512542 (± 5)	0.706670	0.512527	-1.8

Note: *1 $^{87}Sr/^{86}Sr_i$, $^{143}Nd/^{144}Nd_i$ $^{206}Pb/^{204}Pb_i$, $^{207}Pb/^{204}Pb_i$, $^{208}Pb/^{204}Pb_i$: age corrected for 14 Ma. *2 Nd_i: deviation in parts per 10^4 from bulk earth values at 14 Ma.

Table 9.2. (Continued)

| SAMPLE		$^{206}Pb/^{204}Pb$	$^{207}Pb/^{204}Pb$	$^{208}Pb/^{204}Pb$	$^{206}Pb/^{204}Pb\ i$	$^{207}Pb/^{204}Pb\ i$	$^{208}Pb/^{204}Pb\ i$
Takakuma yama	57T-305	18.4493 (± 18)	15.6153 (± 16)	38.7268 (± 41)	18.4308	15.6145	38.7192
	57Z-111	18.4434 (± 14)	15.6253 (± 12)	38.7870 (± 29)	18.4213	15.6242	38.7503
Shibisan	SB1601	18.4507 (± 11)	15.6043 (± 10)	38.7547 (± 25)	18.4059	15.6023	38.6838
	SB1602	18.4590 (± 21)	15.6255 (± 20)	38.7914 (± 57)	18.4497	15.6251	38.7637
	SB1705	18.4819 (± 17)	15.6441 (± 14)	38.8668 (± 36)	18.4459	15.6424	38.8160
Ichifusa yama	75KY-115	18.3860 (± 35)	15.6191 (± 34)	38.7692 (± 91)	18.3729	15.6185	38.7499
	75KY-116	18.0534 (± 17)	15.5865 (± 17)	38.6273 (± 46)	18.0354	15.5857	38.6030
	75KY-118	18.4044 (± 20)	15.6281 (± 18)	38.7760 (± 49)	18.3890	15.6274	38.7517
Osuzu yama	75KY-109	18.1753 (± 15)	15.5769 (± 13)	38.5728 (± 34)	18.1625	15.5764	38.5497
	75KY-110	18.3542 (± 34)	15.6240 (± 29)	38.7556 (± 72)	18.3268	15.6227	38.7464
	75KY-112	18.3854 (± 14)	15.6142 (± 12)	38.7312 (± 30)	18.3700	15.6135	38.7113
Okueyama	75OK-100	18.4294 (± 16)	15.6313 (± 13)	38.7672 (± 33)	18.3919	15.6295	38.7324
	75OK-89	18.3795 (± 16)	15.6176 (± 15)	38.6944 (± 37)	18.3641	15.6169	38.6742
	75OK-95	18.4087 (± 14)	15.6272 (± 12)	38.7448 (± 31)	18.3689	15.6254	38.7042
	75OK-98	18.4226 (± 20)	15.6207 (± 18)	38.7193 (± 49)	18.3683	15.6182	38.6915
Obira	75OB-59	18.3884 (± 20)	15.6091 (± 20)	38.7017 (± 53)	18.3675	15.6081	38.6748
	75OB-60	18.3869 (± 26)	15.6150 (± 25)	38.6940 (± 71)	18.3739	15.6144	38.6789
	75OB-65	18.4034 (± 13)	15.6177 (± 11)	38.7161 (± 30)	18.3810	15.6166	38.6861
Okino shima	58A-302	18.4274 (± 19)	15.6202 (± 16)	38.7556 (± 41)	18.4152	15.6197	38.7285
	58A-303	18.4079 (± 18)	15.5355 (± 13)	38.8737 (± 30)	18.3917	15.5347	38.8574
	58A-309	18.4331 (± 53)	15.6074 (± 45)	38.674 (± 111)	18.4201	15.6069	38.6574
Kashiwa jima	58A-328	18.4215 (± 18)	15.6017 (± 18)	38.7212 (± 53)	18.4068	15.6011	38.7049
	58A-331	18.3560 (± 23)	15.6002 (± 21)	38.6490 (± 53)	18.3494	15.5999	38.6397
Mimaki	70S-97	18.3669 (± 18)	15.5880 (± 16)	38.6238 (± 41)	18.3455	15.5870	38.5965
Takatsuki yama	58A-336	18.4111 (± 18)	15.6145 (± 18)	38.7695 (± 51)	18.3599	15.6121	38.7109
	75TS-38	18.3824 (± 15)	15.5905 (± 14)	38.6221 (± 37)	18.3778	15.5903	38.6159
	75TS-44W	18.3751 (± 14)	15.5975 (± 14)	38.6823 (± 36)	18.3461	15.5962	38.6435
Ishizuchi yama	70S-303	18.3615 (± 19)	15.5926 (± 17)	38.6323 (± 46)	18.3445	15.5919	38.6087
	70S-304	18.3799 (± 13)	15.5738 (± 11)	38.5655 (± 28)	18.3680	15.5732	38.5518
Kumano	kumano-4	18.4310 (± 17)	15.5913 (± 18)	38.6543 (± 55)	18.4102	15.5903	38.6132
	kumano-5	18.4738 (± 63)	15.6352 (± 52)	38.762 (± 126)	18.4453	15.6339	38.7438
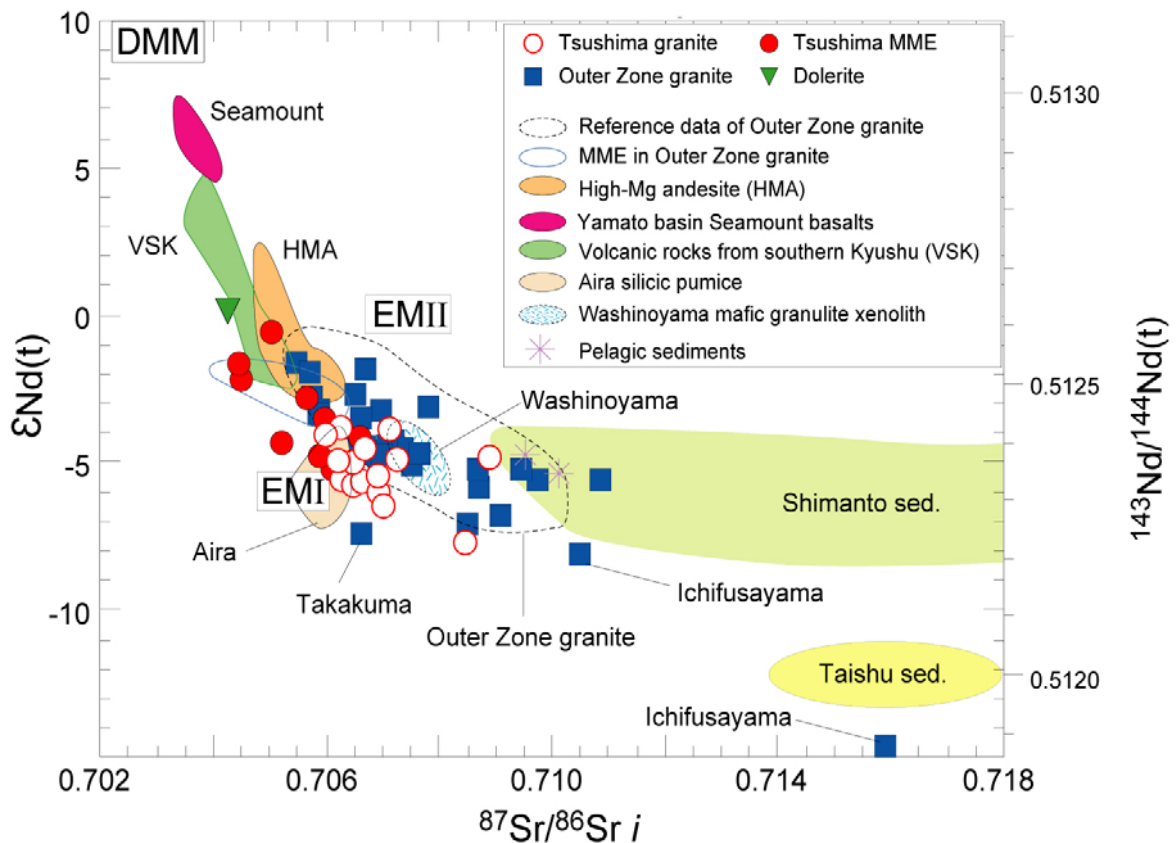
Figure 9.3 Relationship between initial Sr and Nd isotope ratios for the TSUG and the Outer Zone granites of the Southwest Japan. The open dashed area represents Sr-Nd isotopes of the Middle Miocene granites from Southwest Japan (Terakado *et al*., 1988; Dai *et al*., 1993; Shinjoe, 1997; Anma *et al*., 1998). The open solid circle represents MME from the Outer Zone granites (Ishikawa and Kagami, 1992; Shijoe et al., 1997). Data source; Volcanic rocks of the southern Kyushu, Hosono *et al*. (2003); High-Mg andesite, Shimoda et al., (1998) and Tatsumi et al., (2003); Aira silicic pumice, Arakawa et al., (1998); Shimanto Sedimentary rocks, Terakado *et al*. (1988) and Hosono *et al*. (2003); Pelagic sediments, Shimoda et al., (1998). Values for DMM and enriched mantle materials (EMI and EMII) are from Hart (1988).
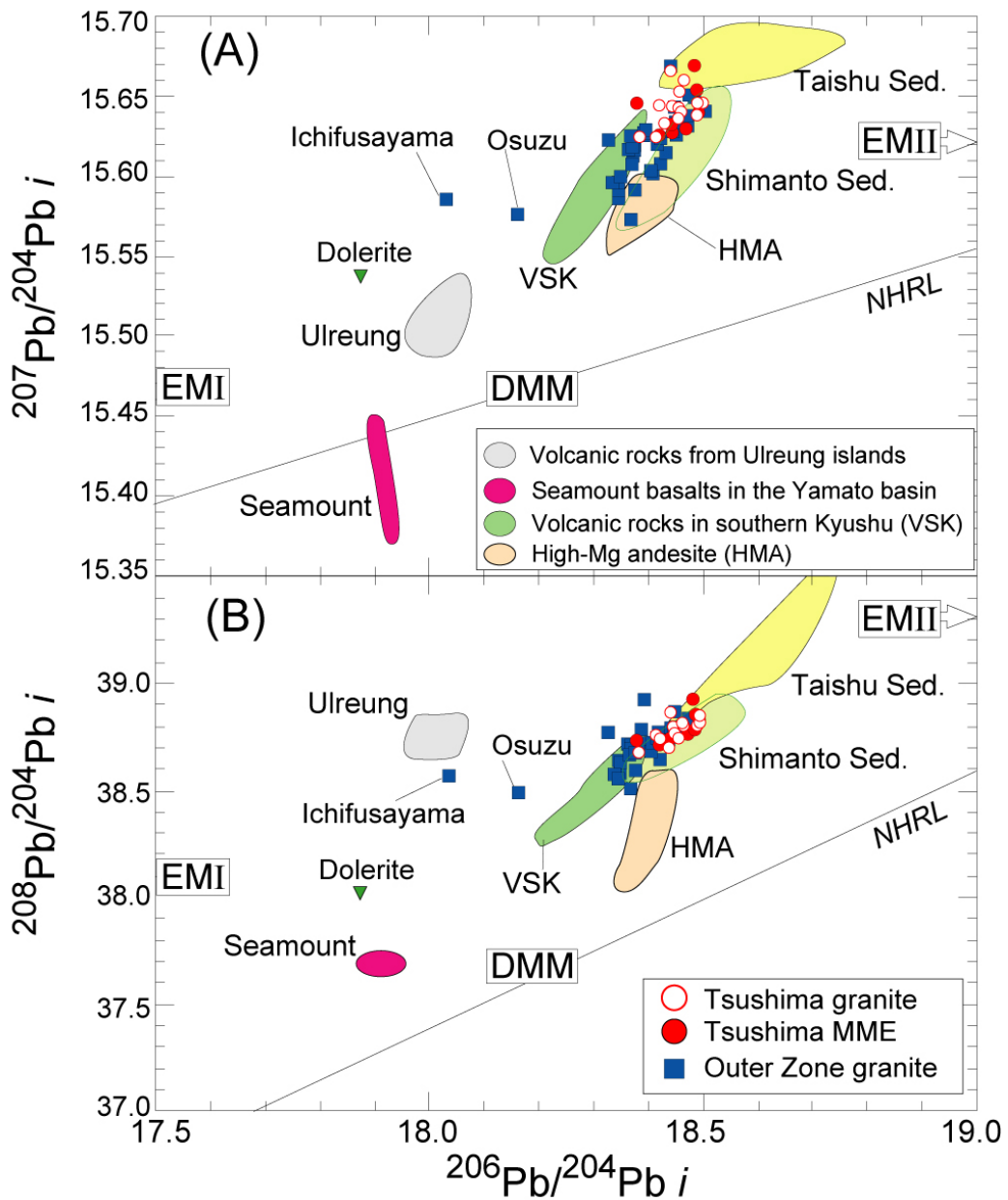
Figure 9.4 Initial Pb isotopic compositions of the TSUG and the Outer Zone granites. Data sources are the same as those indicated in the caption of figure 8.2 and 9.3. Data for Shimanto Sedimentary rocks are from Ishikawa and Nakamura (1994) and Hosono *et al*. (2003). NHRL represents Northern Hemisphere reference line with Th/U = 4.0 (Hart, 1984).

9.5 Source materials of the Middle Miocene granites in Southwest Japan

The Outer Zone granites have distribution of initial Sr isotopic ratios more scattered with increasing SiO_2 contents (Figure 9.5a). The granites also showed both highly fractionated and contaminated isotopic signature (Figure 9.5b) than the TSUG. Moreover, most of the granites plotted on the array between the mantle-generated high-Mg andesites and the Shimanto sedimentary rocks in Sr-Nd diagram (Figure 9.3). This result is consistent with the finding that the Outer Zone granites have contaminated by sedimentary rocks of the Shimanto Group. As reported earlier, these granites have regional chemical and isotopic variations; the Outer Zone granites generally increase the ASI values and initial $^{87}Sr/^{86}Sr$ compositions toward the Nankai trough (Figure 9.6a, b), reflecting increasing contamination by sediments.

The mafic magmas that partially melted the lower crust of the Outer Zone to form felsic (granitic) magmas are considered to be the high-Mg andesites (HMA in Figure 9.3), which have higher Sr and Pb isotopic ratios than the mafic magma of DMM and EMI origin (VSK and YB in Figures 9.3 and 9.4) injected into the crust beneath the TSUG in the back arc region. This isotopic signature of the high-Mg andesites required an involvment of another mantle component for their origin, adding to the DMM and EMI mantle components hypothesized underneath the Inner Zone. Metasomatized mantle component (EMII: contaminated DMM by subducted oceanic sediments) is the most likely candidate of another component in the subarc regions. Thus the mantle beneath the Outer Zone must consist of three mantle components; DMM, EMI and EMII (Figure 9.7).

Possible source materials of the granitic magmas that formed the Outer Zone granites were metabasic rocks in the lower crust (LC in Figure 9.7), as deduced from the TSUG. The hot mantle-derived mafic magma, it is the high-Mg andesite in the Outer Zone, partially melted the mafic lower crust to form felsic magma and to leave basic granulitic
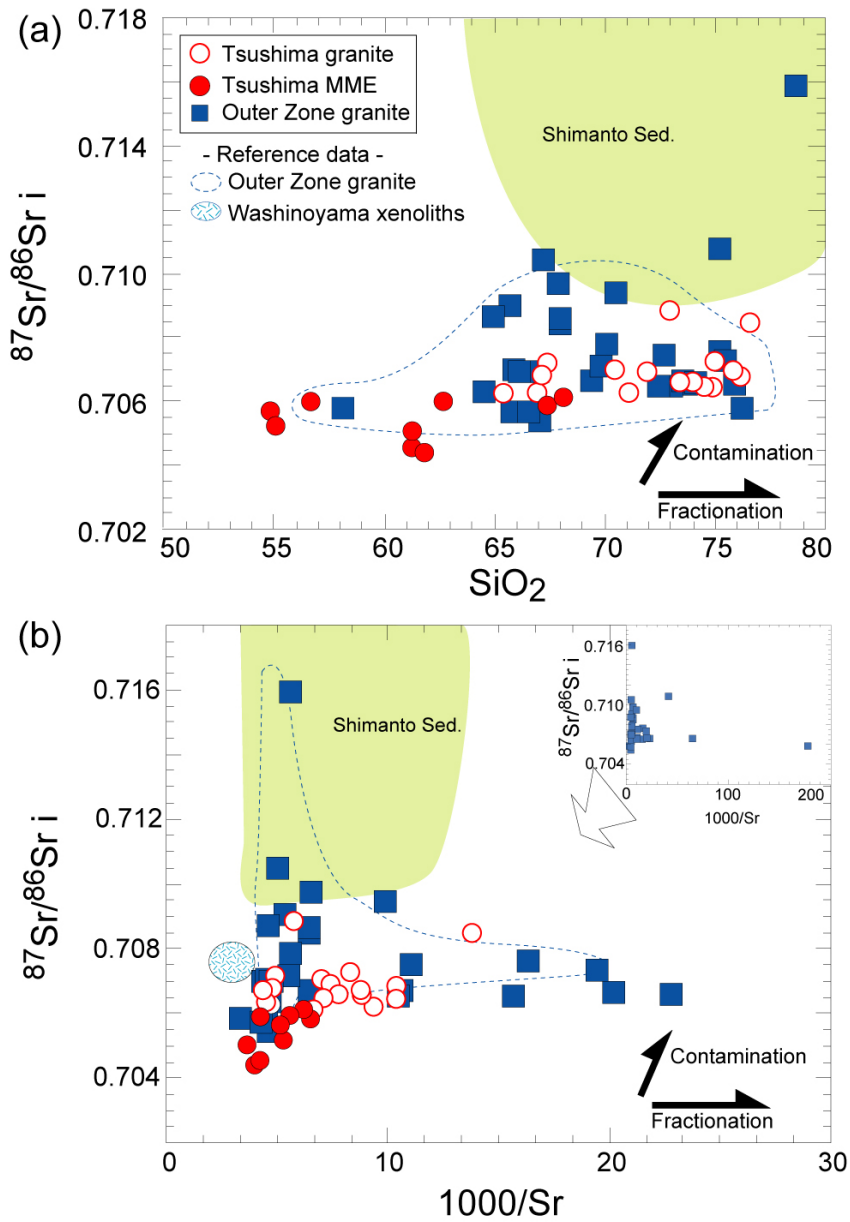
Figure 9.5 a) SiO$_2$ contents vs. initial Sr isotopic ratios diagram. b) 1000/Sr vs. initial Sr isotopic ratios diagram. Data sources are the same those indicated in the caption of figure 8.2.

residues. The Washinoyama granulite xenoliths of mafic compositions are ploted in the granite fields in between the Outer Zone granites and the TSUG in the Sr-Nd isotope diagram (Figure 9.3). The basic compositions of the Washinoyama granulite xenoliths are considered to be residues, left-over after extraction of felsic melts (isotopic compositions do not change during differentiation) from the partially molten source materials in the lower crust beneath the Outer Zone. Thus, the original lower crust must have rather intermediate (andestic) compositions. The felsic magmas of the TSUG and Outer Zone granites could have shared the similar source materials. This hypothesis is supported by regional distribution of low Sr isotopic ratios (Figure 9.6c). The most isotopically primitive rocks (the rocks with the lowest $^{87}Sr/^{86}Sr$ ratios) of most Middle Miocene granite plutons have relatively low initial $^{87}Sr/^{86}Sr$ ratios (0.706-0.707 whiteblue line; Figure 9.6c), though they underwent severe contamination by sediments in the upper crust (UC in Figure 9.7) as observed in Figrue 9.5a and changed the isotopic compositions. The Ichifusayama samples provide an extreme example of the initial $^{87}Sr/^{86}Sr$ ratios increasing with SiO_2 content (Figure 9.5a).

However, several rocks of the Outer Zone granites (ones from the Takakumayama and Ichifusayama granites) were plotted below the simple mixing array between the high-Mg andesites and the Shimanto sediments. The Ichifusayama samples have rather high initial $^{87}Sr/^{86}Sr$ ratios and $\varepsilon_{Nd}(t)$ values much lower than those of the Shimanto sediments. This isotopic ratio cannot be explained by simple mixing between the high-Mg andesite and the sedimentary rocks. Thus the magmas formed the Ichifusayama granite must have been influenced by an evolved materials with high Sr isotope compositions and low $\varepsilon_{Nd}(t)$ values. Since this material cannot be the sediments, it must be an old felsic lower crustal materials. This consideration further suggests that the lower crustal materials were heterogeneously distributed beneath the Outer Zone of Southwest Japan.

Recent studies on volcanic rocks in southern Kyushu strongly suggested that the EMI-derived magmas had important roles in forming felsic magmas (Aira pumice: Arakawa et al., 1998; Hishikari dacite: Hosono et al., 2003). This was also verified in the Tsushima granites. In contrast, in the Outer Zone granites, such EMI signature is obliterated by rather strong EMII influence. High degree of contamination by sediments might also dilute the EMI signature under the compressional tectonic environments in the Outer Zone.

In the Outer Zone, mafic magmas of mantle origin, felsic magmas of lower crust origin, and sediments in the upper crust were highly interactive during the ascent and emplacement of the granites. In contrast, the Tsushima granites that intruded into back arc extensional environments emplaced and cooled rapidly, and hardly had time to be mixed and/or contaminated with middle to upper crustal materials. This contrast might be attributed to difference in tectonic regime; in the compressive tectonic region (the forearc Outer Zone) the granite melts experienced more difficulty to find access to rise through the middle-upper crust, whereas rise of the granite melts were enhanced by the crustal thinning and open fractures in the back arc region.

9.6 Sediment assimilation and influence of fluid

Regional variation in Pb isotopic ratios is shown in the Figure 9.6d. The granites in the Shikoku have relatively low values of $^{207}Pb/^{204}Pb$ ratios, and the values increase toward both east and west directions. This variation could be attributed either to isotopic heterogeneity of the source materials or to difference in the Pb isotope composition of assimilated sediments or fluids, as deduced form the TSUG. Pb isotopic ratios of the sedimentary rocks of the Shimanot group (n = 9 form two area, green line) were rather homogenious (Ishikawa and Nakamura, 1994; Hosono et al, 2003) and latitudinal variaion
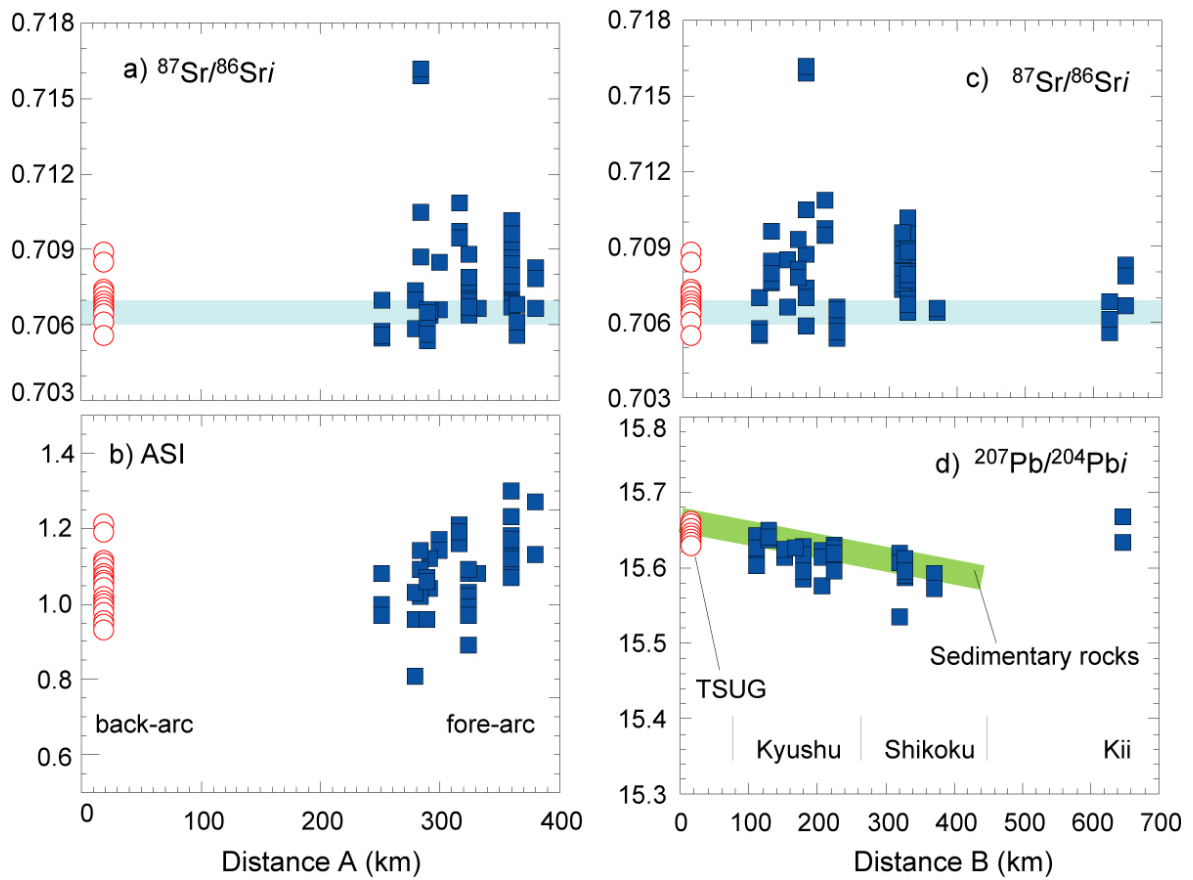
Figure 9.6 Regional chemical and isotopic variations of the Middle Miocene granites from the Southwest Japan. A represent across arc distance from the Tsushima islands to the dirction of Nankai through, and B represent along arc latitudinal distance from Tsushima islands to east.

of Sr*i* (that is a measure of the sediment contamination) of the Outer Zone granite was rather scattered but has no tendency (Figure 9.6c). Thus, the influence of the degree of sediment contamination on Pb isotopes may not be a major reason. The Outer Zone granites have in general only few miarolitic cavities and lower Pb isotope ratio than the TSUG, implying that the influence of fluid, unlike the TSUG, was not severe. There is no Pb isotope data available from the lower crust of the Outer Zone. Thus, this Pb isotopic variation is considered to have resulted from heterogeneous Pb isotope compositions of the source materials in the lower crust or crustal fluids.

10. CONCLUSIONS

The Tsushima pluton, which is contemporaneous with the latest opening stage of the East Sea at 15 Ma, is located in the innermost part among the many Middle Miocene plutons in Southwest Japan. The Tsushima granites (TSUG) consist of leucocratic granite, numerous MMEs, and gray granite, and accompanied hydrothermal activity, which formed the lead–zinc deposits. The TSUG have a metaluminous to slightly peraluminous composition. Only a few xenoliths of the host Taishu sedimentary rocks were observed. The author deduced the source materials of the TSUG and reconstructed the magmatic processes that might explain the field observations, petrography, mineralogy, and geochemical and isotopic compositions.

The framework of the Tsushima granite pluton was developed by the injection of a high-temperature mafic magma with low viscosity into a viscous leucocratic magma containing quartz–plagioclase–hornblende crystals in the shallow crust (2–6 km depth). Mingling of the felsic magma with the mafic magma formed the quenched globules of the MMEs, which contain ovoid quartz. The mafic magma originated from two mantle sources: DMM and EMI. The felsic magma formed by the partial melting of metabasic rocks in the lower crust induced by injection of mafic magmas of EMI origin. Both mafic and felsic magmas ascended separately through the lower crust to the shallow emplacement level, where they eventually mixed and mingled. The rapid cooling and crystallization of the mingled magma at the shallow emplacement level generated hydrothermal fluid, which led to the mobilization of B, Cl, Pb, and alkali elements. The Pb isotopic compositions imply that Pb in the host Taishu sediments was incorporated into the magmas by the fluid circulation.

The Outer Zone granites generally have comparable geochemical compositions to those of the TSUG. However, the Outer Zone granites have relatively enriched Pb, Rb, and

Ta content, and depleted in CaO and Sc content than those of the TSUG. The Outer Zone granites show rather fractionated and contaminated feature in chemical and isotopic ratio diagrams. Many Outer Zone granites are plotted on an array between mantle-generated high-Mg andesite and the Shimanto sedimentary rocks. The high-Mg andesites, considered to have melted the lower crust of the Outer Zone, have higher Sr and Pb isotopic ratios than the mantle-derived mafic magma in the back arc region. The isotopic signature of the high-Mg andesites required involvement of another mantle component for their generation, such as subarc metasomatized mantle contaminated by oceanic sediments (EMII) adding to DMM and EMI mantles hypothesized beneath the Inner Zone.

The felsic magmas were generated from partial melting of the mafic lower crust by injection of hot mantle-derived magma. The mafic lower crustal materials must be widely distributed underneath Southwest Japan. However, isotopically enriched samples from the Ichifusayama granite pluton suggest involvement of another crustal component with enriched Sr-Nd isotope compositions. This material is most likely an older felsic material in the lower crust. This further suggests the heterogeneous lower crust beneath the Outer Zone in the Southwest Japan.

Compressional environments in the forearc region must have stimulated interaction between the mafic mamga and the felsic magma during ascent and emplacement of the Outer Zone granites. Further contamination of sedimentary rocks also played an important role to modify their geochemical and isotopic compositions. Thus, the Outer Zone granites are mainly composed of three components; granitic magma derived from mafic lower crustal materials, mafic magma of the mantle origin (DMM+EMI+EMII), and sedimentary rocks of the upper crust.

These results further suggest the deep mantle/crustal structure of Southwest Japan: the mantle beneath the Inner Zone can be characterized by a deep mantle of DMM

composition, overlain by subcontinental lithospheric mantle of EMI-like composition, whereas that beneath the Outer Zone consists of EMII-like mantle adding to DMM and EMI mantle. The lower crust of mafic/felsic granulites must underlie the upper crust consisting mainly of the sedimentary rocks (Figure 10.1) beneath the Southwest Japan arc.

Upwelling of the hot mantle associated with the opening of the East Sea and the decompression due to crustal thinning must have generated mafic magmas in the mantle and felsic magmas in the lower crust. Transport of the mafic and felsic magmas to the shallow emplacement level interacted variously depends on their tectonic environments; high interaction and contamination occurred in compressional region of the forearc, whereas no interaction was promoted in the relatively extensional environment of the back arc region, respectively.
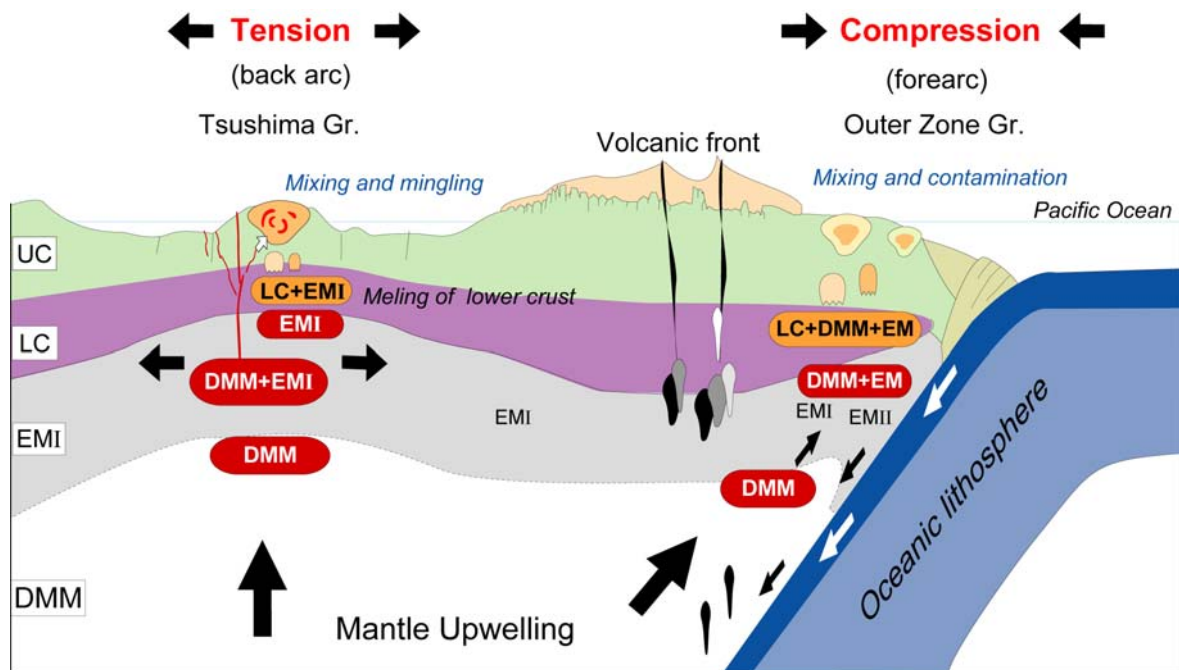
Figure 10.1 Schematic illustration of the generation of felsic and mafic magmas in forearc and back arc regions in Southwest Japan. Abbreviations: UC, upper crust; LC, lower crust; EM, enriched mantle; DMM, depleted MORB mantle.

ACKNOWLEDGEMENTS

abroad for their encouragement and support.

REFERENCES

Anderson, J. L. and Smith, D. R. (1995) The effects of temperature of fO_2 on the Al-in-hornblende barometer. *Am. Mineral.,* 80, 549-559.

Anma, R., Kawano, Y. and Yuhara, M. (1998) Compositional zoning and its implication in a toroidal circulation inside the Yakushima pluton, SW Japan. *Mem. Natl. Inst. Polar Res. Spec. Issue,* 53, 157-176.

Arai, S., Hirai, H. and Uto, K. (2000) Mantle peridotite xenoliths from the Southwest Japan arc: a model for the sub-arc upper mantle structure and composition of the Western Pacific rim. *J. Min. Pet. Sciences* 95, 9-23.

Arakawa, Y., Kurosawa, M., Takahashi, K., Kobayashi, Y., Tsukui, M. and Amakawa, H. (1998) Sr-Nd isotopic and chemical characteristics of the silicic magma reservoir of the Aira pyroclastic eruption, southern Kyushu, Japan. *J. Volcan. Geotherm. Res.,* 80, 179-194.

Aramaki, S., Hirayama, K. and Nozawa, T. (1972) Chemical composition of the Japanese granites, part2. Variation trends and average composition of 1200 analyses. *J. Geol. Soc. Japan*, 78, 39-49.

Audétat, A., Günther, D. and Heinrich, C. A. (2000) Causes for large-scale metal zonation around mineralized plutons: fluid inclusion LA-ICP-MS evidence from the Mole granite, Australia. *Bull. Soc. Econ. Geologists* 95, 1563-1581.

Barbarin, B. (1991) Enclaves of the Mesozoic calc-alkaline granitoids of the Sierra Nevada Batholith, California. *In* Didier, J. and Barbarin, B. (ed*.) Enclaves and Granite Petrology*. Elsevier, Amsterdam, 135-53.

Barbarin, B. and Didier, J. (1991) Conclusions: enclaves and granite petrology. *In* Didier, J. and Barbarin, B. (ed.) *Enclaves and Granite Petrology.* Elsevier, Amsterdam,

545-549.

Barbarin, B. and Didier, J. (1992) Genesis and evolution of mafic microgranular enclaves through various types of interaction between coexisting felsic and mafic magmas. *Trans. R. Soc. Edin. Earth Sci.,* 83, 145-153.

Beard, J. S. and Lofgren, G. E. (1991) Dehydration melting and water-saturated melting of basaltic and andesitic greenstones and amphibolites at 1, 3, and 6.9kb. *J. Petrol.,* 32, 365-401.

Blundy, J.D., Holland, T.J.B., 1990. Calcic amphibole equilibria and a new amphibole-plagioclase geothermometer. *Contrib. Mineral. Petrol.,* 104, 208-224.

Condie, K. C. (1998) Episodic continental growth and supercontinents: a mantle avalanche connection? *Earth Planet. Sci. Lett.,* 163, 97-108.

Cousens, B. L. and Allan, J. F. (1992) A Pb, Sr, and Nd isotopic study of basaltic rocks from the Sea of Japan, Legs 127/128. *In* Tamaki, K., Suyehiro, K., Allan, J. and McWilliams M. (ed.) *Proc. Ocean Drill. Program, Sci. Results*, 127/128, part 2, 805-817.

Dai, K., Tsusue, A. and Honma, H. (1993) Petrological study of granitic rocks from the Kashiwajima-Okinoshima district in the southwestern part of Kochi Prefecture. *J. Mineral. Petrol. Econ. Geology,* 88, 247-264.*

Faure, G. and Mensing, T. M. (2005) *Isotopes: principles and applications.* Wiley, New Jersey, 897p.

Giret, A., Bonin, B. and Leger, J. (1980) Amphibole compositional trends in oversaturated and undersaturated alkaline plutonic ring-complexes. *Can. Mineral.,* 18, 481-495.

Geological Survey of Japan (1992) *Geological Atlas of Japan*, 2nd edn. Asakura Pub.

Hamasaki, S. (1997) K-Ar ages of igneous activity in the Amakusa area, Kumamoto prefecture: an investigation of Miocene magmatic activity in Inner and Zone of

Kyushu, southwestern Japan. *Resource Geol.,* 47, 121-129.

Hart, S. R. (1984) A large-scale isotope anomaly in the southern hemisphere mantle. *Nature,* 309, 753-757.

Hart, S. R. (1988) Heterogeneous mantle domains: Signatures, genesis, and mixing chronologies. *Earth Planet. Sci. Lett.*, 90, 273-296.

Hibbard, M. J. (1981) The magma mixing origin of mantled feldspar. *Contrib. Mineral. Petrol.,* 76, 158–170.

Holland, H. D. (1972) Granites, Solutions, and base metal deposits. *Bull. Soc. Econ. Geologists,* 67, 281-301.

Hosono, T., Nakano, T. and Murakami, H. (2003) Sr-Nd-Pb isotopic compositions of volcanic rocks around the Hishikari gold deposit, southwest Japan: implications for the contribution of a felsic lower crust. *Chem. Geology*, 201, 19-36.

Huppert, H. E. and Sparks, R. S. J. (1988) The generation of granitic magmas by intrusion of basalt into continental crust. *J. Petrol.,* 29, 599-624.

Ibaraki, M. (1994) Geologic ages and paleoenvironments of the Tertiary deposits in northwestern Kyushu on the basis of planktonic foraminiferal fauna. *The Earth Monthly (Gekkan Chikyu)* 16, 150-153.**

Ikeda, Y., Nagao, K. and Kagami, H. (2001) Effects of recycled materials involved in a mantle source beneath the southwest Japan arc region: evidence from noble gas, Sr, and Nd isotopic systematics. *Chem. Geology,* 175, 509-522.

Ikemi, H., Shimada, N. and Chiba, H. (2001) Thermochronology for the granitic pluton related to lead-zinc mineralization in Tsushima, Japan. *Resource Geol.,* 51, 229-238.

Imai, H. (1973) The geologic structure and mineralization at the Taishu mine, Nagasaki Prefecture, Japan. *J. mining Metal. Inst. Japan,* 89, 509-514.*

Imai, H., Takenouchi, S. and Kihara, T. (1971) Fluid inclusion study at the Taishu Mine, Japan, as related to geologic structure. *Mining Geol., Spec. Issue* 3, 321-326.

Ishihara, S. (1977) Magnetite-series and ilmenite-series granitic rocks. *Mining Geol.,* 27, 293-305.

Ishihara, S. and Imai, A. (2000) Genesis of high chlorine and silver-lead-zinc-mineralized granitoids in Tsushima, Japan. *Resource Geol.*, 50, 167-178.

Ishihara, S. and Matsuhisa, Y. (1999). Oxygen isotopic constraints on the geneses of the Miocene Outer Zone granitoids in Japan. *Lithos,* 46, 523-534.

Ishizaka, K. and Ishikawa, N. (1990) Sr and Nd isotopic study of Tertiary granitic rocks in the Tsushima and Goto Islands. *Earth Sci. Rep. Colle. Lib. Art. Sci. Kyoto Univ.*, 24, 15-22.**

Ishikawa, A. and Kagami, H. (1992) Isotopic composition of igneous and metamorphic xenoliths within the Takatsukiyama granitic mass. *Geol. Rept. Shimane Univ.,* 11, 1-6.**

Ishikawa, T. and Nakamura, E. (1994) Origin of the slab component in arc lavas from across-arc variation of B and Pb isotopes. *Nature,* 370, 205-208.

Ishikawa, N. and Tagami, T. (1991) Paleomagnetism and fission-track geochronology on the Goto and Tsushima islands in the Tsushima strait area: implications for the opening mode of the Japan Sea. *J. Geomag. Geoelectr.*, 43, 229-253.

Ishikawa, N., Torii, M. and Koga, K. (1989) Paleomagnetic study on the Tsushima islands, Southern margin of the Japan Sea. *J. Geomag. Geoelectr.*, 41, 797-811.

Isozaki, Y. and Maruyama, S. (1991). Studies on orogeny based on plate tectonics in Japan and new geotectonic division of the Japanese islands. *Journal of Geography (Tokyo)*, 100, 697-761.

Johannes, W. and Holtz, F. (1996) *Petrogenesis and Experimental Petrology of Granitic*

Rocks. Springer, Berlin. p.335.

Johnston, A. D. and Wyllie, P. J. (1988) Interaction of granitic and basic magmas: experimental observations on contamination processes at 10kbar with H_2O. *Contrib. Mineral. Petrol.,* 98, 352-362.

Kagami, H., Iizumi, S., Iwata, M., and Nureki, T. (1993) Sr-Nd isotope systematics of xenoliths in Cenozoic volcanic rocks from SW Japan. *Proc. Japan Acad.,* 69, ser. B, 1-6.

Kagami, H., Owada, M., Ohishi, Y. and Iwata, M. (1995) Temporal variation in Sr and Nd isotopic composition of Jurassic to Miocene igneous rocks in Seto Inland Sea and Kinki Districts of the Ryoke Belt, Southwest Japan Arc. *Mem. Geol. Soc. Japan,* 44, 309-320.*

Kaneko, K. and Yaguti, S. (1980) Uchiyama granite in Shimo-jima, Tsushima. *Mem. Fac. Edu., Miyazaki Univ., Nat. Science,* 48, 27-40.*

Kanno, S. (1995) Tertiary molluca from Taishu Mine, Tsushima, Nagasaki Prefecture, Japan. *Trans. Proc. Palaeont. Soc. Japan, N. S.,* 18, 31-36.

Karakida, Y. (1987) K-Ar ages of the igneous rocks in Tsushima Shimojima, Nagasaki Prefecture. *J. Nikkan Tunnel Study Group,* 7, 32-42.**

Kawahara, K. S., Tsukahara, T. T., and Kamogawa, N. (1984) The late Miocene volcanism in Nakadorijima, Goto islands, Nagasaki Prefecture, Japan. *Mem. Geol. Soc. Japan 24, 77-92.* *

Kemp, A. I. S. and Hawkesworth, C. J. (2003) Granitic perspectives on the generation and secular evolution of the continental crust. *In* Rudnick, R. L. (Eds.) *The Crust (Treatise in Geochemistry,* Vol. 3) (pp. 349 – 410). Elsevier, Amsterdam

Kitai, T. (1969) On the basic and intermediate plutonic rocks from Goto Islands and Tsushima Island. *J. Japanese Assoc. Min. Petro. Econ. Geology,* 62, 18-35.*

Kretz, R. (1982) Transfer and exchange equilibria in a portion of the pyroxene quadrilateral as deduced from natural and experimental data. *Geochim. Cosmochim. Acta*, 46, 411-422.

Kurosawa, M., Jackson, S. and Sueno, S. (2002) Trace Element Analysis of NIST SRM 614 and 616 glass reference materials by laser ablation microprobe-inductively coupled plasma-mass spectrometry. *Geostand. Newslett. J. Geostand. Geoanalysis,* 26, 75-84.

Leake, B. E., Woolley, A. R., Arps, C. E. S. *et al.* (1997) Nomenclature of amphiboles: report of the subcommittee on amphiboles of the International Mineralogical Association, Commission on New Minerals and Mineral Names. *Eur. J. Mineral.,* 9, 623-651.

Le Maitre, R. W.(editor), Streckeisen, A., Zanettin, B. *et al.* (2002) *Igneous Rocks: A Classification and Glossary of Terms (2nd ed.) Recommendations of the International Union of Geological Sciences Subcommission on the Systematics of Igneous rocks.* Blackwell Scientific Publications, Oxford. p.236.

Linnen, R.L., Keppler, H., 2002. Melt composition control of Zr/Hf fractionation in magmatic processes. *Geochim. Cosmochim. Acta*, 66, 3293-3301.

Marshall, C. P. and Fairbridge, R. W. (1999). *Encyclopedia of Geochemistry.* Kluwer Academic pub. 712 pp.

Maruyama, S. (1997) Pacific-type orogeny revisited: Miyashiro-type orogeny proposed. *Island Arc*, 6, 91-120.

Matsuhashi, S. (1968) Analysis of structural control and results of prospecting for bedding plane veins in the Taishu mine. *Mining Geol.,* 18, 161-172.*

Matsumoto, Y. and Takahashi, K. (1987) Igneous activities in the Tsushima islands, Nagasaki Prefecture, Japan. *Mono. Assoc. Geol. Collaboration*, 33, 1-20.*

Miller, C.F., McDowell, S.M., Mapes, R.W., 2003. Hot and cold granites? Implications of zircon saturation temperatures and preservation of inheritance. *Geology*, 31, 529-532.

Ministry of International Trade and Industry (MITI) (1972) Report on the regional geological survey, Tsushima-Kamiagata district of the 1971' fiscal year Geological Survey. 29p.**

Ministry of International Trade and Industry (MITI) (1973) Report on the regional geological survey, Tsushima-Kamiagata district of the 1972' fiscal year Geological Survey. 34p.**

Ministry of International Trade and Industry (MITI) (1974) Report on the regional geological survey, Tsushima-Kamiagata district of the 1973' fiscal year Geological Survey. 52p.**

Na, C., Nakano, T., Tazawa, K., Sakagawa, M. and Ito, T. (1995) A systematic and practical method of liquid chromatography for the determination of Sr and Nd isotopic ratios and REE concentrations in geological samples. *Chem. Geology*, 123, 225-237.

Nakada, S. (1983) Zoned magma chamber of the Osuzuyama acid rocks, southwest Japan. *J. Petrol.*, 24, 471-494.

Nakada, S. and Takahashi, M. (1979) Regional variation in chemistry of the Miocene intermediate to felsic magmas in the Outer Zone and the Setouchi Province of Southwest Japan. *J. Geol. Soc. Japan*, 85, 571-582.*

Nakada, S. and Okamoto, Y. (1984) Petrogenetic model of I- and S-type felsic magma in the Outer Zone, SW Japan, in terms of Sr isotopic compositions. *Mem. Geol. Soc. Japan*, 24, 187-198. *

Nakajo, T. and Funakawa, S. (1996) Eocene radiolarians from the Lower Formation of the

Taishu Group, Tsushima Islands, Nagasaki Prefecture, Japan. *J. Geol. Soc. Japan,* 102, 751-754. *

Nakajo, T. and Maejima, W. (1998) Morpho-dynamic development and facies organization of the Tertiary delta system in the Taishu Group, Tsushima Islands, southwestern Japan. *J. Geol. Soc. Japan*, 104, 749-763.

Nakano, T. and Ito, T. (1990) Pulverization experiment on geological materials using automated pulverizer: 1-appraisal of recovery and contamination. *Ann. Rep. Inst. Geosci. Univ. Tsukuba*, 16, 78-80.

Nakano, T., Jeon, S. R. and Sueno, S. (1997) X-ray fluorescence analysis of rock samples using Philips PW1404 (1): Simultaneous determination of major and trace elements using glass beads of GSJ igneous rocks reference samples. *Ann. Rep. Inst. Geosci. Univ. Tsukuba,* 23, 63-68.

Okada, H. and Fujiyama, I. (1970) Sedimentary cycles and sedimentation of the Taishu Group in the Shiohama area, central Tsushima, Kyushu. *Mem. Natl. Sci. Museum,* 3, 9-18. *

Okamoto, K., Kinoshita, O., Nonaka, K. and Yagi, S. (1987) Magma mixing model of the Tertiary granitic rocks of the southern Kyusyu. *J. Japanese Assoc. Mineral. Petrol. Econ. Geol.*, 82, 257-268.

Otofuji, Y., Hayashida, A. and Torii, M. (1985) When was the Japan Sea opened?: Paleomagnetic evidence from Southwest Japan. *In* Nasu, N., Kushiro, I., Kobayashi, K. *et al*. (Eds.) *Formation of Active Oceanic margins* (pp. 551-566). Terra Publication, Tokyo.

Ohyama and Shimada (1988) Genetical relationships between lead-zinc ore deposits and the Uchiyama granitic body – (1) Zonal arrangement of magnetic susceptibility (abstr.) *Mining Geol.,* 38, 71-71.**

Pearce, N. J. G., Perkins, W. T., Westgate, J. A. *et al*. (1997) A complication of new and published major and trace element data for NIST SRM 610 and NIST SRM 612 glass reference materials. *Geostand. Newslett. J. Geostand. Geoanalysis,* 21, 115-144.

Piccoli, P. M. and Candela, P. A. (2002) Apatite in igneous systems. *Rev. Mineral. Geochem.,* 48, 255-292.

Pitcher, W.S. (1997) *The Nature and Origin of Granite*. 2nd Edi. Chapman & Hall, 387 pp.

Pouclet, A., Lee, J., Vidal, P., Cousens, B. and Bellon, H. (1995) Cretaceous to Cenozoic volcanism in South Korea and in the Sea of Japan: magmatic constraints on the opening of the back-arc basin. *In* Smellie, J. L. (ed.) *Volcanism Associated with Extension at Consuming Plate Margins. Geol. Soc. Spec. Pub.*, 81, 169-191.

Rudnick, R.L., and Fountain, D.M. (1995) Nature and composition of the continental crust: a lower crustal perspective. Rev. *Geophysics,* 33, 267-309.

Rudnick, R. L. and Gao, S. (2003) Compositions of the continental crust. *In* Rudnick, R. L. (Eds*.) The Crust (Treatise in Geochemistry*, Vol. 3) (pp. 1 – 64). Elsevier, Amsterdam.

Sakai, H. and Nishi, H. (1990) Geologic age of the Taishu Group and the Katsumoto Formation in the Tsushima and Iki Islands, off northwest Kyushu on the basis of planktonic foraminifers. *J. Geol. Soc. Japan,* 96, 389-392.

Sakai, H. and Yuasa, T. (1998) K-Ar ages of the Mogi and Ugetsuiwa subaqueous pyroclastic flow deposits in the Taishu Group, Tsushima Islands. *Mem. Natl. Sci. Museum,* 31, 23-28. *

Sato, K., Ishihara, S. and Shibata, K. (1992). Granitoid map of Japan. *In* Kato, H. and Inoki, Y. (Eds.) *Geological Map of Japan*. Asakura Publishing, Tokyo.

S'edin, V. T. and Sato, H. (1996). Volcanic rocks. *In* Isenaki, N. et al., (Eds.) *Geology and*

Geophysics of the Japan Sea (Japan-USSR Monograph Series) (pp. 353-368). Terra Publication, Tokyo.

Shibata, K. and Ishihara, S. (1979). Initial $^{87}Sr/^{86}Sr$ ratios of plutonic rocks from Japan. *Contrib. Mineral. Petrol.*, 70, 381-390.

Shimada, N. (1977) Lead-zinc ore deposits of the Tsushima Islands, Nagasaki Prefecture, with special reference to Shigekuma-type mineralization. *Mem. Fac. Sci., Kyushu Univ., Series D, Geology,* 23, No 3, 417-480.

Shimada, N., Ohyama, Y. and Ikemi, H. (2000) Characterization of magnetically zoned pluton, Tsushima, Japan. *Resource Geol.,* 50, 65-73.

Shimoda, G., Tatsumi, Y., Nohda, S., Ishizaka, K. and Jahn, B. M. (1998) Setouchi high-Mg andesites revisited: geochemical evidence for melting of subducting sediments. *Earth Planet. Sci. Lett*., 160, 479-492.

Shinjo, R., Chung, S. -L., Kato, Y. and Kimura, M. (1999) Geochemical and Sr-Nd isotopic characteristics of volcanic rocks from the Okinawa Trough and Ryuku Arc: implications for the evolution of a young, intracontinental back arc basin. *J. Geoph.. Research*, 104, 10591-10608.

Shinjoe, H. (1997) Origin of the granodiorite in the forearc region of southwest Japan: Melting of the Shimanto accretionary prism. *Chem. Geol*., 134, 237-255.

Shinjoe, H., Orihashi, Y., Wada, Y., Sumii, T. and Nakai, S. (2007) Regional variation of whole rock chemistry of the Miocene felsic igneous rocks in the Kii Peninsula, southwest Japan. *J. Geol. Soc. Japan,* 113, 310-325.

Sisson, T. W., Ratajeski, K., Hankins, W. B. and Glazner, A. F. (2005) Voluminous granitic magmas from common basaltic sources. *Contrib. Mineral. Petrol*., 148, 635-661.

Stein, G., Charvet, J., Lapierre, H. And Fabbri, O. (1994). Geodynamic setting of volcano-plutonic rocks in so-called "paleo-accretionary prisms": Fore-arc activity or post-collisional magmatism? The Shimanto belt as a case study. *Lithos,* 33, 85-107.

Sterner, S. M., Hall, D. L. and Bodnar, R. J. (1988) Synthetic fluid inclusions. V. Solubility relations in the system NaCl-KCl-H2O under vapor-saturated conditions. *Geochim. Cosmochim. Acta,* 52, 989-1005.

Sugimura, A. and Uyada, S. (1973) *Island Arcs – Japan and its Environs.* Amsterdam, Elsevier. 247 pp.

Suzaki, Y., Yajima, S. and Tsutsumi, S. (1970) Hakudo and Toseki deposits in the north of Izuhara-machi. *Mem. Natl. Sci. Museum*, 3, 35-44.*

Taira, A. (2001) Tectonic evolution of the Japanese Island arc system. *Ann. Rev. Earth and Planet. Sci.*, 29, 109-134.

Takahashi, K. (1969) A study of the Taishu Group. Bull. Fac. Lib. Arts, *Nagasaki Univ., Natu. Sci.,* 10, 67-82. *

Takahashi, K. and Hayashi, M. (1985) Fission track ages of igneous rocks from Tsushima Islands (I). *Bull. Fac. Lib. Arts, Nagasaki Univ., Natu. Sci.*, 25, 9-19.*

Takahashi, K. and Hayashi, M. (1987) Fission track ages of igneous rocks from Tsushima Islands (II). *Bull. Fac. Lib. Arts, Nagasaki Univ., Natu. Sci.*, 27, 19-31.*

Takahashi, K. and Nishida, T., (1975) On the molluscan fossils from the Lower Formation of the Taishu Group in the Kamiagata district of Tsushima Islands. *Bull. Fac. Lib. Arts, Nagasaki Univ., Nat. Sci.* 25, 19-31.*

Takahashi, M. (1983). Space-Time distribution of late Mesozoic to early Cenozoic magmatism in East Asia and its tectonic implications. *In* Hashimoto, M. and Uyeda, S. (Eds.) *Accretion tectonics in the Circum-Pacific regions* (pp. 69-88).

Terra publication, Tokyo.

Takahashi, M. (1986). Magmatic activity of island arcs before and after the opeining of the Japan Sea. *Kagaku*, 56, 103-111.**

Takahashi, M., Aramaki, S. and Ishihara, S. (1980) Magnetite-series/ilmenite-series vs. I-type/S-type granitoids. *Mini. Geology, special issue*, 8, 13-28.

Tamaki, K. (1995) Opening tectonics of the Japan Sea. *In* Taylor, B. (Eds.), *Backarc Basins: Tectonics and Magmatism* (pp. 407-420). Plenum Press, New York.

Tamaki, K., Suyehiro, K., Allan, J., Ingle, J. C. and Pisciotto, K. A. (1992) Tectonic synthesis and implications of Japan Sea ODP drilling. *In* Tamaki, K., Suyehiro, K., Allan, J. and McWilliams, M. (ed.) *Proc. Ocean Drill. Program, Sci. Results*, 127/128, part 2, 1333-1348.

Tatsumi, Y., Maruyama, S. and Nohda, S. (1990) Mechanism of back opening in the Japan Sea: role of asthenospheric injection. *Tectonophysics,* 181, 299-306.

Tatsumi, Y., Otofuji, Y., Matsuda, T. and Nohda, S. (1989) Opening of Sea of Japan back-arc basin by asthenospheric injection. *Tectonophysics*, 166, 317-329.

Tatsumi, Y., Shukuno, H., Sato, K., Shibata, T. and Yoshikawa, M. (2003) The petrology and geochemistry of high-magnesian andesites at the western tip of the Setouchi volcanic belt, SW Japan. *J. Petrgol.,* 44, 1561-1578.

Tatsumoto, M. and Nakamura, Y. (1991) DUPAL anomaly in the Sea of Japan: Pb, Nd, and Sr isotopic variations at the eastern Eurasian continental margin. *Geochim. Cosmochim. Acta,* 55, 3697-3708.

Taylor, S. R. and McLennan, S. M. (1985) *The Continental Crust: Its Composition and Evolution.* Blackwell, Oxford. 328p.

Terakado, Y., Shimizu, H. and Masuda, A. (1988) Nd and Sr isotopic variations in acidic rocks formed under a peculiar tectonic environment in Miocene Southwest Japan.

Contrib. Mineral. Petrol., 91, 1-10.

Terashima, S. and Ishihara, S. (1980) Anomalous chlorine contents of Miocene granitoids from Tsushima, Japan. *J. Japan. Assoc. Mineral. Petrol. Econ. Geol.*, 75, 62-67.

Tobisch, O. T., Mcnulty, B. A. and Vernon, R. H. (1997) Microgranitoid enclave swarms in granitic plutons, central Sierra Nevada, California. *Lithos*, 40, 321-339.

Tsusue, A., Mizuta, T., Tamai, T. and Ishihara, S. (1987) Granitic rocks of southwest Japan: trace element evidence regarding their differentiation; 1. REE patterns. *Mining Geol.*, 37, 267-278.

Urabe, T. (1987) The effect of pressure on the partitioning ratios of lead and zinc between vapor and rhyolite melts. *Econ. Geology,* 82, 1049-1052.

Uto, K., Hoang, N. and Matsui, K. (2004) Cenozoic lithospheric extension induced magmatism in Southwest Japan. *Tectonophysics*, 393, 281-299.

Vernon, R. H. (1984) Microgranitoid enclaves in granites: globules of hybrid magma quenched in a plutonic environment. *Nature*, 309, 438-439

Vernon, R. H. (1991) Interpretation of microstructures of microgranitoid enclaves. *In* Didier, J. and Barbarin, B. (ed.) *Enclaves and granite petrology, Developments in Petrology,* vol. 13, Elsevier, Amsterdam, 277-291.

Yamada, N., Sato, Y., Hiroshima, T. and Suda, Y. (1990) *1:200,000 Geological map of Izuhara*. Geological Survey of Japan.**

Wedepohl, K. H. (1991) Chemical composition and fractionation of the continental crust. *Geol. Rundsch* 80, 207-223.

Whitney, J.A. (1975) The effects of pressure, temperature, and X_{H2O} on phase assemblage in four synthetic rock compositions. *J. Geol.*, 83, 1-31.

Wiebe, R. A. and Collins, W. J. (1998) Depositional features and stratigraphic sections in granitic plutons: implications for the emplacement and crystallization of granitic

magma. *J. Struct. Geol.*, 20, 1273-1289.

Wyllie, P. J., Cox, K. G. and Biggar, G. M. (1962) The habit of apatite in synthetic systems and igneous rocks. *J. Petrol.*, 3, 238-243.

* in Japanese with English abstract; ** in Japanese.